On Time Machines in Kerr–Newman Spacetime

vorgelegt von

Christian Wüthrich

1999

Leiter der Arbeit: Prof. Petr Hájíček
Institut für theoretische Physik
Universität Bern

On Time Machines in Kerr–Newman Spacetime

Diplomarbeit
der Philosophisch-naturwissenschaftlichen Fakultät
der Universität Bern

vorgelegt von

Christian Wüthrich

1999

Leiter der Arbeit: Prof. Petr Hájíček
                   Institut für theoretische Physik
                   Universität Bern

One cannot choose but wonder. Will he ever return? It may be that he swept back into the past, and fell among the blood–drinking, hairy savages of the Age of Unpolished Stone; into the abysses of the Cretaceous Sea; or among the grotesque saurians, the huge reptilian brutes of the Jurassic times.

H. G. Wells, The Time Machine

Contents

Chapter 1

Introduction

The subject of this essay is the causality violations occuring in an analytical extension of the Kerr–Newman solution of the Einstein–Maxwell equations. We investigate the theoretical possibility of such violations and study timelike curves along which a hypothetical space crew could move in order to travel backwards in time. Prior to the launch of our essay, a few notes should serve as an introduction to the topic. First, we give a short historical account of the field. These remarks are intended to help the reader to gain an idea of where to locate the subsequent thesis and are far from claiming to be complete.

1.1   Historical Remarks

Albert Einstein published in 1915 several remarkable papers which may serve as beautiful historical documents. They give account of the last few developments in the original version of general relativity (GR) after a decade's struggle until Einstein was eventually in the position to declare: "With this step [the final formulation of the field equations], general relativity is finally completed as a logical structure."[1] The formulation of GR may undoubtedly count as one of the finest intellectual achievements of the twentieth century. It opened up a field of research which fascinates to this day.

A few month after the publication of Einstein's field equations, Karl Schwarzschild discovered the first exact solution in his [2]. The solution describes the spacetime curvature induced by a non–rotating star and is asymptotically Newtonian. Today, it gains relevance through its illustration of the clearly non–Euclidean nature of spacetime geometry in case of strong gravity and through its equivalence with the spacetime geometry of a black hole and of a collapsing star when appropriately truncated. Shortly thereafter, Reissner and Nordstrøm found a more general solution of a non–rotating black hole with charge.

In 1924, Eddington was the first to find a coordinate system which was non–singular at $r = 2M$. However, it covered only a part of the Schwarschild geometry. Unfortunately, he seemed not to have recognized the relevance of his findings. It took another nine years until Lemaître did so. Kruskal [3]

---

[1]Einstein, A. "Die Feldgleichungen der Gravitation", *Preuss. Akad. Wiss. Berlin, Sitzber.* 1915, 844–847, quoted according to [1], p. 433.

constructed in 1960 a coordinate system which overcame the difficulties with the incompleteness of former systems, covering both "Schwarzschild patches" and revealing the structure of the Schwarzschild geometry.

The solution to Einstein's vacuum field equations describing an uncharged black hole with an angular momentum was first found by Kerr [4]. Two years later, Newman and his collaborators discovered the charged generalization in [5]. They attributed their solution to a rotating ring of mass and charge. The connection to black holes was found only later, when Hawking and Penrose revised the traditional view. According to the latter, singularities arising in the exact solutions of Schwarzschild and Reissner–Nordstrøm were dismissed as non–physical, due perhaps to the specific assumptions regarding symmetry properties.[2] Penrose [8] concluded that "[...] the existence of a trapped surface implies—irrespective of symmetry—that singularities necessarily develop." Hawking [9] showed that the occurrence of—principally observable—singularities is inevitable if the Einstein equations hold, if matter has normal properties and if the universe satisfies certain reasonable global conditions. Furthermore, he argued that the singularity would not necessarily constitute a beginning of the universe.

Later, these theorems were improved and refined. Uniqueness theorems proven by Israel, Carter, Hawking, Robinson, and Mazur were obtained from the late sixties to the early eighties. Israel [10, 11] proved that a static, spherical black hole is described by the Schwarzschild or the Reissner–Nordstrøm solutions. In 1975, Robinson [12] proved that the Kerr spacetimes are the unique family of black hole solutions of the Einstein vacuum field equations in case of a non–degenerate event horizon. Penrose [13], p. 69 assumed as early as 1969 that the asymptotically flat exterior of an event horizon approaches a Kerr–Newman solution asymptotically with time. In 1982, Mazur [14] showed the uniqueness of the Kerr–Newman solution with $M^2 - a^2 - P^2 - Q^2 > 0$ for a stationary, rotating, electrovacuum black hole with non–degenerate event horizon.

The foundations on which the uniqueness theorems were based were also largely developed in this period. One of the most important findings in this respect is due to Penrose [13] who conjectured that some "cosmic censor" does not allow for "naked singularities" in gravitational collapses, *i.e.* no singularities without an event horizon with respect to asymptotic observers are permitted. Also, the classical instability of naked singularities was shown by de Felice [15]. Thus, the cosmic censorship concept is accepted today.

Hawking justified some basic assumptions on which the uniqueness theorems rely in his famed [16]. These assumptions include that stationary black holes must either be static or axisymmetrical and the event horizon has a spherical topology. Hájíček [17] showed that the outer boundary of an ergosphere must intersect the event horizon and thus demonstrated the existence of a singularity or a black hole within any ergosphere.[3]

---

[2]Lifshitz and Khalatnikov in their [6] for instance seem to be rather sceptical about the physicality of the essential properties of gravitational collapse, a scepticism which condenses in [7].

[3]A detailed review concerning uniqueness and censorship issues is given by Carter in [18] as well as by Mazur in [19].

It seems natural to study the motion of test particles in order to form an understanding of the structure of the respective spacetime. Therefore, several authoritative papers concerned with geodesic motion were published in the aftermath of the discovery of black hole solutions. They include the works of de Felice—*e.g.* [20]—as well as the far–reaching and rather complete account of test particle trajectories by Stewart and Walker [21]. Bičák and Stuchlík [22] analysed latitudinal and radial motion in Kerr spacetime.

Boyer and Lindquist [23] as well as Carter [24, 25] have discovered analytical extensions for Kerr and Kerr–Newman spacetimes based on the removing of the source, analogous to what Eddington, Finkelstein, and Kruskal have done to the Schwarzschild metric. We will briefly discuss this maximal analytical extension in section 2.1, since it constitutes the basis of our subsequent calculations. For reasons not to be elaborated here, it is totally irrelevant to the subject of *physical* black holes.[4]

The study of the causal structures of spacetimes has always been one of the main foci of relativity groups all over the world. Hawking and Penrose [26] presented a new theorem which largely incorporated and generalized previously known results regarding the existence of singularities under the exclusion of the possibility of closed timelike curves. This assumption was supported by Tipler [27], who argued that it is not possible to manufacture a region containing closed timelike curves without the formation of naked singularities, provided normal matter is used in the construction attempt. On the other hand, Carter [25] proved that in all except the spherically symmetric cases there is nontrivial causality violation, *viz.* closed timelike curves. Putting it the other way, this provides another well–founded justification for assuming the event horizon to be smooth and perturbations to die out with time.

In the dawn of systematic research of potential causality violating closed timelike curves, physicists largely studied curves for positive radial coordinates in spacetimes of naked singularities. As far as we know, Brandon Carter [25] was the first to clearly recognize that domains of closed timelike curves *generally* exist in these spacetimes. In the late seventies, de Felice and Calvani widely investigated in a series of papers in *General Relativity and Gravitation* [28, 29, 30] causality violations in Kerr and Kerr–Newman metrics. However, they concentrated on the case $M < a$. In this essay, the argument is strictly confined to black holes with $M > a$. We have thus established the link to our cause.

1.2 Objectives and Methods

As we have seen in the preceding section, it is today commonly agreed among relativists that in general, solutions of the Einstein–Maxwell equations or their respective analytical extensions allow for violations of causality. Such violations may occur either only in restricted areas of the spacetime or unrestrictedly, *i.e.* globally. With "restricted", we refer to closed timelike φ–curves existing in a domain in the analytical extension of the Kerr–Newman solution into negative radii, whereas with "global" (or "unrestricted") causality violations we term

---

[4]Cf. [1], p. 882 f.

closed timelike curves which start in the positive asymptotic region, intersect the horizons, pass by the singularity and run into negative infinity, where we change the frame from the advanced to the retarded Eddington–Finkelstein type of coordinates[5] and return then to another patch of positive infinity. If we identify the latter patch including positive infinity with the one where we started from, we allow global closed timelike curves. But this would imply that the spacetime becomes acausal in the sense that the intersection of the causal past with the causal future of any point on the manifold would include infinitely many points. However, we shall focus on the local case in what follows.

Even when we talk of "spacetimes", it is important to point out that "space" and "time" are not treated on a perfectly equal footing. In every point of any given metrical manifold obeying the laws of general relativity, we have a local inertial frame provided by the Minkowski metric. It is in this simple metric, however, that we recognize the inequality between "time" and "space" the clearest. The differing sign between the diagonal element referring to the time coordinate and those referring to the spatial coordinates draws a line of distinction. This line allows the foundation of a causal structure. The distinction enables the astrophysicist to construct light cones locally and thus to differentiate between timelike and spacelike motion. Without this basic feature, we would not be in the position to define a chronological orientability of spacetimes and eventually to introduce a notion of causality, as we shall do in section 2.1.

Our objective will thus be the investigation of the domain of causality violations dependent upon the parameters of the spacetime and the assessment of curves spiralling into the past within these domains. We shall always keep the practicability of such time travel in the back of our mind when discussing our results.

The methodological approach should be governed by common sense regarding what serves our ends. In the preliminary considerations, it will be natural to restrict ourselves to analytical calculations. Generally however, the method chosen in later chapters will be less formal. We will usually begin with quantitative analyses accomplished with the aid of computer algebraic programmes. Interpreting the results thus obtained, we will try to recognize prevailing trends in the data output. With a clear notion of what to expect, we nevertheless hope to achieve some analytical results of the quantities considered. The calculations performed will be quite straightforward. The obstacles will be found in the interpretations rather than in the results themselves, for some will tend to be lengthy and will therefore not be easily treated. Wherever this will happen, we will try to gain some qualitative information on the quantity and its dependence on the spacetime or trajectory parameters. In cases where even this strategy brakes down, we will content ourselves with purely numerical analysis.

1.3   Outline of the Thesis

After a short account on the structure of the Kerr–Newman spacetime and the notion of causality in general relativity, we shall discuss the tetrad and

---

[5]See appendix B.

Newman–Penrose formalisms in chapter 2. The main reason for starting from the null tetrad of Newman and Penrose is found in the boost invariance of the curvature in the plane of the degenerate principal null directions as well as its rotational invariance with respect to the symmetry of the spacetime. We thus take advantage of the algebraically special directions manifest in the Newman–Penrose formalism to construct a tetrad frame in advanced Eddington–Finkelstein type coordinates. The simplicity of the Riemann curvature tensor with respect to this tetrad frame reveals that feature. The components of the Riemann curvature tensor are later used to derive the tidal forces encountered on the journey to the domains of potential causality violation and on the time travel itself.

In chapter 3 we shall discuss the itinerary of the journey along timelike geodesics, starting from asymptotic flatness at positive infinity, along the axis of symmetry of the singular ring into the realm of causality violation inside the negative patch of the external Kerr–Newman spacetime. Even though the spacecraft follows geodesics, energy will be needed in order to complete this part of the journey. This is necessitated by hills in the effective potential, overlooking the potential in the asymptotic region. We will calculate this energy and the elapsed proper time as well as the tidal forces on the axis to which the crew will be subjected. We will argue that the duration of such a trip does not generally pose a problem for its completion. Also, the tidal accelerations do not exceed a relatively harmless threshold, provided that the mass of the singularity is sufficiently large. On the other hand, as we will learn, that energy requirements outmatch the resources generally available by far, even for the most favourable combinations of parameters. Closing the chapter, we will cite the familiar argument that the charge of a black hole is not very likely to be large enough to cause a notable change in our considerations since the electromagnetic force is much stronger than the gravitational one and leads to its own neutralization in the course of time.

In chapter 4 on the domains Γ of closed timelike φ–curves—*i.e.* curves where all coordinates except φ are held constant—following thereafter, we have computed their extension in (r, ϑ)–space. Their shape will depend on the mass M, the angular momentum a, and the charge Q of the singularity. These domains are rotationally symmetrical on $(t = \text{const})$–surfaces with respect to the φ–coordinate and form a distorted torus. They are confined to the negative leg of r, unless the singular ring carries electromagnetic charge. The larger the latter is, the more the domain stretches into positive r's. However, as we will have learnt in chapter 3, the charge is restricted to very low values and the penetration of Γ into zones of positive radial coordinate is therefore limited. The aim of this chapter is to provide calculations and graphs which should give the reader an impression of the extension of the realm of causality violation.

Chapter 5 will present the analysis of curves spiralling within Γ. These spirals should not only be timelike and future pointing, but they are supposed to lead into the past. The idea is that a spacecraft following such a curve would travel backwards in time with respect to an asymptotic observer, but that its crew members would nevertheless biologically age. We shall give evidence to prove that these spirals occur in the same domain as the closed φ–curves.

The quantities introduced in order to account for the appeal of the spirals

to a conceived time traveller include the gain in time, the elapsed proper time
during the enterprise, the tidal forces on the time travel, and the energy con-
sumption necessary to keep on track. The latter will only be investigated in
the last chapter. The gain in time which we are striving for is, of course, the
main objective for the whole journey. This quantity, however, is rather useless
unless we relate it to the proper time elapsed during the respective time gain.
The time gain per revolution (or, synonymously, per period) divided by the
duration of the same revolution will therefore provide a—unitless—quantity of
relevance for our analysis.

    The principal purpose of the last chapter is to calculate the energy consumed
when following any elected spiralling curve. To this end, we shall first calculate
the acceleration to be withstood in order to follow specific spirals. Then, we
aim at finding the formula for the relative mass exhaust of fuel per duration
of one complete revolution. We shall analyse the result afterwards, taking the
contemporary technological level of propulsion systems into account. Unfortu-
nately, the conclusion will be rather unwelcome: the energy problem will render
the time travel impossible despite all conceivable efforts.

Chapter 2

Preliminaries

This chapter is intended to offer a brief account on the relevant notions of what follows hereafter. Above all, it has to provide an idea of the solution in question of the Einstein equations, namely the Kerr–Newman spacetime. It is further intended to give a coherent introduction to the tetrad and Newman–Penrose formalisms of [31]. Finally, we present the explicit calculation of several important quantities in the spacetime mentioned. In general, the formulae will be expressed in a system of "natural" units, where $c = G = \mu_0 = 1$.[1] Wherever the issue is numerical, we will make use of the SI–units. However, this change of units will always be indicated.

2.1 Preparing the Stage

For the gravitational collapse of a realistic star with only small asymmetries and a small net charge, perturbative calculations predict that the spacetime will correspond to a solution of the electro–vacuum state. Such a solution has to satisfy the system of equations

$$
\begin{aligned}
G_{\mu\nu} &= 8\pi T_{\mu\nu}, \\
\nabla_\rho F^{\mu\rho} &= 0, \\
F_{\mu\nu} &= \partial_\mu A_\nu - \partial_\nu A_\mu, \\
T_{\mu\nu} &= -\frac{1}{4\pi}\left(F_{\mu\rho}F_\nu{}^\rho - \frac{1}{4}g_{\mu\nu}F_{\rho\sigma}F^{\rho\sigma}\right),
\end{aligned} \tag{2.1}
$$

where $G_{\mu\nu}$ is the Einstein tensor, canonically defined through the Ricci tensor $R_{\mu\nu} \doteq R^\rho{}_{\mu\rho\nu}$ and the curvature scalar $R \doteq g^{\mu\nu}R_{\mu\nu}$ by

$$
G_{\mu\nu} \doteq R_{\mu\nu} - \frac{1}{2}Rg_{\mu\nu}.
$$

Further, we have in (2.1) the energy-momentum or stress-energy tensor $T_{\mu\nu}$, the electromagnetic field tensor $F_{\mu\nu}$, the corresponding four–potential A_μ, and the metric $g_{\mu\nu}$ which is determined by the mass distribution in the relevant

---

[1]cf. Appendix A

spacetime. Multiplying the Einstein equations $G_{\mu\nu} = 8\pi T_{\mu\nu}$ by $g^{\mu\nu}$ yields

$$R = -8\pi g^{\mu\nu} T_{\mu\nu}. \tag{2.2}$$

It is clear that an energy–momentum tensor as determined above is traceless,

$$\begin{aligned} g^{\mu\nu} T_{\mu\nu} &= -\frac{1}{4\pi}\left(g^{\mu\nu} F_{\mu\rho} F_\nu{}^\rho - \frac{1}{4} g^{\mu\nu} g_{\mu\nu} F_{\rho\sigma} F^{\rho\sigma}\right) \\ &= -\frac{1}{4\pi} F_{\rho\sigma} F^{\rho\sigma}\left(1 - \frac{1}{4} g^{\mu\nu} g_{\mu\nu}\right) \\ &= 0, \end{aligned} \tag{2.3}$$

since we have always $g^{\mu\nu} g_{\mu\nu} = 4$ in four dimensions. Hence, in every solution of the system (2.1), the curvature scalar R vanishes.

The starting point of our research will be the Kerr–Newman solution of the Einstein–Maxwell equations (2.1). Every solution describing completely collapsing stars supposedly converges eventually to the Kerr–Newman family. Though this is not yet proved rigorously, many theorems suggest that a stationary black hole is determined by the hole's mass M, angular momentum a, and charge Q. Thus, a singularity has no other independent characteristics as *e.g.* the baryon number. In collapse, the baryon number is therefore probably not conserved. Poetically afflicted relativists have named this property "black holes have no hair".[2]

Unless specified otherwise, we will use the generalized Boyer–Lindquist coordinates:

$$ds^2 = \frac{\Delta}{\Sigma}(dt - a\sin^2\vartheta d\varphi)^2 - \frac{\sin^2\vartheta}{\Sigma}[adt - (r^2 + a^2)d\varphi]^2 - \frac{\Sigma}{\Delta}dr^2 - \Sigma d\vartheta^2 \tag{2.4}$$

where

$$\begin{aligned} \Delta &\doteq r^2 - 2Mr + a^2 + Q^2, \\ \Sigma &\doteq r^2 + a^2\cos^2\vartheta. \end{aligned} \tag{2.5}$$

The associated electromagnetic potential is

$$A_\mu dx^\mu = \frac{Qr}{\Sigma}(dt - a\sin^2\vartheta d\varphi). \tag{2.6}$$

This solution describes the stable spacetime of a generic black hole with mass M, angular momentum per unit mass a, and electric charge Q where $M^2 > a^2 + Q^2$. We exclude a possible magnetic charge explicitly from our considerations. As the components of this metric do not depend upon the azimuthal angle φ nor on the time coordinate t we have a stationary spacetime which is axisymmetrical.

In accordance to its causal structure, we split this universe into three patches. For this purpose we briefly outline the construction of the delimiting hypersurfaces. The relevant variable for the separation is r. We therefore look at

---

[2]For a more thorough account of this aspect, see [1], p. 876, [32], p. 110ff, and [33], p. 292ff.

hypersurfaces of constant r. On these, the length of curves is given by

$$\gamma_{kl} \quad \dot{=} \quad g_{\mu\nu} \frac{\partial x^\mu}{\partial y^k} \frac{\partial x^\nu}{\partial y^l}, \tag{2.7}$$

where we define γ_{kl} as the metric induced on the hypersurface by $g_{\mu\nu}$, *i.e.* the components of γ_{kl} are the scalar products of the basis vectors $\frac{\partial x^\mu}{\partial y^k}$. On hypersurfaces with $r = const$, we find for the induced metric

$$\gamma_{kl} \quad = \quad \frac{1}{\Sigma} \begin{pmatrix} \Delta - a^2 \sin^2 \vartheta & a \sin^2 \vartheta (r^2 + a^2 - \Delta) & 0 \\ a \sin^2 \vartheta (r^2 + a^2 - \Delta) & \Delta a^2 \sin^4 \vartheta - \sin^2 \vartheta (r^2 + a^2)^2 & 0 \\ 0 & 0 & -\Sigma^2 \end{pmatrix}.$$

The signature of the hypersurfaces is unequivocally determined by the determinant D of the induced metric: the hypersurface is timelike iff[3] $D > 0$, spacelike iff $D < 0$ and null iff $D = 0$. A simple computation yields $D = \Delta \Sigma \sin^2 \vartheta$. As Σ and ϑ generally do not vanish, we find the following roots for $\Delta = 0$:

$$r_\pm \quad = \quad M \pm \sqrt{M^2 - a^2 - Q^2}. \tag{2.8}$$

These hypersurfaces define the boundaries between the above mentioned regions: the external Kerr–Newman spacetime with small or negative radial component (EKN−) where $-\infty < r < r_-$, the internal Kerr–Newman spacetime (IKN) where $r_- < r < r_+$, and the external Kerr–Newman spacetime with positive radial component (EKN+) where $r_+ < r < +\infty$. The hypersurfaces $r = const$ are timelike in the external and spacelike in the internal case respectively. The two null surfaces at $r = r_\pm$ are horizons to the asymptotic observers in the external regions.

Due to the fact that the maximal analytical extension of the Kerr–Newman spacetime does not allow closed global timelike curves, it is possible to find continuous timelike vector fields and thus to define an *orientation of time*. Locally time's arrow is determined by the properties of the vacuum state in Quantum Field Theory, *i.e.* by β–decay and by K–meson decay. Mathematically, we choose a local inertial frame in an arbitrary point $p \in \mathcal{M}$, where $\mathcal{M}$ is a Riemannian manifold. In the tangential space $\mathcal{T}_p \mathcal{M}$ we have two light cones of a kind such that any timelike vector in p lives either in the future or in the past light cone. Taking the above mentioned physical properties of temporally asymmetrical decays into account, we select an appropriate vector field T^μ as pointing towards the future and thus define the corresponding light cone as directed accordingly. If the scalar product of two nonvanishing, non–spacelike vectors in p is positive, then they both lie in the same light cone, and if it turns out to be negative, they are found in different light cones. We call a curve $x^\mu(\lambda)$ in a time–oriented spacetime $(\mathcal{M}, g, T)$ an *oriented causal curve* (OCC) iff (a) $\dot{x}^\mu_\pm(\lambda)$ is well defined everywhere ("$\pm$" representing derivatives operating from the left or the right side respectively), and (b)

$$g_{\mu\nu} T^\mu \dot{x}^\nu_\pm \quad \geq \quad 0,$$
$$g_{\mu\nu} \dot{x}^\mu_\pm \dot{x}^\nu_\pm \quad \geq \quad 0.$$

---

[3]We use "iff" as a shortcut for "if and only if".

A hypersurface is said to be *orientable* iff the normal vector can be chosen to form a continuous vector field on the whole of the concerned hypersurface. If a spacetime $\mathcal{M}$ with metric g can be oriented in time, then all non–timelike hypersurfaces in $\mathcal{M}$ are orientable.[4] The continuous field of the normal vector can therefore always be directed to the future light cone. If $n^\mu(x)$ is such a normal vector field, then $g_{\mu\nu}\dot{x}_\pm^\mu n^\nu \geq 0 \ \forall p \in (C \cap S)$, where C is an OCC and S a non-timelike hypersurface in a time–oriented spacetime $(\mathcal{M}, g, T)$. Equality will only hold when both vectors are linearly dependent null vectors. But in this case, one would find that C is tangential to S and does not intersect it. Thus we come to understand that S can be crossed by C in only one way, namely from the past to the future side. The future side of the mentioned horizons at $r = r_+$ and $r = r_-$ can hence be turned towards or away from a defined observer depending on whether he or she lives in EKN+ or EKN− and on the coordinate system.

In order to study the structural properties of the above constructed space-time more accurately, we introduce at this place coordinates of an Eddington–Finkelstein type.[5] These so-called advanced and retarded Kerr–Newman co-ordinates will show us a way to find the maximal analytical extension.[6] Our motivation for these transformations is to avoid the coordinate singularities of the metric at $r = r_\pm$. For an asymptotic observer in EKN+, we recognize in the advanced extension the two null hypersurfaces as event horizons, whereas in the retarded coordinates they are "horizons of influence", which our observer cannot penetrate under any circumstances, not even if he or she is a photon. Of course, causal questions should always be coordinate–independent. In the present case, however, we are dealing with different patches and therefore with different horizons, to be precise.

A last word on the singularities. As can be seen from (B.8) and (2.5), we find a ring singularity at $(r = 0, \vartheta = \frac{\pi}{2})$. Viewed from our home planet in the asymptotic region of EKN+, this singular ring is screened by the two intermediate horizons at $r = r_\pm$. But viewed from the asymptotic region in EKN−, the ring is "naked". That the asymptotic region of our universe ($r \rightarrow \pm\infty$) is flat can easily be seen from the expansion of (2.4) in powers of r^{-1}:

$$
\begin{aligned}
g_{tt} &= 1 - 2M\frac{1}{r} + Q^2\frac{1}{r^2} + \mathcal{O}\left(r^{-3}\right), \\
g_{t\varphi} &= 4Ma\sin^2\vartheta\frac{1}{r} - 2Qa\sin^2\vartheta\frac{1}{r^2} + \mathcal{O}\left(r^{-3}\right), \\
g_{\varphi\varphi} &= -r^2\sin^2\vartheta\left(1 + a^2\frac{1}{r^2} + \mathcal{O}\left(r^{-3}\right)\right), \\
g_{rr} &= -\left(1 + 2M\frac{1}{r} + \left(4M - a^2\sin^2\vartheta - Q^2\right)\frac{1}{r^2} + \mathcal{O}\left(r^{-3}\right)\right), \\
g_{\vartheta\vartheta} &= -r^2\left(1 + a^2\cos^2\vartheta\frac{1}{r^2} + \mathcal{O}\left(r^{-3}\right)\right);
\end{aligned}
$$

---

[4]The proof for this theorem shall here be omitted. It can be found in [34], p. 208.

[5]For an explicit account of these coordinates see Appendix B.

[6]For more details, see [23], [24], [32], p. 128 ff, and [34], p. 217f.

expanding the potential (2.6) accordingly yields:

$$A_\mu = \left(Q\frac{1}{r}, -Qa\sin^2\vartheta\frac{1}{r}, 0, 0 \right) + \mathcal{O}\left(r^{-2} \right).$$

Information can be gained about the multipoles of the source from the coefficients of the expansion of the metric and its accompanying electromagnetic potential. For instance, the coefficient of r^{-1} in the expansion of A_t equals the electromagnetic charge of the source. Similarly, we recognize the coefficient of $-2r^{-1}$ in g_{tt} as the mass of the source and that of $4r^{-1}\sin^2\vartheta$ in $g_{t\varphi}$ as its total angular momentum.

The asymptotic observer in EKN+ thus perceives the source as an object of mass M, angular momentum $J = Ma$, and charge Q. Supposing an observer who lives at a large negative radial component, we state bewilderedly that we see not only an object with an angular momentum $J = -Ma$ and a charge $-Q$—which is still fine—, but also with negative mass $-M$! As it is a canonical procedure in (at least classical) physics to consider mass as a parameter running over positive, real numbers, we perform a sign–changing transformation $r \mapsto -r$ in our universe. But thus transforming, we will not avoid any of the problems since the horizons at $r = r_\pm$ would only flip to the other side of the ring and the trouble with the negative mass would rise anew, this time with respect to our home planet in EKN+. Luckily, the fact that observers in EKN+ and EKN− realize different signs when measuring the parameters of the ring singularity does not violate the condition $M^2 > a^2 + Q^2$ for generic black holes. This is to be understood in the sense that if an astrophysicist in EKN+ discerns the source as a generic black hole satisfying the latter condition, his colleague in EKN− would do likewise.

2.2   Tetrad Formalism

In this section we will obtain some results which will later prove useful for our purposes. Since it has appeared advantageous in many contexts to overcome the former standard procedure of solving problems in general relativity by considering a local coordinate basis adapted to the problem at hand, we will introduce a so–called "tetrad basis".[7] This tetrad formalism consists of the construction of four linearly independent vector fields and of the projection of the relevant quantities onto the tetrad basis. The choice of the tetrad basis depends on the underlying structure of the spacetime in question and is somewhat a part of the problem. Thereafter, one only has to consider the equations satisfied by the projected quantities.

We first provide a brief introduction to the basic definitions necessary for the understanding of the following. This account follows in its main lines the book of Chandrasekhar [33]. We define at each point of the spacetime in question a

---

[7]Tetrad formalisms have proved advantageous in many respects. For instance, according to Estabrook and Wahlquist, "The dyadic formalism [...] has the advantages of physical *interpretability,* mathematical *completeness,* and wide *applicability.*" [35] The dyadic formalism mentioned is derived from a tetrad formalism by basing it on a preferred congruence.

tetrad basis of four linearly independent, contravariant vectors

$$e_a{}^\mu \qquad (a = 1, 2, 3, 4), \tag{2.9}$$

where Latin letters label tetrad indices and Greek letters tensor indices. Associated with the contravariant vectors we have the covariant vectors

$$e_{a\mu} = g_{\mu\nu} e_a{}^\nu, \tag{2.10}$$

where $g_{\mu\nu}$ denotes the metric tensor. In addition, we also define the inverse $e^b{}_\mu$ of the matrix $e_a{}^\mu$ (where the tetrad index is labeling the rows and the tensor index the columns) in such a way that

$$e_a{}^\mu e^b{}_\mu = \delta^b_a \quad \text{and} \quad e_a{}^\mu e^a{}_\nu = \delta^\mu_\nu. \tag{2.11}$$

The Einsteinian summation convention also holds for the tetrad indices here and elsewhere. Further, we assume that

$$g_{\mu\nu} e_a{}^\mu e_b{}^\nu = \eta_{ab}, \tag{2.12}$$

where η_{ab} is the Minkowski metric. This is the case because we choose the basis vectors $e_a{}^\mu$ to be orthonormal.

Given an arbitrary tensor field of a general rank, we obtain its tetrad components by projecting it onto the tetrad frame. Thus,

$$H^{a\cdots m}_{n\cdots z} = e^a{}_\alpha \cdots e^m{}_\mu \, e_n{}^\nu \cdots e_z{}^\omega \, H^{\alpha\cdots\mu}_{\nu\cdots\omega}, \tag{2.13}$$

$$\text{and} \quad H^{\alpha\cdots\mu}_{\nu\cdots\omega} = e_a{}^\alpha \cdots e_m{}^\mu \, e^n{}_\nu \cdots e^z{}_\omega \, H^{a\cdots m}_{n\cdots z}. \tag{2.14}$$

In particular, we find for the Riemann tensor

$$R_{abcd} = e_a{}^\mu e_b{}^\nu e_c{}^\rho e_d{}^\sigma R_{\mu\nu\rho\sigma},$$

$$\text{and} \quad R_{\mu\nu\rho\sigma} = e^a{}_\mu e^b{}_\nu e^c{}_\rho e^d{}_\sigma R_{abcd}.$$

The reader should not feel uncomfortable with the simultaneous appearance of indices of different sorts, since there is no ambiguity providing that the preceding operational rules are strictly followed.

2.3   A Tetrad for the Kerr–Newman Spacetime

Starting off with the Newman–Penrose choice of basis (null) vectors, we construct an orthonormal tetrad. The novelty of this formalism is its efficacy for showing the inherent symmetries of the concerned spacetime. The choice made by Penrose and Newman was a tetrad of null vectors $l, n, m,$ and $\bar{m}$, where l and n are real and m and $\bar{m}$ are the complex conjugates of one another. They are required to satisfy the orthogonality conditions,

$$l \cdot m = l \cdot \bar{m} = n \cdot m = n \cdot \bar{m} = 0.$$

At the same time they are to be null:

$$l \cdot l = n \cdot n = m \cdot m = \bar{m} \cdot \bar{m} = 0.$$

In addition, we impose the normalization requirements,

$$l \cdot n = 1 \quad \text{and} \quad m \cdot \bar{m} = -1.$$

Then, we have found a null basis of contravariant vector fields,

$$e_1 = l, \quad e_2 = n, \quad e_3 = m, \quad \text{and} \quad e_4 = \bar{m}.$$

The corresponding covariant basis reads

$$e^1 = e_2 = n, \quad e^2 = e_1 = l, \quad e^3 = -e_4 = -\bar{m}, \quad \text{and} \quad e^4 = -e_3 = -m.$$

If the null vectors l and n are chosen to be in the principal null directions[8], then the components of the Riemann tensor simplify considerably. In particular, they are independent of a boost in the (l, n)–hypersurface in our case. The null vectors must therefore be chosen according to the spacetime at hand. In the Boyer–Lindquist coordinates $x^\mu = (t, r, \vartheta, \varphi)$ of the Kerr–Newman spacetime such a null basis is given by [33], p. 299

$$l^\mu = \frac{1}{\Delta} \left(r^2 + a^2, +\Delta, 0, a \right),$$

$$n^\mu = \frac{1}{2\Sigma} \left(r^2 + a^2, -\Delta, 0, a \right),$$

$$m^\mu = \frac{1}{\bar{\rho}\sqrt{2}} \left(ia \sin\vartheta, 0, 1, i \csc\vartheta \right),$$

where

$$\bar{\rho} = r + ia\cos\vartheta \quad \text{and} \quad \bar{\rho}^* = r - ia\cos\vartheta.$$

We change the order of the coordinates to $x^\mu = (t, \varphi, r, \vartheta)$. Furthermore, we separate the real and the imaginary part of m. Altogether, this yields

$$l^\mu = \frac{1}{\Delta} \left(r^2 + a^2, a, +\Delta, 0 \right),$$

$$n^\mu = \frac{1}{2\Sigma} \left(r^2 + a^2, a, -\Delta, 0 \right),$$

$$m^\mu = \frac{1}{\sqrt{2}\Sigma} \left(a^2 \sin\vartheta \cos\vartheta + ira\sin\vartheta, \right.$$

$$\left. a \cot\vartheta + ir \csc\vartheta, 0, r - ia\cos\vartheta \right).$$

We construct the desired orthonormal tetrad out of the null basis. At the same time we boost the tetrad in the (l, n)–plane by a boost parameter α. This action will help to avoid any troubles that will arise at the horizons of the spacetime. Applying the combination rule

$$e_1^{\ \mu} = \pm \frac{1}{\sqrt{2}} \left(e^\alpha l^\mu + e^{-\alpha} n^\mu \right),$$

$$e_2^{\ \mu} = \pm \frac{1}{\sqrt{2}} \left(e^\alpha l^\mu - e^{-\alpha} n^\mu \right),$$

$$e_3^{\ \mu} = \frac{1}{\sqrt{2}} \left(m^\mu + \bar{m}^\mu \right),$$

$$e_4^{\ \mu} = \frac{-i}{\sqrt{2}} \left(m^\mu - \bar{m}^\mu \right), \tag{2.15}$$

---

[8]Every Weyl tensor (see equation (2.21)) defines four principal null directions.

we obtain the comoving tetrad frame

$$
\begin{aligned}
e_1{}^\mu &= \pm\frac{1}{\sqrt{2}}\left((r^2+a^2)\left(\frac{e^\alpha}{\Delta}+\frac{e^{-\alpha}}{2\Sigma}\right), a\left(\frac{e^\alpha}{\Delta}+\frac{e^{-\alpha}}{2\Sigma}\right), \Delta\left(\frac{e^\alpha}{\Delta}-\frac{e^{-\alpha}}{2\Sigma}\right), 0\right),\\
e_2{}^\mu &= \pm\frac{1}{\sqrt{2}}\left((r^2+a^2)\left(\frac{e^\alpha}{\Delta}-\frac{e^{-\alpha}}{2\Sigma}\right), a\left(\frac{e^\alpha}{\Delta}-\frac{e^{-\alpha}}{2\Sigma}\right), \Delta\left(\frac{e^\alpha}{\Delta}+\frac{e^{-\alpha}}{2\Sigma}\right), 0\right),\\
e_3{}^\mu &= \frac{1}{\Sigma}\left(a^2\sin\vartheta\cos\vartheta, a\cot\vartheta, 0, r\right),\\
e_4{}^\mu &= \frac{1}{\Sigma}\left(ra\sin\vartheta, r\csc\vartheta, 0, -a\cos\vartheta\right).
\end{aligned}
\tag{2.16}
$$

This is the comoving frame of four orthogonal vector fields which will provide a home for many of our future calculations. The sign of the two first vector fields of the orthonormal frame corresponds to the part of the spacetime concerned. The "+"–sign will be used in the positive and negative *external* Kerr–Newman spacetime and the "−"–sign in the *internal* respectively. The reason for this will later emerge in a clearer way.

In order to study its regularity, we transform the tetrad into advanced Kerr–Newman coordinates[9] (AKN) $x^\mu = (v, \eta, r, \vartheta)$,

$$
\begin{aligned}
e_1{}^\mu &= \pm\frac{1}{\sqrt{2}}\left(\frac{2(r^2+a^2)}{\Delta}e^\alpha, \frac{2a}{\Delta}e^\alpha, \Delta\left(\frac{e^\alpha}{\Delta}-\frac{e^{-\alpha}}{2\Sigma}\right), 0\right),\\
e_2{}^\mu &= \pm\frac{1}{\sqrt{2}}\left(\frac{2(r^2+a^2)}{\Delta}e^\alpha, \frac{2a}{\Delta}e^\alpha, \Delta\left(\frac{e^\alpha}{\Delta}+\frac{e^{-\alpha}}{2\Sigma}\right), 0\right),\\
e_3{}^\mu &= \frac{1}{\Sigma}\left(a^2\sin\vartheta\cos\vartheta, a\cot\vartheta, 0, r\right),\\
e_4{}^\mu &= \frac{1}{\Sigma}\left(ra\sin\vartheta, r\csc\vartheta, 0, -a\cos\vartheta\right).
\end{aligned}
$$

The reader can easily verify in a straightforward calculation that the orthonormality condition

$$
g_{\mu\nu}e_a{}^\mu e_b{}^\nu = \eta_{ab}
\tag{2.17}
$$

holds. Here $g_{\mu\nu}$ is the metric of the advanced Kerr–Newman solution. We need to make sure that the tetrad is regular at the axis of symmetry where $\vartheta = 0, \pi$. In order to investigate the behavior of the tetrad near $\vartheta = 0$ we introduce "regular" coordinates,

$$
\begin{aligned}
x &= \sin\vartheta\cos\eta,\\
y &= \sin\vartheta\sin\eta.
\end{aligned}
$$

where η is the "angular" coordinate. This means that the advanced Kerr–

---

[9]Appendix B

Newman coordinates transform in the following manner:

$$
\begin{aligned}
v &\mapsto v, \\
\eta &\mapsto \arctan\left(\frac{y}{x}\right), \\
r &\mapsto r, \\
\vartheta &\mapsto \arcsin\left(\sqrt{x^2 + y^2}\right).
\end{aligned}
$$

For the Jacobian, we have

$$
\begin{aligned}
\frac{\partial v}{\partial v} &= 1, & \frac{\partial r}{\partial r} &= 1, \\
\frac{\partial x}{\partial \eta} &= -y, & \frac{\partial x}{\partial \vartheta} &= \sqrt{\frac{1 - (x^2 + y^2)}{x^2 + y^2}}\, x, \\
\frac{\partial y}{\partial \eta} &= x, & \frac{\partial y}{\partial \vartheta} &= \sqrt{\frac{1 - (x^2 + y^2)}{x^2 + y^2}}\, y.
\end{aligned}
$$

We finally obtain the tetrad in the "regular" advanced Kerr–Newman frame $x^\mu = (v, r, x, y)$,

$$
\begin{aligned}
e_1^\mu &= \pm\frac{1}{\sqrt{2}}\left(\frac{2(r^2 + a^2)}{\Delta}e^\alpha, \Delta\left(\frac{e^\alpha}{\Delta} - \frac{e^{-\alpha}}{2\Sigma}\right), -\frac{2a}{\Delta}e^\alpha y, \frac{2a}{\Delta}e^\alpha x\right), \\
e_2^\mu &= \pm\frac{1}{\sqrt{2}}\left(\frac{2(r^2 + a^2)}{\Delta}e^\alpha, \Delta\left(\frac{e^\alpha}{\Delta} + \frac{e^{-\alpha}}{2\Sigma}\right), -\frac{2a}{\Delta}e^\alpha y, \frac{2a}{\Delta}e^\alpha x\right), \\
e_3^\mu &= \frac{1}{\Sigma}\sqrt{\frac{1 - (x^2 + y^2)}{x^2 + y^2}}\left(a^2\left(x^2 + y^2\right), 0, -ay + rx, ax + ry\right), \\
e_4^\mu &= \frac{1}{\Sigma\sqrt{x^2 + y^2}}\bigg(ra(x^2 + y^2), 0, -ry - ax\left(1 - (x^2 + y^2)\right), \\
&\qquad rx - ay\left(1 - (x^2 + y^2)\right)\bigg).
\end{aligned}
$$

The direction of our approaching the axis of symmetry does not influence the "induced" tetrad on the axis substantially. Only the two latter components of the third and the fourth leg are affected by the φ–angle we choose to approximate the $(\vartheta = 0)$–hyperspace. Independently from φ though, both will eventually vanish at $\vartheta = 0$. Without loss of generality we set $\varphi = 0$, *i.e.* we first move to the x–axis and from there to the origin. As a result we obtain

$$
\begin{aligned}
\lim_{\vartheta \to 0} e_1^\mu &= \pm\frac{1}{\sqrt{2}}\left(\frac{2(r^2 + a^2)}{\Delta}e^\alpha, \Delta\left(\frac{e^\alpha}{\Delta} - \frac{e^{-\alpha}}{2(r^2 + a^2)}\right), 0, 0\right), \\
\lim_{\vartheta \to 0} e_2^\mu &= \mp\frac{1}{\sqrt{2}}\left(\frac{2(r^2 + a^2)}{\Delta}e^\alpha, \Delta\left(\frac{e^\alpha}{\Delta} + \frac{e^{-\alpha}}{2(r^2 + a^2)}\right), 0, 0\right), \\
\lim_{\vartheta \to 0} e_3^\mu &= \frac{1}{r^2 + a^2}\left(0, 0, r, a\right), \\
\lim_{\vartheta \to 0} e_4^\mu &= \frac{1}{r^2 + a^2}\left(0, 0, -a, r\right),
\end{aligned}
$$

where $x^\mu = (v, r, x, y)$. We consider the tetrad as a matrix $e_a{}^\mu$ and calculate its determinant in order to check its regularity. We have

$$\det e_a{}^\mu = \frac{1}{r^2 + a^2}.$$

Since a is required to be non–zero, $\det e_a{}^\mu \neq 0$ ($\forall r \in \mathbf{R}$) and the matrix is therefore regular on the axis. But is it still an orthonormal tetrad? This can easily be seen by checking whether relation (2.17) is satisfied. The reader will hardly be surprised if we state that this is the case.

We have to apply a Lorentz transformation in order to control the regularity of the tetrad at the horizons, due to the way the tetrad is formulated in (2.17), the first two legs diverge at $\Delta = 0$. Since we have previously shown the regularity on the axis and the orthonormality for all boost parameters α, our choice of α will not be restricted. If we then fix the boost as

$$\alpha = \ln \frac{|\Delta|}{\mathrm{m}^2},$$

we prevent our tetrad from diverging. The absolute value of the argument is used in order to give sense to the equation in IKN, where Δ is negative. The denominator "m^2" designates the unit of area for a two–dimensional surface and originates from our desire to calculate in correct units. The endangered two vectors of the orthonormal tetrad thus transform to

$$
\begin{aligned}
e_1{}^\mu &= \frac{1}{\sqrt{2}} \left(\frac{2(r^2 + a^2)}{\mathrm{m}^2}, \frac{2a}{\mathrm{m}^2}, \frac{\Delta}{\mathrm{m}^2} - \frac{\mathrm{m}^2}{2\Sigma}, 0 \right), \\
e_2{}^\mu &= \frac{1}{\sqrt{2}} \left(\frac{2(r^2 + a^2)}{\mathrm{m}^2}, \frac{2a}{\mathrm{m}^2}, \frac{\Delta}{\mathrm{m}^2} + \frac{\mathrm{m}^2}{2\Sigma}, 0 \right),
\end{aligned}
\tag{2.18}
$$

These vectors are clearly regular at $\Delta = 0$. For this reason, the whole tetrad is regular at the horizons near the ring singularity to be found towards the future of the asymptotic observer.

One word to the "$\pm$" prefix of two of the vectors. This sign is introduced in order to prevent the tetrad from flipping direction at the horizon. Thus, we provide a *continuous* tetrad of vector fields through the horizons. Clearly, the sign has disappeared in (2.18). In this way, we omit an ambiguity which would arise otherwise since the limit at the horizons would depend upon the side we are approaching the horizon from.

2.4   The Curvature of the Kerr–Newman Spacetime

In the present section we will apply the newly constructed formalism in order to calculate the curvature of the Kerr–Newman spacetime, the Ricci tensor and the curvature scalar. These quantities will be relevant subsequently, *e.g.* for the consideration of the tidal forces that would tear and squeeze the "timeonauts" on their mission to violate causality.

The Riemann tensor is canonically obtained from the metric by first calculating the Christoffel symbols,

$$\Gamma^\mu_{\alpha\beta} = \frac{1}{2} g^{\mu\kappa} \left(g_{\alpha\kappa,\beta} + g_{\beta\kappa,\alpha} - g_{\alpha\beta,\kappa} \right), \tag{2.19}$$

and then the Riemann by means of the Christoffel symbols,

$$R^\mu_{\nu\rho\sigma}(x) \quad = \quad \Gamma^\mu_{\nu\sigma,\rho}(x) - \Gamma^\mu_{\nu\rho,\sigma}(x) + \Gamma^\alpha_{\nu\sigma}\Gamma^\mu_{\alpha\rho} - \Gamma^\alpha_{\nu\rho}\Gamma^\mu_{\alpha\sigma}. \qquad (2.20)$$

With a non–trivial metric, we find ourselves quickly in the predicament of an annoying and rather lengthy calculation with nearly infinitely many opportunities to make mistakes. For this reason we suggest an alternative procedure which roughly follows Chandrasekhar in his [33]. We express the Riemann tensor as a function of the Weyl tensor C_{abcd}, the Ricci tensor R_{ab}, and the curvature scalar R. The Weyl tensor is something like the "trace–free" part of the Riemann tensor and thus has 10 independent components, and so has the Ricci tensor. Hence, the Weyl tensor can be represented by five complex scalars Ψ_a. We term these scalars *Weyl scalars* and borrow their values for the Kerr–Newman spacetime from Chandrasekhar. The Ricci tensor can be obtained by calculating the energy–momentum tensor from the electromagnetic potential of the Kerr–Newman solution.

2.4.1 The Weyl Tensor for the Kerr–Newman Solution

The Weyl tensor is defined by

$$\begin{aligned}
C_{abcd} \quad &= \quad R_{abcd} - \frac{1}{(n-2)}\left(g_{ac}R_{bd} + g_{bd}R_{ac} - g_{bc}R_{ad} - g_{ad}R_{bc}\right) \\
&\quad + \frac{1}{(n-1)(n-2)}\left(g_{ac}g_{bd} - g_{ad}g_{bc}\right)R,
\end{aligned} \qquad (2.21)$$

where n means the dimensionality of the concerned spacetime and will be set to $n = 4$. Obviously, the tensor constructed in this manner shows all the symmetries of the Riemann tensor, but

$$g^{bd}C_{abcd} = 0, \quad \text{whereas} \quad g^{bd}R_{abcd} = R_{ac}. \qquad (2.22)$$

If we consider the tensor in the comoving frame, the metric $g_{\mu\nu}$ will be represented by the Minkowski metric and (2.22) will mutate to

$$C_{a1b1} - C_{a2b2} - C_{a3b3} - C_{a4b4} = 0. \qquad (2.23)$$

If written out explicitly for $a = b$, these equations reduce the list of the independent and non–vanishing components of the Weyl tensor from the same 20 as the Riemann tensor to 16. If we set $a \neq b$, another reduction of six elements can be achieved and we are down to ten. A complete set of independent components could read as follows:

$$\begin{array}{ccccc}
C_{1212} & C_{1213} & C_{1214} & C_{1223} & C_{1224} \\
C_{1234} & C_{1313} & C_{1314} & C_{1323} & C_{1324}
\end{array}$$

In the Newman–Penrose formalism of a null tetrad $l, n, m,$ and $\bar{m}$, the metric in (2.22) becomes slightly different from the Minkowski case since the tetrad is not orthonormal. This difference will lead us to a different set of independent

components. Following Chandrasekhar [33], p. 43f, we obtain in terms of the Weyl scalars

$$
\begin{array}{llll}
C_{lnln} & = & -\Psi_2 - \Psi_2^* \qquad & C_{lnm\bar{m}} & = & \Psi_2 - \Psi_2^* \\
C_{lnlm} & = & -\Psi_1 & C_{lmlm} & = & -\Psi_0 \\
C_{lnl\bar{m}} & = & -\Psi_1^* & C_{l\bar{m}l\bar{m}} & = & -\Psi_0^* \\
C_{lnnm} & = & \Psi_3 & C_{nmnm} & = & -\Psi_4^* \\
C_{lnn\bar{m}} & = & \Psi_3^* & C_{n\bar{m}n\bar{m}} & = & -\Psi_4
\end{array}
$$

where C_{lnln} is one of the Weyl components in the null frame defined as $C_{lnln} = C_{\mu\nu\rho\sigma}\, l^\mu n^\nu l^\rho n^\sigma$. The remaining components are constructed analogously.

We now have to specify the Weyl scalars of the Kerr–Newman spacetime. All but one vanish [33], p. 579f

$$
\begin{aligned}
\Psi_0 & = & \Psi_1 = \Psi_3 = \Psi_4 = 0, \\
\Psi_2 & = & -\frac{M}{(\bar{\rho}^*)^3} + \frac{Q^2}{\bar{\rho}\,(\bar{\rho}^*)^3},
\end{aligned}
$$

where $\bar{\rho} = r + ia\cos\vartheta$ and $\bar{\rho}^* = r - ia\cos\vartheta$. In order to split the real and the imaginary part, we eliminate the division by complex numbers and get

$$
\Psi_2 = \frac{1}{\Sigma^3}\left(-M\bar{\rho}^3 + Q^2\bar{\rho}^2\right),
$$

from where we can easily derive that

$$
\begin{aligned}
\mathrm{Re}\,\Psi_2 & = & \frac{1}{\Sigma^3}\left[-Mr\left(r^2 - 3a^2\cos^2\vartheta\right) + Q^2\left(r^2 - a^2\cos^2\vartheta\right)\right], \\
\mathrm{Im}\,\Psi_2 & = & \frac{a\cos\vartheta}{\Sigma^3}\left[-M\left(3r^2 - a^2\cos^2\vartheta\right) + 2Q^2 r\right].
\end{aligned}
$$

The only nonvanishing components of the Weyl tensor in the frame of the null tetrad are therefore

$$
\begin{aligned}
C_{lnln} & = & \frac{2}{\Sigma^3}\left[Mr\left(r^2 - 3a^2\cos^2\vartheta\right) - 2Q^2\left(r^2 - a^2\cos^2\vartheta\right)\right], \\
C_{lnm\bar{m}} & = & \frac{2ia\cos\vartheta}{\Sigma^3}\left[-M\left(3r^2 - a^2\cos^2\vartheta\right) + 2Q^2 r\right].
\end{aligned}
\tag{2.24}
$$

Finally, we project the Weyl tensor unto the orthonormal tetrad frame of (2.16), i.e.

$$
C_{abcd} = C_{\alpha\beta\gamma\delta}\, e_a{}^\alpha e_b{}^\beta e_c{}^\gamma e_d{}^\delta,
$$

where Latin letters indicate the orthonormal tetrad and Greek ones the null tetrad.

Since the transformation between the two frames is governed by (2.15), the $e_a{}^\alpha$ vector fields are given by these equations. The velocity $e_1{}^\mu$ of the spacecraft is naturally changed through the boost we included in the construction there by the velocity $\beta = \tanh\alpha$. (Thus we make sure that no addition of an arbitrary velocity can possibly hurt the special relativistic condition $\beta \leq 1$.) Luckily, the boost factors e^α and $e^{-\alpha}$ cancel everywhere except in those components which

vanish in the Kerr–Newman spacetime. The Weyl tensor is hence independent of a boost in the (l, n)–plane in our case. This independence means that our calculations are not altered by a varying of the speed during the journey. Due to their irrelevance in the present case, we omit the boost factors in the following.

For the above mentioned null tetrad, equation (2.22) leads to

$$C_{l\alpha\beta n} + C_{n\alpha\beta l} - C_{m\alpha\beta\bar{m}} - C_{\bar{m}\alpha\beta m} = 0.$$

Explicitly, these are the subsequent ten equations:

$$C_{lml\bar{m}} = C_{nmn\bar{m}} = C_{lmnm} = C_{l\bar{m}n\bar{m}} = 0,$$

and

$$
\begin{array}{rclrcl}
C_{lnlm} & = & -C_{lmm\bar{m}}, & C_{lnl\bar{m}} & = & C_{l\bar{m}m\bar{m}}, \\
C_{lnnm} & = & C_{nmm\bar{m}}, & C_{lnn\bar{m}} & = & -C_{n\bar{m}m\bar{m}}, \\
C_{lnln} & = & C_{m\bar{m}m\bar{m}}, & C_{lmn\bar{m}} & = & \frac{1}{2}\left(C_{lnm\bar{m}} - C_{lnln}\right).
\end{array}
$$

These relations indicate the path to the already stated set of independent components of the Weyl tensor with respect to the null tetrad.

Using the symmetry properties of the Weyl tensor which are common to the Riemann tensor yields

$$
\begin{aligned}
C_{1212} & = C_{lnln}, \\
C_{1213} & = -\frac{1}{2}\left(C_{lnlm} + C_{lnl\bar{m}} + C_{lnnm} + C_{lnn\bar{m}}\right), \\
C_{1214} & = \frac{i}{2}\left(C_{lnlm} - C_{lnl\bar{m}} + C_{lnnm} - C_{lnn\bar{m}}\right), \\
C_{1223} & = \frac{1}{2}\left(-C_{lnlm} - C_{lnl\bar{m}} + C_{lnnm} + C_{lnn\bar{m}}\right), \\
C_{1224} & = \frac{i}{2}\left(C_{lnlm} - C_{lnl\bar{m}} - C_{lnnm} + C_{lnn\bar{m}}\right), \\
C_{1234} & = -i\, C_{lnm\bar{m}}, \\
C_{1313} & = \frac{1}{4}\left(C_{lmlm} - 2C_{lnln} + C_{l\bar{m}l\bar{m}} + C_{nmnm} + C_{n\bar{m}n\bar{m}}\right), \\
C_{1314} & = -\frac{i}{4}\left(C_{lmlm} - C_{l\bar{m}l\bar{m}} + C_{nmnm} - C_{n\bar{m}n\bar{m}}\right), \\
C_{1323} & = \frac{1}{4}\left(C_{lmlm} + C_{l\bar{m}l\bar{m}} - C_{nmnm} - C_{n\bar{m}n\bar{m}}\right), \\
C_{1324} & = -\frac{i}{4}\left(C_{lmlm} - C_{l\bar{m}l\bar{m}} - C_{nmnm} + C_{n\bar{m}n\bar{m}} + 2C_{lnm\bar{m}}\right).
\end{aligned}
$$

By inserting (2.24), we get for the Weyl tensor transformed into the comoving

tetrad frame

$$
\begin{aligned}
C_{1212} &= \frac{2}{\Sigma^3}\left[Mr\left(r^2 - 3a^2\cos^2\vartheta\right) - Q^2\left(r^2 - a^2\cos^2\vartheta\right)\right], \\
C_{1213} &= C_{1214} = C_{1223} = C_{1224} = 0, \\
C_{1234} &= \frac{2a\cos\vartheta}{\Sigma^3}\left[-M\left(3r^2 - a^2\cos^2\vartheta\right) + 2Q^2r\right], \\
C_{1313} &= -\frac{1}{2}\,C_{1212} = -\frac{1}{\Sigma^3}\left[Mr\left(r^2 - 3a^2\cos^2\vartheta\right) - Q^2\left(r^2 - a^2\cos^2\vartheta\right)\right], \\
C_{1314} &= C_{1323} = 0, \\
C_{1324} &= \frac{1}{2}\,C_{1234} = \frac{a\cos\vartheta}{\Sigma^3}\left[-M\left(3r^2 - a^2\cos^2\vartheta\right) + 2Q^2r\right]. \qquad (2.25)
\end{aligned}
$$

Thus, the first part of the calculation of the Riemann tensor is completed.

2.4.2 The Ricci Tensor for the Kerr–Newman Solution

According to the definition of the Einstein tensor in section 2.1, an obvious way to compute the Ricci tensor $R_{\mu\nu}$ is through the Einstein–Maxwell equations as the energy–momentum tensor $T_{\mu\nu}$ is implicitly given by the corresponding electromagnetic potential A_μ of the Kerr–Newman solution. We start with the electromagnetic field tensor $F_{\mu\nu}$ whose nonvanishing components we easily get from (2.1) and (2.6),

$$
\begin{aligned}
F_{tr} &= \frac{Q}{\Sigma^2}\left(r^2 - a^2\cos^2\vartheta\right), \\
F_{t\vartheta} &= -\frac{2Qra^2\sin\vartheta\cos\vartheta}{\Sigma^2}, \\
F_{\varphi r} &= -\frac{Qa\sin^2\vartheta}{\Sigma^2}\left(r^2 - a^2\cos^2\vartheta\right), \\
F_{\varphi\vartheta} &= \frac{2Qra\sin\vartheta\cos\vartheta}{\Sigma^2}\left(r^2 + a^2\right).
\end{aligned}
$$

Needless to say for the attentive reader, we have used the canonical Boyer–Lindquist frame here. The electromagnetic field tensor has the manifest symmetry $F_{\mu\nu} = -F_{\nu\mu}$. We raise the second index by calculating $F_\mu{}^\nu = g^{\nu\rho}F_{\mu\rho}$,

where $g^{\mu\nu}$ denotes the inverted Kerr–Newman metric. The result is

$$F_t{}^r = -\frac{\Delta Q}{\Sigma^3} \left(r^2 - a^2 \cos^2 \vartheta\right),$$

$$F_t{}^\vartheta = \frac{2Qra^2}{\Sigma^3} \sin\vartheta \cos\vartheta,$$

$$F_\varphi{}^r = \frac{\Delta Qa}{\Sigma^3} \sin^2\vartheta \left(r^2 - a^2 \cos^2 \vartheta\right),$$

$$F_\varphi{}^\vartheta = -\frac{2Qra}{\Sigma^3} \sin\vartheta \cos\vartheta \left(r^2 + a^2\right),$$

$$F_r{}^t = -\frac{Q}{\Delta\Sigma^2} \left(r^2 - a^2 \cos^2 \vartheta\right)\left(r^2 + a^2\right),$$

$$F_r{}^\varphi = -\frac{Qa}{\Delta\Sigma^2} \left(r^2 - a^2 \cos^2 \vartheta\right),$$

$$F_\vartheta{}^t = \frac{2Qra^2}{\Sigma^2} \sin\vartheta \cos\vartheta,$$

$$F_\vartheta{}^\varphi = \frac{2Qra}{\Sigma^2} \cot\vartheta.$$

The same symmetry properties as for the covariant tensor field $F_{\mu\nu}$ hold for its contravariant counterpart $F^{\rho\sigma} = g^{\rho\nu} F_\nu{}^\sigma$. We find

$$F^{tr} = -\frac{Q}{\Sigma^3} \left(r^2 - a^2 \cos^2 \vartheta\right)\left(r^2 + a^2\right),$$

$$F^{t\vartheta} = \frac{2Qra^2}{\Sigma^3} \sin\vartheta \cos\vartheta,$$

$$F^{\varphi r} = -\frac{Qa}{\Sigma^3} \left(r^2 - a^2 \cos^2 \vartheta\right),$$

$$F^{\varphi\vartheta} = \frac{2Qra}{\Sigma^3} \cot\vartheta.$$

We can now derive the scalar $F_{\rho\sigma} F^{\rho\sigma}$,

$$
\begin{aligned}
F_{\rho\sigma} F^{\rho\sigma} &= 2\left(F_{tr} F^{tr} + F_{t\vartheta} F^{t\vartheta} + F_{\varphi r} F^{\varphi r} + F_{\varphi\vartheta} F^{\varphi\vartheta}\right) \\
&= -\frac{2Q^2}{\Sigma^4}\left[\left(r^2 - a^2 \cos^2 \vartheta\right)^2 - 4r^2 a^2 \cos^2 \vartheta\right].
\end{aligned}
$$

The factor of two appears because of the antisymmetry of the electromagnetic field tensor. The next step is to calculate the ten independent components of the stress–energy tensor $T_{\mu\nu}$. They are quickly obtained from (2.1) and read as

follows:

$$
\begin{aligned}
T_{tt} &= \frac{Q^2}{8\pi\Sigma^3}\left(\Delta + a^2\sin^2\vartheta\right), \\
T_{t\varphi} &= -\frac{Q^2 a}{8\pi\Sigma^3}\sin^2\vartheta\left(\Delta + r^2 + a^2\right), \\
T_{tr} &= T_{t\vartheta} = 0, \\
T_{\varphi\varphi} &= \frac{Q^2}{8\pi\Sigma^3}\sin^2\vartheta\left[\Delta a^2\sin^2\vartheta + \left(r^2 + a^2\right)^2\right], \\
T_{\varphi r} &= T_{\varphi\vartheta} = 0, \\
T_{rr} &= -\frac{Q^2}{8\pi\Delta\Sigma}, \\
T_{r\vartheta} &= 0, \\
T_{\vartheta\vartheta} &= \frac{Q^2}{8\pi\Sigma}.
\end{aligned}
\tag{2.26}
$$

As we have learnt in (2.2) and (2.3), the curvature scalar vanishes in the Kerr–Newman case. The components of the Ricci tensor are therefore very readily obtained through the Einstein equations,

$$
\begin{aligned}
R_{tt} &= \frac{Q^2}{\Sigma^3}(\Delta + a^2\sin^2\vartheta), \\
R_{t\varphi} &= -\frac{Q^2 a}{\Sigma^3}\sin^2\vartheta(\Delta + r^2 + a^2), \\
R_{\varphi\varphi} &= \frac{Q^2}{\Sigma^3}\sin^2\vartheta\left[\Delta a^2\sin^2\vartheta + (r^2 + a^2)^2\right], \\
R_{rr} &= -\frac{Q^2}{\Delta\Sigma}, \\
R_{\vartheta\vartheta} &= \frac{Q^2}{\Sigma}.
\end{aligned}
$$

The next task is to project the Ricci tensor into the boosted tetrad frame (2.16), applying the rules (2.13). Since $R_{\mu\nu} = R_{\nu\mu}$, we are confronted with ten independent components which read

$$
\begin{array}{llll}
R_{11} &= \dfrac{Q^2}{\Sigma^2}, & R_{23} &= 0, \\
R_{12} &= 0, & R_{24} &= 0, \\
R_{13} &= 0, & R_{33} &= \dfrac{Q^2}{\Sigma^2}, \\
R_{14} &= 0, & R_{34} &= 0, \\
R_{22} &= -\dfrac{Q^2}{\Sigma^2}, & R_{44} &= \dfrac{Q^2}{\Sigma^2}.
\end{array}
\tag{2.27}
$$

Again, we point out that the result is obviously independent of the boost we introduced in (2.15) and thus independent of the value of the velocity of our spacecraft.

Here ends the second task to be completed in order to receive the Riemann tensor of the Kerr–Newman metric. We are now only a short computation away from our goal.

2.4.3   The Riemann Tensor for the Kerr–Newman Solution

We put the results of (2.25) and (2.27) into (2.21) and obtain the 20 independent components of the Riemann tensor for the Kerr–Newman solution in the tetrad frame as defined in (2.16):

$$
R_{1212} \;=\; R_{3434} \;=\; \frac{1}{\Sigma^3}\left[2Mr(r^2 - 3a^2\cos^2\vartheta) - Q^2(3r^2 - a^2\cos^2\vartheta)\right],
$$

$$
R_{1234} \;=\; 2R_{1324} \;=\; \frac{2a\cos\vartheta}{\Sigma^3}\left[-M(3r^2 - a^2\cos^2\vartheta) + 2Q^2 r\right],
$$

$$
\begin{aligned}
R_{1313} \;=\; & R_{1414} \;=\; -R_{2323} \;=\; -R_{2424} \\
\;=\; & -\frac{1}{\Sigma^3}\left[Mr(r^2 - 3a^2\cos^2\vartheta) - Q^2(r^2 - a^2\cos^2\vartheta)\right],
\end{aligned}
\tag{2.28}
$$

and

$$
R_{1213} = R_{1214} = R_{1223} = R_{1224} = R_{1314} = R_{1323} =
$$
$$
R_{1334} = R_{1424} = R_{1434} = R_{2324} = R_{2334} = R_{2434} = 0.
$$

This list will prove very useful when considering the tidal forces near the ring singularity. With these results we conclude the preliminary discussion to our essay on causality violations in the Kerr–Newman spacetime.

Chapter 3

Travel to the End of the World

3.1 Itinerary

In order to complete the time travel in question, we first have to reach the proximity of the singularity in EKN− before we are in the position to violate causality. Living on our home planet in the approximately Euclidean asymptotic region of EKN+, we therefore need to make a passage through the inhospitable internal district of Kerr–Newman spacetime to the nearly flat asymptotic part of EKN−. Arrived there, we will build up a base camp from which we embark upon the main part of our journey afterwards.

The aim of this chapter is to find this passage without getting lost in the singularity. Especially near the ring singularity at $r = 0$, we will meet a challenging travelling hazard: the tidal forces of the strong curvature. We need to make sure that our spaceship will not be torn asunder. Furthermore, we must pay attention to our fuel supply while trying to minimize the time of travel. Consequently, a geodesic will be an ideal path.

For the calculation of the itinerary we use the advanced Kerr–Newman coordinates (AKN). Thus we make sure that the horizons are passable because the future side of the null hypersurfaces are turned away from EKN+ in the sense of section 2.1. Our home planet has the following coordinates in AKN:

$$
\begin{aligned}
v_0 &= \lambda_0 + X(r_0), \\
\eta_0 &= \varphi_0 + Y(r_0), \\
r_0 &= \zeta r_+, \\
\vartheta_0 &= \vartheta_0,
\end{aligned}
$$

where the subscript "0" labels constant initial values. Without loss of generality, we assume $\vartheta \in [0, \frac{\pi}{2}]$. The factor ζ introduced in the radial component assures that the initial distance from the horizon at $r = r_+$ is large: $\zeta \gg 1$.

The basic idea now consists in splitting up the trip into a "tangential" and a "radial" portion. The first leg will bring us near the "North Pole" of the universe, *i.e.* to the axis of symmetry at $\vartheta = 0$, while r and φ will remain

unchanged. After having reached the axis of symmetry, we will travel along it through a large range of decreasing r.

3.2   Tangential Journey

3.2.1   Parameterization

The tangential section of our journey will certainly be no geodesic as the $\Gamma^{\mu}_{\alpha\beta}$'s do not vanish, while the second derivatives with respect to λ of the curve of our path will be zero. For the whole tangential journey we stay in the nearly flat spacetime. Hence the astronauts will not yet be exposed to any tidal forces of a noteworthy size. The curve has the following parameterization,

$$
\begin{aligned}
v &= r_0\lambda + X(r_0), \\
\eta &= \varphi_0 + Y(r_0) \doteq \eta_0, \quad (= const) \\
r &= \zeta r_+ \doteq r_0, \quad (= const) \\
\vartheta &= -\alpha\lambda,
\end{aligned}
\tag{3.1}
$$

where $\alpha > 0$ and $\lambda \in [-\frac{\vartheta_0}{\alpha}, 0]$. The installed parameter α is a measure for the speed of our spacecraft and can therefore be chosen only up to a certain value α_{max} (speed of light). But once chosen, α remains constant for the sake of simplicity. The well–known condition for timelikeness of a vector $\dot{x}^{\mu}$ is:

$$
g_{\mu\nu}\dot{x}^{\mu}\dot{x}^{\nu} > 0
\tag{3.2}
$$

where a dot means a derivative with respect to λ. With the chosen parameterization, we find

$$
\dot{x}^{\mu} = \begin{pmatrix} r_0 \\ 0 \\ 0 \\ -\alpha \end{pmatrix}.
\tag{3.3}
$$

Since $\Sigma > 0$ outside the singularity we get

$$
\alpha_{max} = \frac{\sqrt{\Delta - a^2 \sin^2\vartheta}}{\Sigma}r_0.
\tag{3.4}
$$

In order to make sure that the argument of the square root remains positive, our reasoning will be as follows. It will only be positive if the coordinates of the spacecraft satisfy the condition

$$
r^2 + a^2\cos^2\vartheta - 2Mr + Q^2 > 0.
$$

Rearranging this condition leads to

$$
(r - M)^2 > M^2 - a^2\cos^2\vartheta - Q^2.
$$

This is not only the inequality which is to be obeyed in order to render the argument of the square root in (3.4) positive, but also the one which defines the exterior bound of the domain called *ergosphere*. The ergosphere is

the region outside the horizon of the singularity where we do not find an analogue to the classical gravitational potential and where particles may thus have arbitrarily small negative energies. Its boundaries are fixed by the inequality $M + \sqrt{M^2 - a^2 - Q^2} < r < M + \sqrt{M^2 - a^2 \cos^2 \vartheta - Q^2}$. Since the tangential journey proceeds exclusively in the approximately Euclidean outer space of EKN+, there is no danger of entering the ergoshere and thus achieving imaginary velocities according to (3.4).

3.2.2 Proper Time

In this subsection we calculate the time s_1 used for the tangential leg of our journey. Starting at $\lambda_0 = -\frac{\vartheta_0}{\alpha}$ and reaching the axis of symmetry at $\lambda_1 = 0$, a simple computation yields

$$
\begin{aligned}
s_1 &= \int_{\lambda_0}^{\lambda_1} d\lambda \sqrt{g_{\mu\nu} \dot{x}^\mu \dot{x}^\nu} \\
&= \int_{\lambda_0}^{\lambda_1} d\lambda \sqrt{\frac{-\alpha^2 a^4 \cos^4(\alpha\lambda) + (1 - 2\alpha^2) r_0^2 a^2 \cos^2(\alpha\lambda) + \mathcal{K}}{a^2 \cos^2(\alpha\lambda) + r_0^2}}
\end{aligned}
$$

where

$$
\mathcal{K} \doteq (1 - \alpha^2) r_0^4 - 2M r_0^3 + Q^2 r_0^2.
$$

We expand the cosine in powers of α. As we expect α to be small compared to the speed of light, all orders larger than α^2 will be suppressed henceforth. We get

$$
s_1 = \sqrt{\frac{A}{B}} \int_{\lambda_0}^{\lambda_1} d\lambda \sqrt{\frac{1 - \frac{r_0^2 a^2 \alpha^2}{A} \lambda^2}{1 - \frac{a^2 \alpha^2}{B} \lambda^2}}
$$

where

$$
\begin{aligned}
A &\doteq -(r_0^2 + a^2)^2 \alpha^2 + r_0^2 \Delta(r_0), \\
B &\doteq r_0^2 + a^2.
\end{aligned}
$$

Obviously, both terms are constants along the tangential curve. Still bearing $\alpha < 1$ in mind, we expand the fraction and the root in terms of α and find

$$
\begin{aligned}
s_1 &= \sqrt{\frac{A}{B}} \int_{\lambda_0}^{\lambda_1} d\lambda \left[1 + \frac{a^2 \alpha^2}{2} \left(\frac{1}{B} - \frac{r_0^2}{A} \right) \lambda^2 \right] \\
&= \sqrt{\frac{A}{B}} \frac{\vartheta_0}{\alpha} \left[1 + \frac{a^2 \vartheta_0^2}{6} \left(\frac{A - r_0^2 B}{AB} \right) \right]. \tag{3.5}
\end{aligned}
$$

This part of the journey is strictly restricted to the asymptotic region of the spacetime. For this reason, we may neglect the second term in our approximation which depends on r_0 like $1/r_0$ for $r_0 \gg 1$. The latter condition certainly holds for the asymptotic region. Thus, we obtain

$$
s_1 = \frac{\vartheta_0}{\alpha} \sqrt{\frac{r_0^2 \Delta}{r_0^2 + a^2} - \alpha^2 (r_0^2 + a^2)}.
$$

Again, we use $r_0 \gg 1$ which simplifies the expression further,

$$s_1 \quad = \quad \frac{\vartheta_0 r_0}{\alpha} \sqrt{1 - \alpha^2}. \tag{3.6}$$

In order to check whether our estimate is correct, we compare it with the result obtained in Minkowski space. It should look the same after our many approximations, where we principally used the huge distance from the central body. In the Minkowskian spacetime, we have a diagonal metric which appears in spherical coordinates as

$$ds^2 = dt^2 - dr^2 - r^2 \left(d\vartheta^2 + \sin^2 \vartheta \, d\varphi^2 \right). \tag{3.7}$$

We parameterize the curve in a similar way as was done for the curved spacetime. We want the first derivative with respect to λ to be precisely the same as in (3.3). In order to make sure that our motion proceeds in a timelike fashion, we apply the well known restriction upon α, *viz.*

$$\alpha < 1 \tag{3.8}$$

where α is again something like an "angular velocity". To carry out the calculation of the "Minkowskian proper time s_1^M"—as we might name it—we integrate with the same limits as we did in the non–Minkowskian case. We obtain as a result

$$s_1^M \quad = \quad \frac{\vartheta_0 r_0}{\alpha} \sqrt{1 - \alpha^2}, \tag{3.9}$$

in perfect agreement with (3.6). Assuming the angular velocity to be non–relativistic (since we have to save our fuel) we may even cut away the higher order. In the end of this section we will return to the comparison between (3.5) and its Minkowskian counterpart (3.9). Before that, we will calculate the tidal forces to learn more about the parameters of the black hole. Next, however, we complete our journey.

3.3   Radial Journey

Before we take off for the second half of our space travel, we have to take a closer look on the various singularities of our metric. In case of $a = 0$, there results a spherical singularity and there is no passing through to the other side of the singularity. There is simply no "other side" of the Schwarzschild solution. Unless stated differently, we therefore assume for all our subsequent calculations a to be non-zero. We find a singularity at $(r = 0, \vartheta = \pi/2)$. Investigating the hyperspace $r = v = 0$, we deduce the induced metric (2.7)

$$ds^2 \quad = \quad -\tan^2 \vartheta \left(a^2 \cos^2 \vartheta - Q^2 \sin^2 \vartheta \right) d\eta^2 - a^2 \cos^2 \vartheta d\vartheta^2.$$

This is a space of two disks, given by $\varphi \in [0, 2\pi], \vartheta \in [0, \pi/2[$ and by $\varphi \in [0, 2\pi], \vartheta \in]\pi/2, \pi]$ respectively. The singularity at $\vartheta = \pi/2$ splits the two halves of the axis in a $(\vartheta = 0)$–axis and in a $(\vartheta = \pi)$–axis which render hopping

from one to another impossible. This separation generates two "worlds". In turn, they open the field to an analytical extension of the disks along curves of constant ϑ to negative values of r into the realm of possible causality violations. Without loss of generality, we henceforth strictly consider civilizations on the upper disk with the rotational axis at $\vartheta = 0$.

Moreover, it is necessary to ascertain that the degeneracy of the advanced Kerr–Newman metric on the rotational axis is purely due to a bad choice of coordinates. To check this we carry out the following local transformation:

$$
\begin{aligned}
x &= \sin \vartheta \cos \eta, \\
y &= \sin \vartheta \sin \eta.
\end{aligned}
$$

We find for the differentials

$$
\begin{aligned}
d\vartheta &= \frac{x dx + y dy}{\sqrt{(1 - (x^2 + y^2))(x^2 + y^2)}}, \\
d\eta &= \frac{-y dx + x dy}{x^2 + y^2}.
\end{aligned}
$$

When inserted into (B.6) this transformation leads to

$$
\begin{aligned}
ds^2 &= \frac{\Delta (dv + ay dx - ax dy)^2 - (x^2 + y^2)\left(a dv + \frac{(r^2 + a^2)(y dx - x dy)}{x^2 + y^2}\right)^2}{r^2 + a^2(1 - (x^2 + y^2))} \\
&\quad - 2 dr (dv + ay dx - ax dy) - \frac{r^2 + a^2(1 - (x^2 + y^2))}{(1 - (x^2 + y^2))(x^2 + y^2)}(x dx + y dy)^2.
\end{aligned}
$$

One recognizes easily that the transformed AKN line element is symmetrical in x and y except for the signs of the terms linear in x or y. For a combined limiting process where x and y both approach zero, the direction in the (x, y)– plane does therefore not influence the limit at $x = y = 0$. We obtain as a result of the aforementioned limit on the axis of symmetry with respect to (v, r, x, y)

$$
g_{\mu\nu} = \begin{pmatrix} \frac{\Delta}{r^2 + a^2} & -1 & 0 & 0 \\ -1 & 0 & 0 & 0 \\ 0 & 0 & -(r^2 + a^2) & 0 \\ 0 & 0 & 0 & -(r^2 + a^2) \end{pmatrix}.
$$

This metric has the determinant $det(g_{\mu\nu}) = -(r^2 + a^2)^2$ and is therefore regular for all r, since we restrict ourselves to real numbers. We confine the further course of the travel to the two–dimensional submanifold (v, r) of the axis of rotation. The calculation of the there induced metric γ_{kl} gives rise to

$$
\gamma_{kl} = \begin{pmatrix} \frac{\Delta}{r^2 + a^2} & -1 \\ -1 & 0 \end{pmatrix}. \tag{3.10}
$$

This matrix clearly has a constant, non–vanishing determinant and is thus also regular in the entire subspace for all parameters of the black hole. Hence, we will not crash into the singularity when reaching the axis of rotation nor when travelling along it.

3.3.1   Equations of Motion

We intend to derive the equations of motion for the radial leg of our journey into the unknown world of EKN−. For this purpose, we consider an uncharged spaceship of mass m moving in the two-dimensional space of (3.10). Making use of the proper time $ds = d\lambda\sqrt{g_{\mu\nu}\dot{x}^\mu\dot{x}^\nu}$, given the canonical momentum $p_\mu = mg_{\mu\nu}\frac{dx^\nu}{ds}$ and the Lagrangian $\mathcal{L} = m\sqrt{g_{\mu\nu}\dot{x}^\mu\dot{x}^\nu}$, we apply the conservation of the four–momentum

$$\frac{\partial\mathcal{L}}{\partial\dot{x}^\mu} \quad = \quad \text{const.}$$

For an uncharged body of an energy $p_v = e$ with respect to positive infinity we then have the two equations

$$
\begin{aligned}
e &= \gamma_{vk}\dot{x}^k \\
m^2 &= \gamma_{kl}\dot{x}^k\dot{x}^l
\end{aligned}
\tag{3.11}
$$

where

$$ds \quad = m\,d\lambda. \tag{3.12}$$

There are two solutions of (3.11). We pick the one which corresponds to $\dot{r} < 0$:

$$\dot{r}^2 + V_{\text{eff}}^a(r) \quad = \quad 0 \tag{3.13}$$

$$\dot{v} \quad = \quad \frac{r^2 + a^2}{\Delta}\left(e - \sqrt{-V_{\text{eff}}^a(r)}\right) \tag{3.14}$$

with

$$V_{\text{eff}}^a(r) \quad = \quad -e^2 + \frac{m^2\Delta}{r^2 + a^2}$$

There are only implicit solutions of this system of differential equations. Fortunately, it will prove unnecessary for our intent to solve them explicitly. What is important though is the fact that motion is only possible where $V_{\text{eff}}^a(r)$ is negative. Building the limit at infinity, we find $\lim_{r\to\pm\infty} V_{\text{eff}}^a(r) = -e^2 + m^2$ and for this reason $e^2 > m^2$.

We have to check whether $V_{\text{eff}}^a(r) < 0$ is satisfied everywhere on the axis of symmetry. Discussing the effective potential $V_{\text{eff}}^a(r)$, we obtain for the first derivative

$$\frac{\partial V_{\text{eff}}^a(r)}{\partial r} \quad = \quad \frac{2m^2}{(r^2 + a^2)^2}\left(Mr^2 - Ma^2 - rQ^2\right),$$

from which we find the global maximum of the function $V_{\text{eff}}^a(r)$ at

$$r_{\text{maxpot}} \quad = \quad \frac{Q^2 - \sqrt{Q^4 + 4a^2M^2}}{2M}. \tag{3.15}$$

If we study an uncharged black hole, we hence obtain $r_{\text{maxpot}} = -a$ (and a minimum at $r_{\text{minpot}} = +a$). We define the shortcut

$$\rho \;\doteq\; \frac{e^2 - m^2}{m^2}. \tag{3.16}$$

In order to ascertain that $V_{\text{eff}}^a(r) < 0$ ($\forall\, r$) remains valid even at the maximum, ρ is restricted by (3.15) through a lower bound,

$$\rho \;>\; \frac{2M^2}{\sqrt{Q^4 + 4M^2 a^2} - Q^2}. \tag{3.17}$$

Physically, this means that the potential at the maximum along the radial travel is higher than in the asymptotic region. Therefore our spacecraft needs a certain given amount of fuel in order to overcome the barrier of the potential and to reach its destination which lies behind it.

As we will later see, it is highly improbable that the black hole carries a charge with it which should be accounted for in our calculations. Confining Q to zero, we obtain

$$\rho \;>\; \frac{M}{a}.$$

After rescaling to units of M, $\bar{a} \doteq a/M$ and $\bar{Q} \doteq Q/M$, our considerations yield the minimal energy necessary to complete the radial leg of our journey in case the singularity is uncharged,

$$e_{\min} \;=\; m\sqrt{\frac{1 + \bar{a}}{\bar{a}}}. \tag{3.18}$$

We shall provide numerical results of the minimal energy for several combinations of a and Q in section 3.5. If we differentiate (3.18) with respect to $\bar{a}$, we obtain

$$\frac{\partial e_{\min}}{\partial \bar{a}} \;=\; -\frac{m}{2M\bar{a}^2}\sqrt{\frac{\bar{a}}{1 + \bar{a}}},$$

which is clearly negative for all values of $\bar{a} \in [0, 1]$. For this reason, it proves favourable to look for a black hole with large angular momentum. From (3.18), we may also conclude that the larger the mass m of the spacecraft or the mass M of the singularity becomes, the higher is the minimal energy required to pass through the ring and to complete the radial leg of our outward journey to EKN$-$.

Eventually, the kinetic energy necessary in order to surmount the maximum of the effective potential is

$$e_{\text{kinmin}} \;=\; m\left(\sqrt{\frac{1 + \bar{a}}{\bar{a}}} - 1\right). \tag{3.19}$$

For an extreme black hole, we find the minimal kinetic energy $e_{\text{kinmin}} = m(\sqrt{2} - 1)$, which is smaller than the rest energy of the spacecraft. However, it is not strictly necessary to burn that much energy in order to reach the domain of causality violation, since for an uncharged singularity, we do not need any kinetic energy to reach $r = 0$ and the domain starts right after we have passed the singular ring.
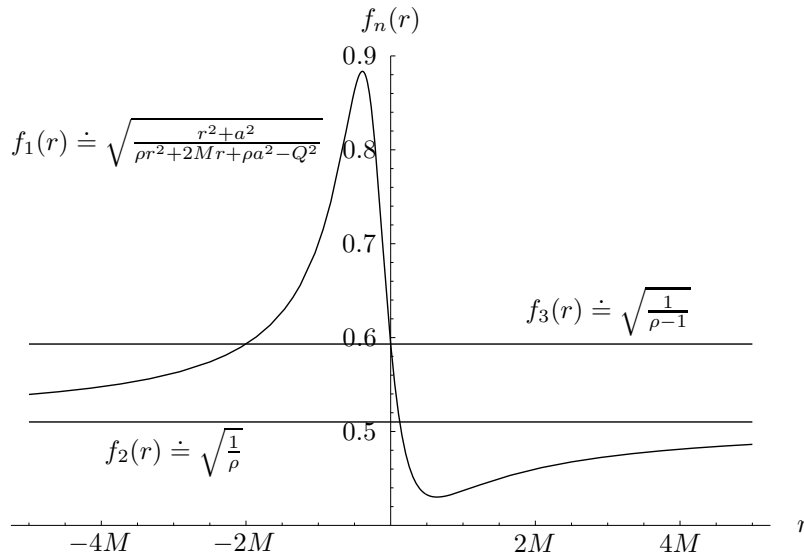
3.3.2 Proper Time

In this subsection we estimate the proper time for the second part of our travel.
Starting with (3.13) and using (3.12), we obtain

$$ds \quad = \quad -\frac{m}{\sqrt{-V_{\text{eff}}^a}}\, dr. \tag{3.20}$$

The sign corresponds to the direction of our journey from EKN+ to EKN−.
Integration of (3.20) then yields (the subscript "2" designates the second leg of
the trip)

$$s_2 \quad = \quad \int_{\zeta r_-}^{\zeta r_+} dr \sqrt{\frac{r^2 + a^2}{\rho r^2 + 2Mr + \rho a^2 - Q^2}}. \tag{3.21}$$

PSfrag replacements

Figure 3.1: $f_1(r)$ is the integrand of (3.21) with $a = Q = 0.5M$ and $\rho = 1.5\rho_{min}$
defined in (3.17). For different values of the parameters, the plot is only
quantitatively but not qualitatively changed. We clearly recognize that
for a small positive r the travelling speed will be high, whereas for a small
negative r the spacecraft will be slowed down. One can also understand
the splitting of the integral (3.21) by means of this figure.

Since we only estimate the order of the time required for our journey, we
split the right-hand side into three integrals with constant integrands which
exceed the original function everywhere. As the integrand approximates $\sqrt{1/\rho}$

for large r, we choose the following convenient separation:

$$s_2 \quad < \quad \int_{-\zeta r_+}^{-M-\sqrt{M^2+Q^2-a^2}} dr \sqrt{\frac{1}{\rho-1}} \;+$$
$$\int_{-M-\sqrt{M^2+Q^2-a^2}}^{Q^2/2M} dr \sqrt{\frac{Q^2-\sqrt{4a^2M^2+Q^4-2a^2\rho}}{2M^2+2\rho(Q^2-a^2\rho)}} \;+$$
$$\int_{Q^2/2M}^{\zeta r_+} dr \sqrt{\frac{1}{\rho}}.$$

Rescaling to units of M we obtain for the proper time of the radial flight

$$s_2\left(\bar{a},\bar{Q},\zeta,\rho,M\right) \quad < \quad M\Bigg[\left(\sqrt{\frac{1}{\rho}}+\sqrt{\frac{1}{\rho-1}}\right)\left(1+\sqrt{1-\bar{a}^2-\bar{Q}^2}\right)\zeta$$
$$-\sqrt{\frac{1}{\rho-1}}\left(1+\sqrt{1-\bar{a}^2+\bar{Q}^2}\right)-\sqrt{\frac{1}{\rho}}\frac{\bar{Q}^2}{2} \qquad (3.22)$$
$$+\sqrt{\frac{\bar{Q}^2-\sqrt{4\bar{a}^2+\bar{Q}^4-2\bar{a}^2\rho}}{2+2\rho\left(\bar{Q}^2-\bar{a}^2\rho\right)}}\left(1+\sqrt{1-\bar{a}^2+\bar{Q}^2}\right)\Bigg],$$

where $\bar{a}$, $\bar{Q}$, ζ, and ρ are the known dimensionless parameters. We get two restrictions on these quantities:

$$\bar{a}^2+\bar{Q}^2 < 1$$
$$\rho > \frac{2}{\sqrt{4\bar{a}^2+\bar{Q}^4}-\bar{Q}^2} \qquad (3.23)$$

We briefly analyze the resulting function $s_2\left(\bar{a},\bar{Q},\zeta,\rho,M\right)$ for the proper time. Clearly, s_2 depends linearly on M. For large ζ, we can easily see that s_2 will also grow linearly. The evaluation of the characteristics of the a– and Q–dependence prove much more complicated. In addition, we see from (3.23) that if $\bar{a}$ is small or if $\bar{Q}$ is large, our spacecraft will consume a higher energy than vice versa. As we will later learn in section 3.5, this is generally not to be expected. In order to get an impression of how the proper time will be influenced by the angular momentum and the electric charge of the black hole, the reader may consult Fig. 3.2.

Studying the figures, one needs to be aware of the fact that the inclusive variable ρ depends as mentioned before on $\bar{a}$ and $\bar{Q}$ itself. Trivially, the statement holds that for larger energies ρ the time required decreases. This shortening of time happens nonlinearly, as Fig. 3.3 illustrates. A short consideration of (3.22) leads us to the conviction that the proper time asymptotically approaches zero for arbitrarily large ρ.

3.4 Tidal Forces

Due to the increasingly changing gravitational potential, our spacecraft and its pilots will be more imperiled by tidal forces the closer to the singularity

(a) $\bar{a}$–dependence with constant $\bar{Q} = 0.5$ **(b)** $\bar{Q}$–dependence with constant $\bar{a} = 0.5$
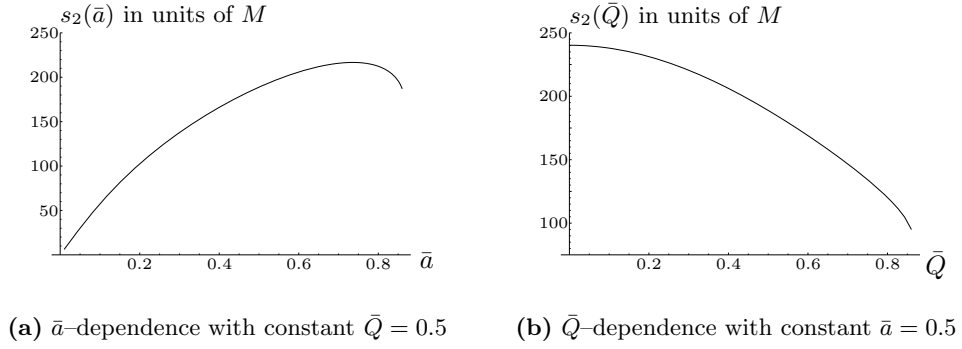
Figure 3.2: Dependences of s_2 of $\bar{a}$ and $\bar{Q}$ while holding $\zeta = 100$ constant. ρ takes the value $3/(\sqrt{4\bar{a}^2 + \bar{Q}^4} - \bar{Q}^2)$, *i.e.* $\rho = 1.5\rho_{\min}$.
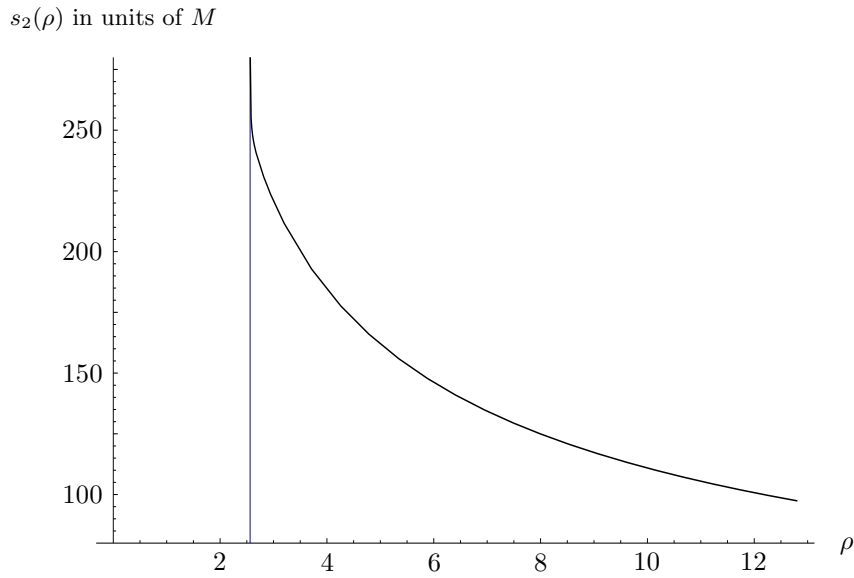
Figure 3.3: ρ-dependence of s_2 with constant $\zeta = 100, \bar{a} = \bar{Q} = 0.5$. The area left of the gridline at $\rho = 2.56$ is prohibited if the spacecraft is to have enough energy to complete the journey.

they get. For an estimation of these forces, we first have a look at the relative acceleration affecting the travellers. Any estimation of numerical values of the tension and pressure encountered will have to rely upon the calculation of the Riemann tensor in an orthonormal, co–moving tetrad frame as completed in Section 2.4.3.

3.4.1 Geodesic Deviation

In order to estimate the tidal forces to be expected when passing through the ring singularity, we derive the equation of geodesic deviation, which will provide a measure of the relative acceleration between two neighbouring mass points. These mass points are at a distance δx from each other and move according to the corresponding geodesic equations respectively:

$$\frac{d^2 x^\mu}{d\lambda^2} + \Gamma^\mu_{\beta\gamma}(x)\frac{dx^\beta}{d\lambda}\frac{dx^\gamma}{d\lambda} = 0,$$

$$\frac{d^2}{d\lambda^2}\left(x^\mu + \delta x^\mu\right) + \Gamma^\mu_{\beta\gamma}(x + \delta x)\frac{d}{d\lambda}(x^\beta + \delta x^\beta)\frac{d}{d\lambda}(x^\gamma + \delta x^\gamma) = 0.$$

Subtracting the upper equation from the lower leads up to the first order in δx^μ to

$$\frac{d^2 \delta x^\mu}{d\lambda^2} + \frac{\partial \Gamma^\mu_{\beta\gamma}}{\partial x^\rho}\delta x^\rho \frac{dx^\beta}{d\lambda}\frac{dx^\gamma}{d\lambda} + 2\Gamma^\mu_{\beta\gamma}\frac{dx^\beta}{d\lambda}\frac{d\delta x^\gamma}{d\lambda} = 0. \tag{3.24}$$

On the other hand, we calculate the second covariant derivative of δx^μ. Since the covariant derivative of any given vector field V^μ is defined by

$$\frac{DV^\mu}{D\lambda} \doteq \frac{dV^\mu}{d\lambda} + \Gamma^\mu_{\beta\gamma}\frac{dx^\beta}{d\lambda}V^\gamma,$$

we obtain

$$\frac{D^2}{D\lambda^2}\delta x^\mu = \frac{d^2 \delta x^\mu}{d\lambda^2} + \Gamma^\mu_{\beta\gamma}\dot{x}^\beta\frac{d\delta x^\gamma}{d\lambda} + \frac{d}{d\lambda}\left(\Gamma^\mu_{\beta\rho}\dot{x}^\beta\delta x^\rho\right) + \Gamma^\mu_{\sigma\gamma}\Gamma^\sigma_{\beta\rho}\dot{x}^\beta\dot{x}^\gamma\delta x^\rho,$$

where we used $\dot{x}^\mu \doteq \frac{dx^\mu}{d\lambda}$. After executing the derivative of the product with respect to the parameter λ, regrouping the terms, applying the chain rule, and eliminating the second derivatives by means of the geodesic equation and (3.24) we arrive at

$$\begin{aligned}
\frac{D^2}{D\lambda^2}\delta x^\mu &= -\frac{\partial \Gamma^\mu_{\beta\gamma}}{\partial x^\rho}\dot{x}^\beta\dot{x}^\gamma\delta x^\rho + \frac{\partial \Gamma^\mu_{\beta\rho}}{\partial x^\gamma}\dot{x}^\beta\dot{x}^\gamma\delta x^\rho \\
&\quad -\Gamma^\mu_{\sigma\rho}\left(\Gamma^\sigma_{\beta\gamma}\dot{x}^\beta\dot{x}^\gamma\right)\delta x^\rho + \Gamma^\mu_{\sigma\gamma}\Gamma^\sigma_{\beta\rho}\dot{x}^\gamma\dot{x}^\beta\delta x^\rho.
\end{aligned}$$

We finally employ the canonical definition of the Riemannian curvature tensor $R^\mu_{\beta\gamma\rho}$ to find the *equation of geodesic deviation*:

$$\frac{D^2}{D\lambda^2}\delta x^\mu = R^\mu_{\beta\gamma\rho}\dot{x}^\beta\dot{x}^\gamma\delta x^\rho. \tag{3.25}$$

3.4.2   Stress on the Journey

The relative acceleration of the preceding considerations is termed b^μ and given by

$$b^\mu \doteq \frac{D^2}{D\lambda^2}\delta x^\mu.$$

If we compute b^μ in the co–moving frame (2.16), the four-velocity $\dot{x}^\alpha$ is given by the first vector of the tetrad, and the distance δx^μ can be conveniently measured in the frame of the spacecraft itself. Using the manipulations of the tetrad formalism discussed in section 2.2, we obtain the relative acceleration in co–moving frame,

$$b^a \;=\; \eta^{ab}R_{1b1c}\delta x^c, \tag{3.26}$$

where Latin letters mark quantities measured in the tetrad frame. Extracting yields

$$\begin{aligned}
b^1 &= 0,\\
b^2 &= -R_{1212}\delta x^2,\\
b^3 &= -R_{1313}\delta x^3,\\
b^4 &= -R_{1414}\delta x^4.
\end{aligned}$$

Since $R_{1313} = R_{1414}$, we have only two different, nonvanishing relative accelerations, which exert their influence in the longitudinal and transverse directions respectively. These relative accelerations between head and feet, left and right of the astronauts induce a tidal force upon their bones, muscles, and organs. For simplicity's sake, we idealize both, the human body and the space shuttle, as a homogeneous rectangular box of mass m, of length l in the $e_2^{\;\mu}$ direction, and of width and depth w in the $e_3^{\;\mu}$ and $e_4^{\;\mu}$ directions. The index "A" will always denote the astronaut's measures while "S" indicates the spacecraft.

   We calculate the stresses that organic and inorganic matter has to withstand in order to retain its shape. For the longitudinal force acting on the center of mass, we consider a mass element dm located at a height h above the center of mass of the box. This distance h is naturally measured along $e_2^{\;\mu}$. To prevent the acceleration of the mass element away from the center of mass, cosmonautic life and gear must sustain a force

$$dF_{\text{long}} = b^2\, dm = -R_{1212}\, h\, dm.$$

The upper index of b should not be taken for a exponent, it indicates the direction of the relative acceleration. Then, the total force across the horizontal plane of the center of mass is the sum of the forces on all mass elements above it,

$$\begin{aligned}
F_{\text{long}} &= \int_{\text{(Volume above plane)}} b^2\, dm \;=\; -\int_0^{l/2} R_{1212}\, h\left(\frac{m}{lw^2}\right)w^2 dh\\
&= -R_{1212}\frac{ml}{8},
\end{aligned}$$

where we used $dV = w^2 dh$ and the density m/lw^2. The stress is defined as "force per area", F_{long} divided by the cross–sectional area w^2 in our case,

$$T_{\text{long}} = -R_{1212}\frac{ml}{8w^2}, \tag{3.27}$$

where the sign decides whether the stress is a tension ($T < 0$) or rather a pressure ($T > 0$). Does the sign in (3.27) agree with the present situation? We have to delay the resolution of this issue until we know a bit more about it.

Similarly, we get for the transverse force in the e_3^μ and e_4^μ directions

$$F_{\text{trans}} = -R_{1313}\frac{mw}{8}$$

or, accordingly

$$T_{\text{trans}} = -R_{1313}\frac{m}{8l}. \tag{3.28}$$

Since we travel along the axis of symmetry, we may set $\vartheta = 0$. Remembering (2.28), we recognize that both components of the stress (of the Riemann tensor, to be precise), longitudinal and transverse, appear with an opposing sign. In case of an uncharged singularity $Q = 0$, this effects exactly opposed forces, *viz.* if the box is stretched longitudinally, it is compressed transversely and *vice versa*. As the tide will turn in one direction, it does so in the other simultaneously.

For the Kerr–Newman spacetime, we get for the stress encountered along the axis of the spherically symmetrical spacetime:

$$
\begin{aligned}
T_{\text{long}} &= -\frac{ml}{8w^2(r^2 + a^2)^3}\left[2Mr(r^2 - 3a^2) - Q^2(3r^2 - a^2)\right], \\
T_{\text{trans}} &= \frac{m}{8l\,(r^2 + a^2)^3}\left[Mr(r^2 - 3a^2) - Q^2(r^2 - a^2)\right]. \tag{3.29}
\end{aligned}
$$

If we set $a = Q = 0$ in (3.29), we have the stress suffered in the Schwarzschild solution of a non–rotating, uncharged black hole. We find

$$
\begin{aligned}
T_{\text{long}} &= -\frac{mMl}{4w^2r^3}, \\
T_{\text{trans}} &= \frac{mM}{8lr^3},
\end{aligned}
$$

in accordance with [1], p. 861. Thus, we obtained the correct sign in (3.27). Since we have $r \geq 0$ in the Schwarzschild solution, T_{long} will be negative and T_{trans} positive. Consequently, a venturer challenging the singularity at $r = 0$ would be stretched longitudinally and squashed in the transverse direction.

We render the numerical analysis of the stress components more convenient by rescaling the coordinate r and the parameters a and Q of the black hole:

$$
\begin{aligned}
r &= M\bar{r}, \\
a &= M\bar{a}, \\
Q &= M\bar{Q}. \tag{3.30}
\end{aligned}
$$

The "barred" quantities are all dimensionless in natural units. This scaling to units of mass M has a meaning beyond the achieved simplicity of the expressions. It puts the angular momentum and the charge into relation with the mass. This makes sense, since on the one hand we are not allowed to violate the cosmic censorship with too large parameters. With very low values on the other hand, the influence of these quantities becomes practically irrelevant for super–massive galactic nuclei. But it is exactly this influence which is to be analyzed. The easy–to–handle stress then looks like

$$
\begin{aligned}
T_{\text{long}} &= -\frac{ml}{8w^2 M^2} \frac{1}{(\bar{r}^2 + \bar{a}^2)^3} \left[2\bar{r}(\bar{r}^2 - 3\bar{a}^2) - \bar{Q}(3\bar{r}^2 - \bar{a}^2) \right], \\
T_{\text{trans}} &= \frac{m}{8lM^2} \frac{1}{(\bar{r}^2 + \bar{a}^2)^3} \left[\bar{r}(\bar{r}^2 - 3\bar{a}^2) - \bar{Q}(\bar{r}^2 - \bar{a}^2) \right].
\end{aligned}
\tag{3.31}
$$

These rescaled functions reveal the simple mass–dependence of the stress. Contraintuitively, the stress *decreases* with growing mass of the ring singularity. The relative angular momentum $\bar{a}$ is obviously able to suppress the stress in case there is a strong rotation. We have to find a singularity with a high enough mass in order to keep the stress down even if there is a considerably large rotational contribution. If we assume as a rule of thumb that the tension or pressure should not exceed 10 atmospheres (atm), we are to look for a black hole with mass $M \geq 10^6 M_\odot$. A central body of this mass is likely to be found in a galactic nucleus. Estimations for a super–massive black hole sitting midst of a galaxy range from $10^4 M_\odot$ up to $10^8 M_\odot$.[1] Galaxy M 106 appears to be a promising candidate with an approximate mass $M \approx 36 \cdot 10^6 M_\odot$.[2] Unless stated differently, we henceforth assume in the numerical analysis of this chapter

$$
M = 10^7 M_\odot \approx 10^{37} \text{kg} \sim 10^7 \frac{c^2}{G} R_\odot,
\tag{3.32}
$$

where $R_\odot = 1476.69$m is the gravitational radius of the sun.

Trivially, the stress will be far from constant along the axis. If the object is uncharged, the stress is an antisymmetric function and at the very moment the ring is about to be passed, there will be a dead calm since antisymmetric functions vanish at the origin. With growing charge, we have a remarkable rise of the tidal activity. This increase is due to the cosmic censorship which orders the object to increasingly restrict its angular momentum for a growing charge. Simultaneously, the tidal waves will more and more destroy the peace found at $r = 0$ for $Q = 0$. This interpretation applies for the longitudinal and transverse stresses. In Fig. 3.4 we plot T_{long} for different sets of parameters $\bar{a}$ and $\bar{Q}$. Only the curves for the stress on a human can be found in the figure. Since the ones that affect the craft are very similar if we assume the measures of the craft to be those of the International Space Station[3], we do not show the respective plots. Although out of the range of the given plot, even T_3 will not exceed $T_3^{max} \approx 20.6 \text{Nm}^{-2}$. This tension—for such it is—will not trouble man nor machine.

[1] [1] p. 887

[2] [36] p. 395

[3] Total mass of all modules: $m_S = 455865$kg; Wingspan (End–to–end width): $w_S = 108.6$m; Length: $l_S = 79.9$m. Specifications according to NASA: http://station.nasa.gov/

PSfrag replacements
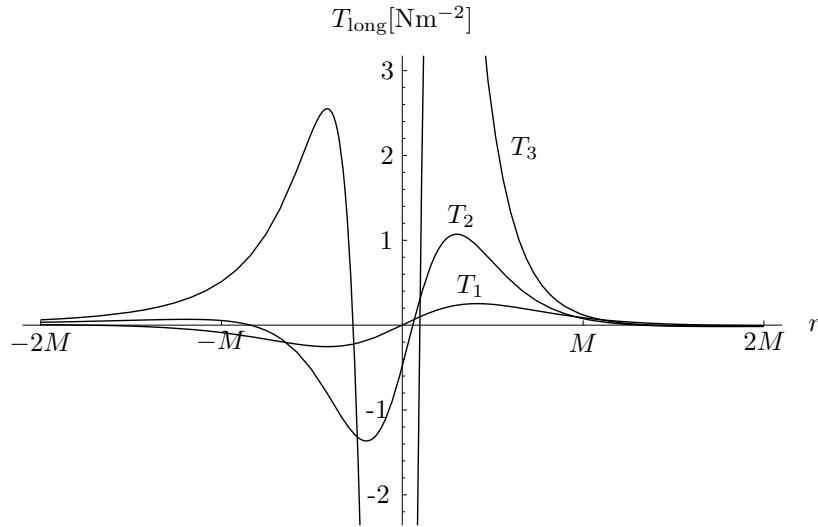
Figure 3.4: The *longitudinal* stress for astronauts ($m_A = 75$kg, $l_A = 1.8$m, $w_A = 0.2$m) as a function of the coordinate r. The three plots represent three different pairs of parameters: T_1 plots the curve for ($\bar{a} = 1, \bar{Q} = 0$), T_2 for ($\bar{a} = 0.6, \bar{Q} = 0.6$), and T_3 for ($\bar{a} = 0.3, \bar{Q} = 0.9$).

PSfrag replacements
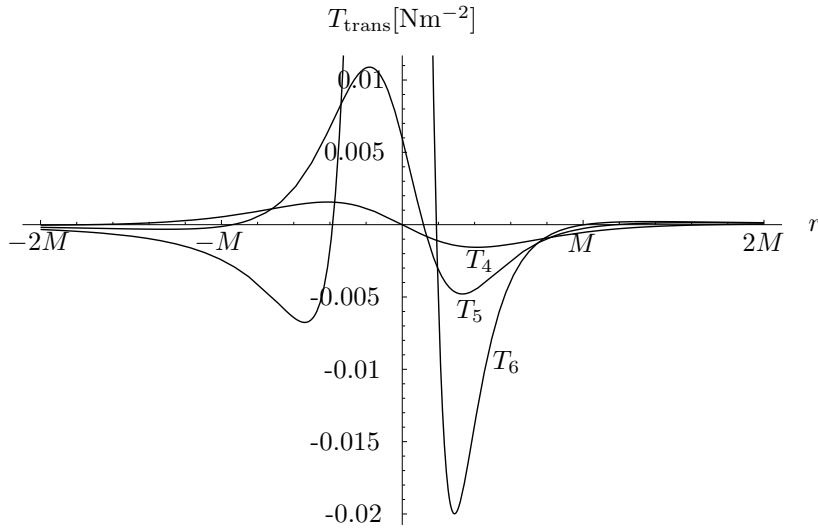
Figure 3.5: The *transverse* stress for astronauts ($m_A = 75$kg, $l_A = 1.8$m, $w_A = 0.2$m) as a function of the coordinate r. The three plots represent three different pairs of parameters: T_4 plots the curve for ($\bar{a} = 1, \bar{Q} = 0$), T_5 for ($\bar{a} = 0.6, \bar{Q} = 0.6$), and T_6 for ($\bar{a} = 0.3, \bar{Q} = 0.9$).

The longitudinal tensions and pressures reach much higher numerical values than the transverse ones. We provide three examples of transverse tidal stress in Fig. 3.5. But unlike the former, in the latter we clearly distinguish between stress affecting astronauts and stress affecting space equipment. Due to the difference of the respective coefficients, we have to multiply the "human" stress by a factor of about 137 in order to get the "technical" stress, assuming again the measures of the International Space Station. Apparently the shape of the graph is not changed in the two cases. The strongest transverse stress for a slowly rotating hole ($\bar{a} = 0.3$) is about $T_6^{max} \approx 0.23 \mathrm{Nm}^{-2}$ for humans and $T_6^{max} \approx 31.5 \mathrm{Nm}^{-2}$ for the ship. This time, the maximum passes for a pressure which is easily withstood by the crew. Without going into details of materials science, we take the solidity of the craft up to the required level for granted. We do not consider such a construction to be only miraculously possible.

The derivatives of the functions (3.31) with respect to $\bar{r}$ have four roots. We pick out those roots which correspond to the global maximum of the absolute values of (3.31) and fix r there. Of course, this "radius of maximal stress" depends on the parameters of the singularity. We have determined its mass in (3.32). Therefore, two variables remain on which equations (3.31) depend. The plot of $T_{long}(\bar{a}, \bar{Q})$ and $T_{trans}(\bar{a}, \bar{Q})$ is shown in Fig. 3.6, 3.7, and 3.8. For the longitudinal T, the size of the stress of crew and craft are comparable, but in the transverse direction, size differs again by a factor of approximately 137. Of course, this factor is only due to our choice of m, l, and w. Hence, we plot the surface graphics for both cases this time. In all three graphics we added a wall which delimits the domain of an eligible combination of angular momentum and charge ($\mathcal{D}$), where travel is nearly stress–free. Every point in the phase space behind this wall is forbidden by cosmic censorship ($\mathcal{F}$).

## 3.5   Choosing a Reasonable Spacetime

Concluding this section, we explicitly calculate the proper time used to cross the plane of the ring singularity from the quasi–flat part of EKN+ to the respective area in EKN− for several possible combinations of the relevant parameters of the black hole. We fix the mass M at $10^7 M_\odot$ as we did in the last section. We discuss four paradigmatic cases,

It is very likely that the galactic nucleus at hand has much angular momentum, since most objects that can collapse to form black holes rotate rapidly.[4] By contrast, it is highly probable that no Kerr–Newman black hole shows a significant charge. The reason is that if we would have $Q \sim M$, the electrostatic force would heavily outscore the gravitational pull. If we consider a test particle with mass m and charge q (either an electron or a proton, depending on the sign of Q), the repulsive electrostatic force dominates the gravitational
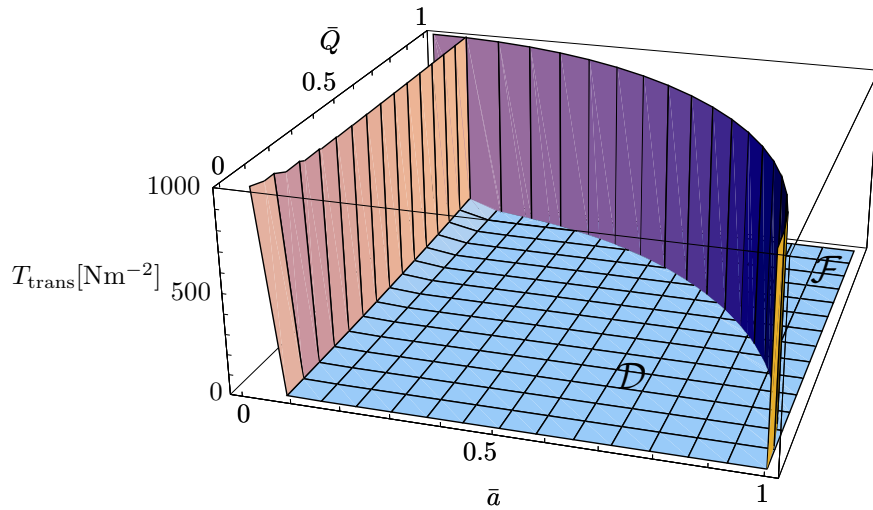
---
[4]cf. [1], p. 885
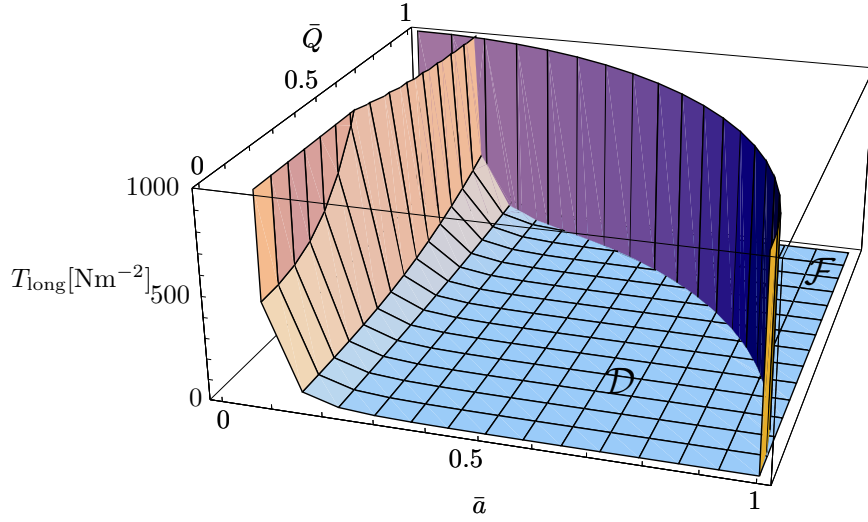
Figure 3.6: The *longitudinal* stress T_{long} for a crew, here plotted as a function of the two parameters $\bar{a}$ and $\bar{Q}$. The coordinate $\bar{r}$ is fixed at the radius of the global maximum for the stress. Again, the stress is calculated for an astronaut with $m_A = 75$kg, $l_A = 1.8$m, $w_A = 0.2$m. $\mathcal{D}$ indicates the region of smooth travel, whereas the domain $\mathcal{F}$ is prohibited by cosmic censorship.

Figure 3.7: $T_{trans}(\bar{a}, \bar{Q})$ for an astronaut where $\bar{r}$ is constantly fixed at the radius of maximal stress.
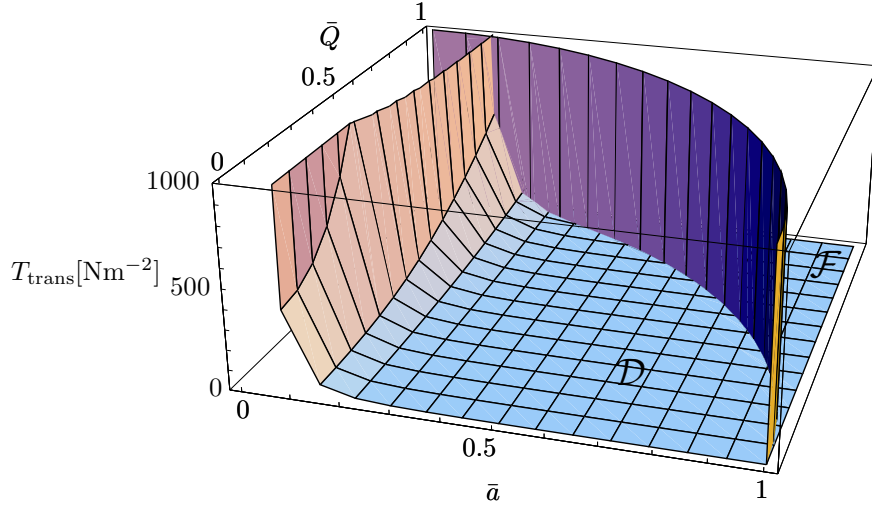
Figure 3.8: $T_{trans}(\bar{a}, \bar{Q})$ for a spacecraft with $m_S = 455865\text{kg}, l_S = 79.9\text{m}, w_S = 108.6\text{m}$.

		Angular Momentum	Charge	
(I)	Large	$\bar{a} = 1.0$	None	$\bar{Q} = 0$
(II)	Middle–sized	$\bar{a} = 0.6$	Middle–sized	$\bar{Q} = 0.6$
(III)	Small	$\bar{a} = 0.3$	Large	$\bar{Q} = 0.9$
(IV)	Tiny	$\bar{a} = 0.1$	Tiny	$\bar{Q} = 0.1$

by a factor

$$\frac{\text{Electrostatic Force}}{\text{Gravitational Force}} = \frac{qQ}{mM} \approx 10^{18}...10^{22}, \tag{3.33}$$

depending on the charge–mass ratio of the test particle. The boundary values apply whether we have a proton or an electron in the potential. If the test particle is an ion with much smaller charge–mass ratio, then the huge differential forces of (3.33) will decrease accordingly. When the total charge–mass ratio of a body near the black hole approaches zero, it will most presumably be torn into pieces and the charged particles will accelerate either towards or away from the singularity, depending on their respective charge. Thus, the black hole is very likely to attract enough charge from outside to be neutralized. In this sense, scenario (III) is highly implausible and we will therefore no longer focus on it. Taking these deliberations into account, we clearly favour scenario (I), but will nevertheless keep track of (II) and (IV) as well.

Finally, we calculate the tangential and radial proper time (3.6) and (3.22) necessary to complete the travel and the appropriate maximal stresses on the radial leg. We still assume $M = 10^7 M_\odot$. Since we have the distance r_0 of our home planet to the horizon at $r = r_+$,

$$r_0 = \zeta M \left(1 + \sqrt{1 - \bar{a}^2 - \bar{Q}^2}\right),$$

we set $\zeta = 100$ in order to make sure that we start in the asymptotic region. For the tangential part, we need to specify the speed of travel α and the location of our home planet ϑ_0. We assume a non–relativistic velocity with $\alpha = 0.01 \ll 1$. We put the home base at $\vartheta_0 = \pi/2$ and choose thus the most unfavourable case where the proper time for the tangential leg becomes maximal.

We confine the available energy ρ consumable on the radial trip to

$$\rho \;=\; \frac{2.01}{\sqrt{4\bar{a}^2 + Q^4} - Q^2}, \tag{3.34}$$

which is only slightly above the required minimum of (3.17). Fig. 3.9 shows the numerical values of s_1, s_2, and the minimal kinetic energy e_{kin} from equation (3.19) for the now fixed values of the parameters $r_0, \vartheta_0, \alpha, \zeta, \rho, M, \bar{a}, \bar{Q}$, and the mass m of the spacecraft according to footnote 3 on page 38.

	s_1 [h]	s_2 [h]	e_{kin} [J]
(I)	214.9	20.71	$1.87 \cdot 10^{22}$
(II)	328.6	3.497	$3.61 \cdot 10^{22}$
(IV)	427.7	1.829	$1.08 \cdot 10^{23}$

Figure 3.9: Explicit tangential and radial proper times s_1 and s_2 in hours and energy consumption in Joule necessary to complete the journey in the respective time.

Equations (3.31) are used to calculate the maximal tension or pressure numerically. Here, we assumed for our human space conquerors the measures

$$\begin{aligned}
m_A &= 75\text{kg}, \\
l_A &= 1.8\text{m}, \\
w_A &= 0.2\text{m}, \tag{3.35}
\end{aligned}$$

and for the space shuttle

$$\begin{aligned}
m_S &= 455865\text{kg}, \\
l_S &= 79.9\text{m}, \\
w_S &= 108.6\text{m}. \tag{3.36}
\end{aligned}$$

The results are given in Fig. 3.10.

Concluding, we state that for all three above discussed scenarios both the proper times as well as the stresses seem to be within the bounds of possibility. The time necessary for the whole trip is astonishingly brief and poses no problem. Only the energy necessary to flee the "square well" potential of the ring singularity might question the feasibility of our adventure. The energy needs of the order 10^{22} J for an spacecraft of the mass of the International Space Station equals approximately 10^4 times the total annual energy consumption of Switzerland...

	T_{long}^A	T_{long}^S	T_{trans}^A	T_{trans}^S
(I)	0.253	0.232	$1.564 \cdot 10^{-3}$	0.214
(II)	1.365	1.249	$1.089 \cdot 10^{-2}$	1.491
(IV)	258.9	236.9	1.678	229.8

Figure 3.10: Maximal longitudinal and transverse stress along the axis for an astronaut (superscript "A") and the spacecraft (superscript "S"). The quantities are measured in Nm^{-2}.

Chapter 4

Domains of Causality Violations near the Singularity

4.1 Kerr–Spacetime with $Q = 0$

Our investigation of causality violations will start from the Kerr solution of a rotating, but uncharged black hole.[1] One of the most startling features of the Kerr spacetime is our finding of domains near the singularity where timelike curves can possibly violate causality. These curves permit us theoretically to influence on our past. We will first calculate the extension of these domains in the case where $Q = 0$. Only in the next section, some considerations on the case $Q \neq 0$ will follow.

The Kerr solution[2] can be written as:

$$ds^2 = \frac{\Delta}{\Sigma}(dt - a\sin^2\vartheta d\varphi)^2 - \frac{\sin^2\vartheta}{\Sigma}(adt - (r^2 + a^2)d\varphi)^2 - \frac{\Sigma}{\Delta}dr^2 - \Sigma d\vartheta^2,$$

which may also be given in matrix form ($x^\mu = t, \varphi, r, \vartheta$):

$$g_{\mu\nu} = \frac{1}{\Sigma}\begin{pmatrix} \Delta - a^2\sin^2\vartheta & 2Mra\sin^2\vartheta & 0 & 0 \\ 2Mra\sin^2\vartheta & \sin^2\vartheta(a^2\Delta\sin^2\vartheta - (r^2 + a^2)^2) & 0 & 0 \\ 0 & 0 & -\frac{\Sigma^2}{\Delta} & 0 \\ 0 & 0 & 0 & -\Sigma^2 \end{pmatrix}.$$

Our subsequent focus will be curves describing orbits "around the inside" of the ring singularity. The curves have constant r and ϑ, but cover the full range of φ. The very special feature of the so–called φ–curves is their providing ways to have a constant t as well, which means that the curves are causally closed.

---

[1] For a short account on the subject of violations of causality due to uncharged singularities, see [33], p. 377ff.

[2] [4], p. 238. It is given here in the form of Boyer and Lindquist [23], p. 270. We changed the signature of the metric to our $(+ - - -)$ convention.

Closed φ–curves may thus be formalized:

$$
\begin{aligned}
t &= t_0 \\
\varphi &= -\lambda \\
r &= r_0 \\
\vartheta &= \vartheta_0
\end{aligned}
$$

where λ runs from zero to 2π to complete a full period. The closed φ–curves will be timelike iff

$$g_{\varphi\varphi} > 0.$$

Hence, the boundary of the domains where causality violations are possible is determined by

$$(r^2 + a^2)^2 - a^2 \Delta \sin^2 \vartheta = (r^2 + a^2)(r^2 + a^2 \cos^2 \vartheta) + 2Ma^2 r \sin^2 \vartheta = 0. \quad (4.1)$$

This equation demands r to be negative, therefore we replace $-r$ by z and rewrite (4.1) as

$$\frac{(z^2 + a^2)^2}{a^2(z^2 + a^2 + 2Mz)} = \sin^2 \vartheta, \qquad (z = -r). \qquad (4.2)$$

In the equatorial plane ($\vartheta = \frac{\pi}{2}$), we can expand (4.2) to the following result:

$$z_{\max}^4 + a^2 z_{\max}^2 - 2Ma^2 z_{\max} = 0,$$

which we reduce to

$$z_{\max}^3 + a^2 z_{\max} - 2Ma^2 = 0. \qquad (4.3)$$

This last step, which brings the equation down to be cubic, is not possible in solutions of charged black holes. We make the ansatz

$$z_{\max} = A \sinh(\frac{\alpha}{3}).$$

Since

$$
\begin{aligned}
\sinh^3(\frac{\alpha}{3}) &= \frac{1}{8}(\exp^\alpha - \exp^{-\alpha} - 3\exp^{\frac{\alpha}{3}} + 3\exp^{-\frac{\alpha}{3}}) \\
&= \frac{1}{4}(\sinh \alpha - 3 \sinh(\frac{\alpha}{3})),
\end{aligned}
$$

we obtain from (4.3)

$$
\begin{aligned}
A^2 &= \frac{4}{3}a^2 \qquad \text{and} \\
\alpha &= \sinh^{-1}(\frac{3M}{a}\sqrt{3}).
\end{aligned}
$$

Thus we get

$$z_{\max} = \frac{2a}{\sqrt{3}} \sinh\left[\frac{1}{3}\sinh^{-1}\left(\frac{3M}{a}\sqrt{3}\right)\right]. \qquad (4.4)$$

This equation delimits the range of z in the equatorial plane:

$$0 \leq z \leq z_{\max}.$$

At this point of the chapter, we include a short consideration on the maximal value of $z_{\max}$. We differentiate (4.4) with respect to a,

$$\frac{\partial z}{\partial a} = \frac{2M}{\sqrt{3}} \left[\sinh \chi - \alpha \cosh \chi \right], \tag{4.5}$$

where $\chi = \frac{1}{3} \sinh^{-1} \left(3\sqrt{3}/\bar{a} \right)$ and $\alpha = \sqrt{3/(\bar{a}^2 + 27)}$. For the total range of $\bar{a} \in [0, 1]$, we find $\alpha < 0$ and $\chi > \chi_{\min}$ because $\sinh^{-1}$ is strictly monotonically increasing. What is the sign of the derivative in (4.5)? In order to answer this question, we argue that

$$\frac{\partial}{\partial \chi} \left(\frac{\partial z}{\partial a} \right) \propto \cosh \chi - \alpha \sinh \chi,$$

which, in turn, is positive everywhere for all $\alpha < 1$, *i.e.* $\partial z / \partial a$ increases for growing χ. In case $\partial z / \partial a$ is positive at $\chi = \chi_{\min}$, we have proved

$$\frac{\partial z}{\partial a} > 0 \quad \forall a \in [0, 1].$$

Since $\chi_{\min} = \frac{1}{3} \sinh^{-1}(3\sqrt{3}) = 0.7834$, we obtain for the derivative

$$\left. \frac{\partial z}{\partial a} \right|_{\chi = \chi_{\min}} = \frac{M}{\sqrt{3}} \left[e^{\chi_{\min}} (1 - \alpha) - e^{-\chi_{\min}} (1 + \alpha) \right].$$

The range of α is very narrow indeed, *i.e.* $\sqrt{3/28} < \alpha < \sqrt{3/27}$. Thus, its variation is negligible. As a result for the derivative, we get

$$\left. \frac{\partial z}{\partial a} \right|_{\chi = \chi_{\min}} = \frac{M}{2} > 0.$$

As $z = z(\bar{a})$ rises all over the full range of $\bar{a}$, it has a supremum at $\bar{a} = 1$, *viz.* $z_{\max} = M$. Finally, we have therefore proved

$$|r| \leq M \quad \forall r \in \Gamma. \tag{4.6}$$

Similarly, the latitudinal—*i.e.* ϑ —direction is bound by

$$\sin^2 \vartheta_{\min} \leq \sin^2 \vartheta \leq 1, \tag{4.7}$$

where

$$\sin^2 \vartheta_{\min} = \min \left[\frac{(z^2 + a^2)^2}{a^2 (z^2 + a^2 + 2Mz)} \right]. \tag{4.8}$$

We find the minimal ϑ–value through calculating the partial derivative with respect to z in (4.8), using the convenient transformation $z = Mx$, and then computing the range of ϑ for different values a of the angular momentum per

unit mass in terms of the mass M. Below, we give a few results for typical values of $\bar{a}$:

$$
\begin{array}{ccccc}
\text{for} & \bar{a} = 0.1 & x = 0.0556 & \sin^2 \vartheta_{\min} = 0.1379 & \vartheta_{\min} = 21.80° \\
& \bar{a} = 0.3 & x = 0.1552 & \sin^2 \vartheta_{\min} = 0.3407 & \vartheta_{\min} = 35.71° \\
& \bar{a} = 0.6 & x = 0.2809 & \sin^2 \vartheta_{\min} = 0.5347 & \vartheta_{\min} = 46.99° \\
& \bar{a} = 1.0 & x = 0.4142 & \sin^2 \vartheta_{\min} = 0.6863 & \vartheta_{\min} = 55.94°
\end{array} \tag{4.9}
$$

Applying equation (4.2), we find a domain where it is possible to have closed, timelike φ–curves. It is exactly these causality violations which are of interest to us. Since we do not consider unphysical black holes, we will again exclude naked singularities with $\bar{a} > 1$. In case we have $\bar{a} = 0$, the spacetime is described by a Schwarzschild solution and there is no analytical extension beyond $r = 0$. Thus, $\bar{a}$ is confined to an interval $]0, 1]$. A rectangular (r, ϑ)–plot of the edge of Γ is given in Fig. 4.1.
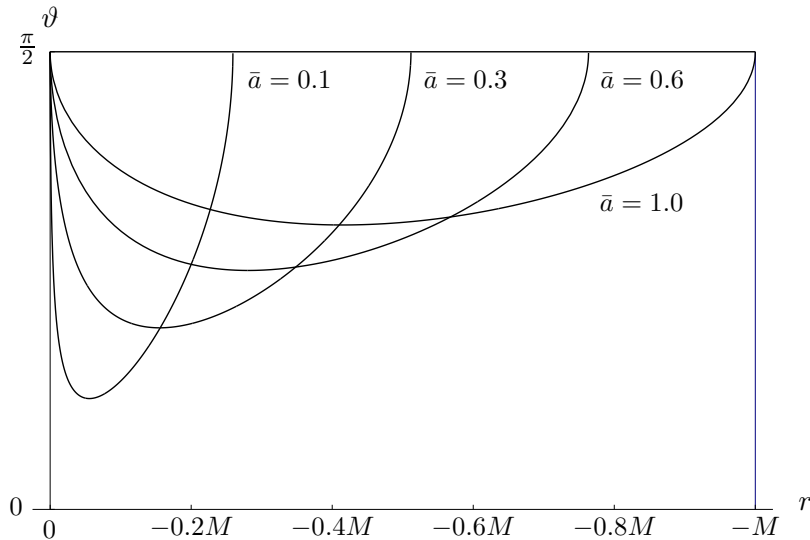
Figure 4.1: Edge of the domain Γ where causality violations are possible. Γ is to be found above the respective graphs.

The plot in Fig. 4.1 shows how the domain Γ contains with increasing angular momentum a larger and larger spread into the r–direction. Simultaneously, the domain stretches less and less towards the poles of the rotational axis. The same result was obtained analytically in (4.4) and (4.8) and numerically in (4.9).

There is another—presumably more instructive—way to present the domain Γ. We plot it in a "quasi–polar" diagram. In order to map the whole range $[-\infty, \infty]$ to a finite interval starting at zero, we apply the transformation

$$
R = \arctan(-z) + \frac{\pi}{2}.
$$

As a result of this transformation, we find $(r = -\infty)$ mapped to the origin, whereas $(r = 0)$ and $(r = \infty)$ are concentric circles of different radius. The

"quasi–polar" plots given in Fig. 4.2 have to be read as rotational bodies around the axis connecting the North Pole ($\vartheta = 0$) and the South Pole ($\vartheta = \pi$). The Γ–domain has a toroidal shape.

(a) $\bar{a} = 0.1$

(b) $\bar{a} = 0.3$

(c) $\bar{a} = 0.6$

(d) $\bar{a} = 1.0$
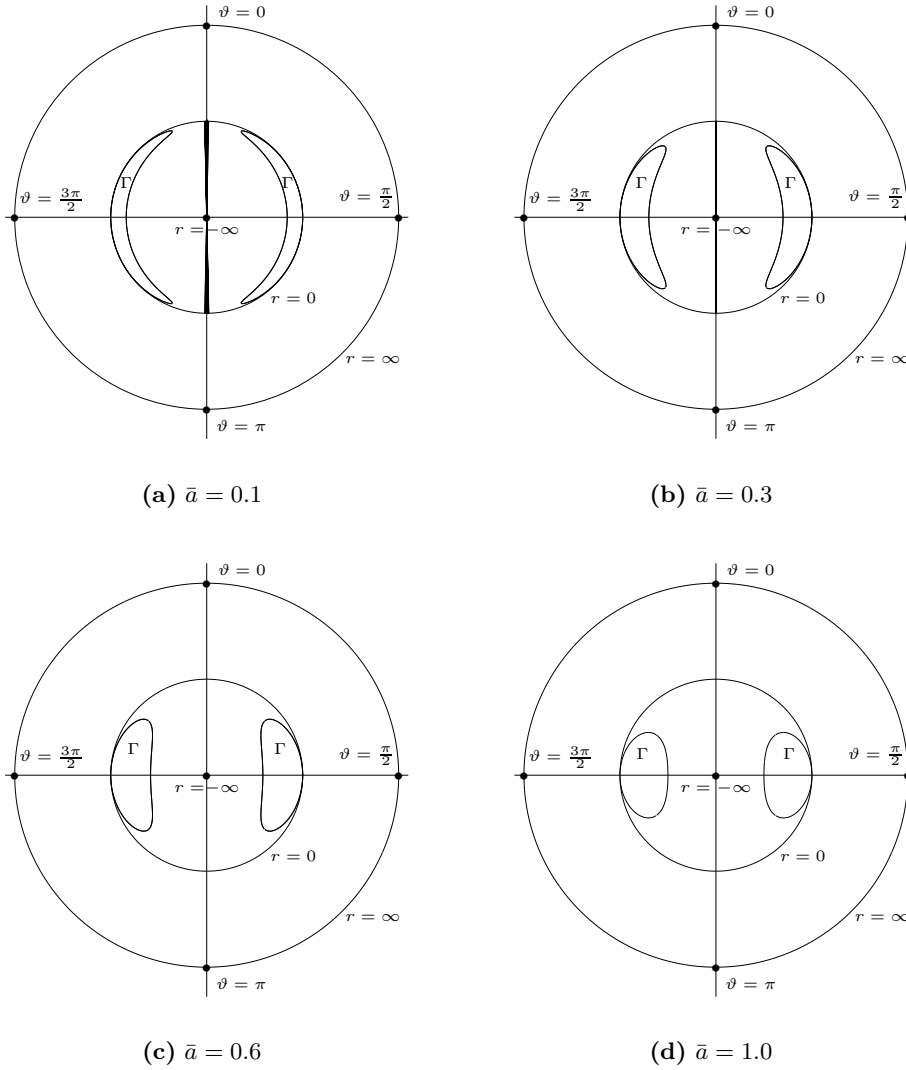
Figure 4.2: The domain Γ of potential causality violation in dependence on the angular momentum $\bar{a} = a/M$ of the black hole. The plots use "polar coordinates" $r \in [-\infty, \infty]$ and $\vartheta \in [0, 2\pi[$, where $r = -\infty$ is mapped to the origin and the radii $r = 0$ and $r = \infty$ are plotted as concentric circles.

Interpreting the diagrams, we can easily see what happens to Γ in case of an increasing angular momentum: it more and more approaches a torus with a circular intersection. This constriction would continue beyond the physical limit of $\bar{a} = 1$. In contrast to that, for a very small $\bar{a}$ we obtain a domain which covers nearly the whole sphere of ($r = 0$) from inside. Finally, as a strict rule clearly visible in (4.3), the domain Γ does not overlap into the section of positive r in case of uncharged singularities. If Q no longer vanishes, then Γ

propagates into the outside of the analytical extension with negative r.

4.2 Kerr–Newman Spacetime with $Q \neq 0$

The calculation of the Γ–domains for the Kerr–Newman solution is analogous to the preceding section on the uncharged case. The most startling feature of the domain of potential causality violation of a charged black hole is the extension into the "Schwarzschild–patch" of positive r. If $Q \neq 0$, equation (4.2) changes to

$$\sin^2 \vartheta = \frac{(z^2 + a^2)^2}{a^2(z^2 + a^2 + Q^2 + 2Mz)}, \qquad (z = -r). \qquad (4.10)$$

In the equatorial plane, this equation simplifies to

$$r^4 + a^2 r^2 + 2Ma^2 r - a^2 Q^2 \leq 0, \qquad (4.11)$$

where we cannot reduce the polynomial to a cubic expression since we have an "inhomogeneity" due to the charge. Though this complicates matters, we can find an analytical solution of equation (4.11). In case of equality, two real and two complex roots may be found. The lengthy form of the solution is confusing and therefore not worth being printed. For this reason, we are satisfied with a purely numerical analysis. This analysis will at least have a pedagogical impact.

In order to find out how much the range Γ extends towards the poles, we have to calculate the minimal ϑ value to which Γ reaches. It is again bound by (4.7), where

$$\sin^2 \vartheta_{\min} = \min \left[\frac{(z^2 + a^2)^2}{a^2(z^2 + a^2 + Q^2 + 2Mz)} \right] \qquad (4.12)$$

this time. We compute the minimum of the bracketed function of the (negative) distance $x = z/M$. We differentiate the right hand side of (4.12) with respect to x and obtain

$$\frac{2(\bar{a}^2 + x^2)(\bar{a}^2(x - 1) + x(2\bar{Q}^2 + x(x + 3)))}{M\bar{a}^2(\bar{a}^2 + \bar{Q}^2 + x(x + 2))^2} = 0.$$

The physical solution is the positive root of this equation. Subsequently, we give the results for several combinations of the parameters $\bar{a}$ and $\bar{Q}$. "x" designates the position of the minimum, and the "$\sin^2 \vartheta_{\min}$"– and "$\vartheta_{\min}$"–columns show the respective numerical results for the bounds of the range. As usually, the ϑ–angle is measured from the North Pole.

We have seen in the preceding section that the bound of ϑ recedes to the equatorial plane with increasing angular momentum. Clearly, in case of constant angular momentum, we have qualitatively the opposite effect for an increasing charge. The higher the charge, the more the domain Γ extends towards the poles. In order not to violate the cosmic censorship, the tables contain for large $\bar{a}$ only small charge $\bar{Q}$. The sprawling of the ϑ–range with increasing charge is also corroborated by Fig. 4.4. Here, the domain reaches much further down in the second subfigure—where we have $\bar{Q} = 0.6$—than in the first one, where $\bar{Q}$ is 0.1.

$\bar{a} = 0.1$			
$\bar{Q}$	x	$\sin^2 \vartheta_{\min}$	$\vartheta_{\min}$
0.1	0.0525	0.1274	20.91°
0.3	0.0341	0.0736	15.74°
0.6	0.0130	0.0261	9.30°
0.9	0.0061	0.0121	6.32°

$\bar{a} = 0.3$			
$\bar{Q}$	x	$\sin^2 \vartheta_{\min}$	$\vartheta_{\min}$
0.1	0.1524	0.3328	35.23°
0.3	0.1318	0.2779	31.81°
0.6	0.0841	0.1674	24.15°
0.9	0.0484	0.0948	17.94°

$\bar{a} = 0.6$			
$\bar{Q}$	x	$\sin^2 \vartheta_{\min}$	$\vartheta_{\min}$
0.1	0.2784	0.5294	46.69°
0.3	0.2597	0.4895	44.40°
0.6	0.2066	0.3831	38.24°

$\bar{a} = 0.9$			
$\bar{Q}$	x	$\sin^2 \vartheta_{\min}$	$\vartheta_{\min}$
0.1	0.3818	0.6521	53.86°
0.3	0.3651	0.6229	52.12°

Figure 4.3: The ϑ–range for several values of the parameters $\bar{a}$ and $\bar{Q}$. For higher angular momenta $\bar{a}$, only smaller values are possible for the charge $\bar{Q}$ due to our decision to confine ourselves to singularities with horizons between the singular ring and positive infinity, and thus respecting cosmic censorship.

Again, the cosmic censorship is respected. It indicates that in Fig. 4.4(b) there are only three examples of Γ–domains. Since $1 - \bar{Q}^2 \approx 0.6$ for $\bar{Q} = 0.6$, the plot for $\bar{a} = 0.6$ is left out as it would have been very similar to the one with $\bar{a} = 0.8$.

The most interesting feature of a domain of potential causality violation caused by a rotating and *charged* singularity is certainly the extension of the domain into the realm of positive radial coordinate, as we have stated earlier. This extension, of course, is more extreme for higher charges. Fig. 4.4 may give an idea of what happens for low and for high charges. With a rising charge, the whole domain migrates more and more into Schwarzschild–like regions of positive r. We have supplied only the "Cartesian" plots since the "quasi–polar" ones do not change qualitatively from Fig. 4.2 and the trespassing of the domain can be detected easier that way.

Concluding, the domain Γ is subjected by a high charge of the singularity to translation towards positive values of r as well as to diffusion into "polar" regions of small ϑ–angles.
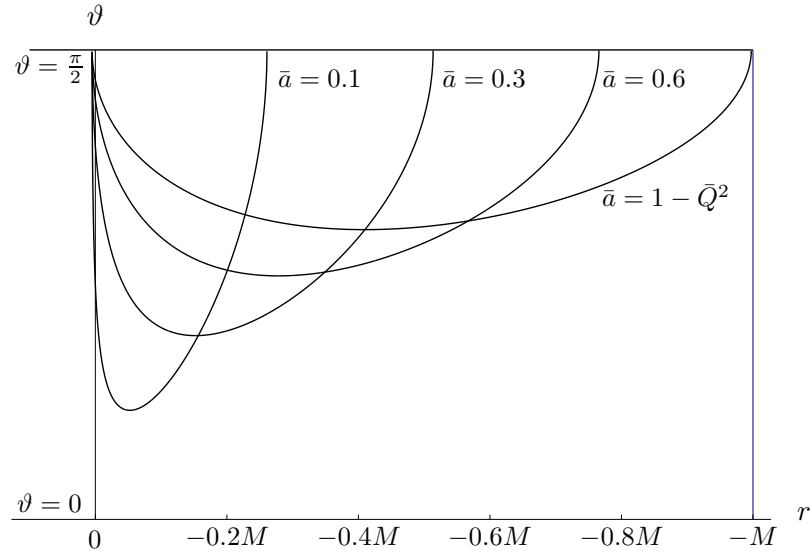
(a) $\bar{Q} = 0.1$
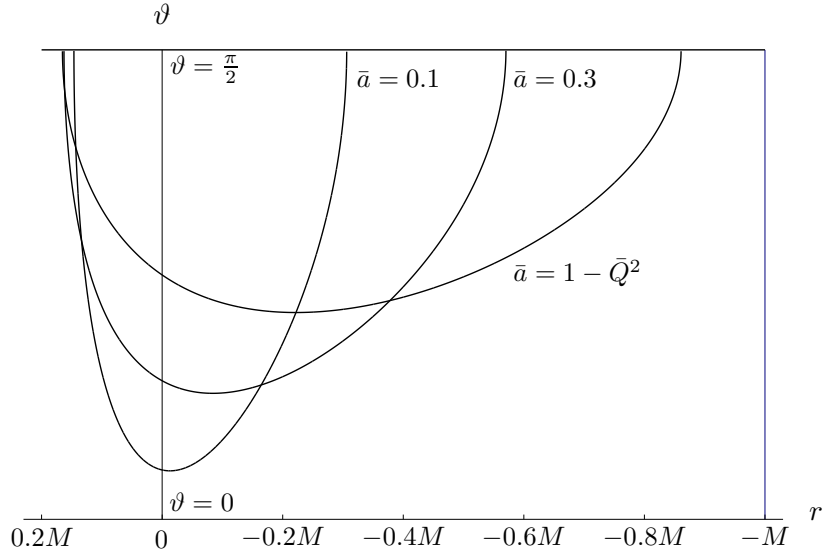
(b) $\bar{Q} = 0.6$

Figure 4.4: The range of potential causality violations for a small and a large charge $\bar{Q} = Q/M$ of the singularity. Here again, Γ is to be found above the lines.

Chapter 5

Time Machines

We are finally equipped with all tools necessary to launch the core issue of this essay. Our astronauts have reached the distant EKN− patch of a massive singularity, presumably situated at the centre of a galaxy. The crew has survived the tidal storm on their dive into the galactic nucleus. The navigator of our space craft knows the precise extension of the domain where the violation of causality is possible in dependence of the parameters of the black hole. The quantitative knowledge of these parameters is thus vital for the success of our enterprise. We have seen in the previous chapter that closed timelike curves along φ–coordinate lines exist in a certain proximity of the ring. As we will argue hereafter, it is even possible to find curves along which we travel backwards in time. Of course, we are not allowed to include null or even spacelike curves in our considerations. Trivially, our time travelling craft has to move on curves directed towards to future, *i.e.* into the future light cone. We impose this condition to make sure the biological clocks of the crew members tick normally. Clearly enough, such travels raise fundamental problems with causality. However, we will not discuss them philosophically. We confine ourselves to the theoretical feasibility of time travel in Kerr–Newman spacetime.

The trajectory of the spaceship has to meet certain requirements. Therefore we build the following conditions into the curve $x^\mu(\lambda)$ (where $x^\mu = (t, \varphi, r, \vartheta)$) which describes the trajectory followed by the spacecraft:

1. The curve needs to be timelike:

$$g_{\mu\nu}\dot{x}^\mu\dot{x}^\nu > 0. \tag{5.1}$$

2. It has to point towards the future:

$$g_{\mu\nu}T^\mu\dot{x}^\nu > 0, \tag{5.2}$$

   where the timelike vector field T^μ designates the future light cone at each point.

3. Finally, a time machine has to yield a gain of time:

$$\dot{t} < 0. \tag{5.3}$$

We employ a simple ansatz for the trajectory of our journey by keeping r and ϑ constant,

$$x^\mu = \begin{pmatrix} \kappa\lambda \\ -\lambda \\ r_0 \\ \vartheta_0 \end{pmatrix}, \tag{5.4}$$

where $\lambda \in [0, 2\pi[$ for one revolution.

Before we launch our spaceship, we should pause and check the foundations of our calculations. Are there curves existing which really show all the properties (5.1) to (5.3)? We will carry through some fundamental considerations beforehand.

The derivatives of x^μ with respect to λ span a four–dimensional tangential space in every event, *i.e.* in every point of the manifold. Since we have $\dot{r} = \dot{\vartheta} = 0$ for the curves at stake, let us therefore consider the two–dimensional intersection with $\dot{t}$ and $\dot{\varphi}$ as basis vectors. Early letters in the Latin alphabet should indicate indices in this two–dimensional intersection. Magic is not part of science and for this reason, the curve has to be timelike, $g_{ab}\dot{x}^a\dot{x}^b > 0$. In order to simplify the calculation we transform to another basis ("σ–basis"),

$$\dot{\sigma}_1 = \sqrt{\frac{\Delta}{\Sigma}}\left(\dot{t} - a\sin^2\vartheta\dot{\varphi}\right),$$
$$\dot{\sigma}_2 = \sqrt{\frac{\sin^2\vartheta}{\Sigma}}\left(a\dot{t} - \left(r^2 + a^2\right)\dot{\varphi}\right).$$

The transformation back to the old basis then reads:

$$\dot{t} = \frac{1}{\sqrt{\Delta\Sigma}}\left[\left(r^2 + a^2\right)\dot{\sigma}_1 - \sqrt{\Delta}a\sin\vartheta\dot{\sigma}_2\right],$$
$$\dot{\varphi} = \frac{1}{\sqrt{\Delta\Sigma}}\left(a\dot{\sigma}_1 - \frac{\sqrt{\Delta}}{\sin\vartheta}\dot{\sigma}_2\right).$$

The property (5.1) simplifies to $(\dot{\sigma}_1)^2 - (\dot{\sigma}_2)^2 > 0$. This condition creates two null cones in the Minkowski–like two–dimensional space. Which one is pointing towards the future? The tangent vector $u = (1,0)$ with respect to the σ–basis is certainly timelike and transforms to

$$\bar{u} = \frac{1}{\sqrt{\Delta\Sigma}}\left(r^2 + a^2, a\right)$$

with respect to the $(\dot{t}, \dot{\varphi})$–basis as well as to the $(\dot{v}, \dot{\eta})$–basis of the advanced Eddington–Finkelstein type of coordinates of Appendix B. According to [34], p. 220, time orientation in AKN is given by

$$T_a^\mu = \left(1, 0, -\frac{r^2 + a^2 - \Delta}{2\Sigma}, 0\right).$$

Now, we are in the position to calculate whether the above mentioned tangent vector points towards the future. The result is easily found:

$$g_{\mu\nu}T_a^\mu\dot{x}_a^\nu = \sqrt{\frac{\Delta}{\Sigma}},$$

which is real and positive everywhere where $\Delta > 0$ because Σ is positive for any real r and ϑ. Concluding, the tangent vector $u = (1,0)$ in the σ–basis is time-like and points towards the future for any external Kerr–Newman spacetime, presuming the spacecraft stays outside IKN. Is there a curve which has not only the properties (5.1) and (5.2), but also property (5.3)? If we set $\dot{\sigma}_1 = \cosh\chi$ and $\dot{\sigma}_2 = \sinh\chi$, we may cover the whole future null cone. The requirement $\dot{t} < 0$ then leads to

$$\sqrt{\frac{1}{\Delta\Sigma}} \left(\left(r^2 + a^2\right)\cosh\chi - \sqrt{\Delta}\, a \sin\vartheta \sinh\chi \right) \quad < \quad 0. \qquad (5.5)$$

In case we find a χ which satisfies inequality (5.5), we have shown the existence of curves meeting all requirements for time travel. The square root is a positive real number for all domains of interest and may therefore be divided out. We obtain a new inequality,

$$\tanh\chi \quad > \quad \frac{r^2 + a^2}{\sqrt{\Delta}\, a \sin\vartheta}.$$

The tanh–function is confined to adopting values between -1 and 1 and ϑ ranges from 0 to π. Hence, we have $\sin\vartheta > 0$.

Obviously, the sign of the angular momentum a does matter here and also for the sign of $g_{t\varphi}$ of the Boyer–Lindquist coordinates, which—in turn—plays a role for the sign of the mixed term of inequality (5.1). Thus, a change in the rotational sense of the singular ring also shifts the light cone, or—technically spoken—the roots of equation $g_{\mu\nu}\dot{x}^\mu\dot{x}^\nu = 0$.

For $a > 0$ (“clockwise”) and the negative sign which was added in (5.4) prospectively, we find both roots in the negative zone of κ. This would meet requirement (5.3). If either the rotation was “counterclockwise” ($a < 0$) or the φ–curve “clockwise” ($\dot{\varphi} > 0$)—but not both—, the roots would shift towards positive κ and inhibit the planned time travel. The situation is symmetrical regarding the orientation of both rotations, the one of the singularity and the one of the space journey. The relevant aspect is just to know that the singularity and the space craft have to rotate with opposing orientation in order to allow the possibility of time travel into the past. Without loss of generality, we inaugurate the conventions $a > 0$ and $\dot{\varphi} < 0$ for the subsequent considerations.

Unfortunately, a convention does not help in making apodictic statements on physical realities. Since tanh is an asymmetrical function, we have proven above the existence of causality violating curves if we find an χ which satisfies the inequality

$$\chi \quad > \quad \tanh^{-1}\left(\frac{r^2 + a^2}{\sqrt{\Delta}\, a \sin\vartheta} \right).$$

Since $\tanh^{-1}$ is only defined for arguments between -1 and 1, the square of the argument must necessarily satisfy

$$\frac{\left(r^2 + a^2\right)^2}{\Delta a^2 \sin^2\vartheta} \quad < \quad 1 \qquad (5.6)$$

if a χ is to comply with (5.6). But inequality (5.6) is equivalent to the condition $g_{\varphi\varphi} > 0$ in (4.11). We have just proved the following theorem:

Theorem 1 *Spiralling curves (5.4) satisfying properties (5.1) to (5.3) are found in the same domain Γ as the closed timelike φ–curves (4.1).*

For these reasons, we are confident about the existence of causality violating curves and may turn our interest towards the actual journey.

5.1 Gain in Time

The main objective of our time travel is—of course—to go back in time as much and as quickly as possible. Thus, the quantity we might call "gain in time" and designate with Δt is introduced. The gain is a function of κ, $\Delta t = \Delta t(\kappa)$. The gain in time per period is defined by

$$\Delta t \;\doteq\; t\,|_{\varphi=2\pi} -t\,|_{\varphi=0}\,.$$

For a curve such as (5.4), we obtain

$$\Delta t \;=\; 2\pi\kappa. \tag{5.7}$$

To reach the past, Δt and therefore κ have to be negative according to condition (5.3). We are striving for a gain in time as large as possibly attainable without either hurting travellers nor physical laws. To this end, κ should be as negative as possible. Timelikeness will eventually define a limit for the negativity of κ. This limit is a function of the parameters of the singularity as well as of in what position the spiraling down along the time–axis takes place. Ultimately, then, the gain in time is also indirectly dependent upon M, a, Q, r, and ϑ. And it is not the only quantity which shall direct our itinerary.

5.2 Duration per Revolution

The duration of one revolution of the space craft is defined as the interval of proper time between two subsequent events of passing by the same spot in space. A central postulate of General Relativity states that the proper time ds between λ and $\lambda + d\lambda$ along a timelike path measured by an ideal clock is given by[1]

$$ds \;=\; d\lambda\sqrt{g_{\mu\nu}\dot{x}^\mu\dot{x}^\nu}. \tag{5.8}$$

This postulate allows us to calculate the time which expires during one period. Again, it is emphasized that we have chosen the convention $\dot\varphi = -1$ and $a > 0$. Clearly, this convention does not alter the duration of the flight, but it is still important for calculating correctly:

$$\begin{aligned}
\Delta s &= \int_0^{-2\pi} \sqrt{g_{ab}\dot{x}^a\dot{x}^b}\,\frac{d\varphi}{\dot\varphi}, \\
&= 2\pi\sqrt{g_{ab}\dot{x}^a\dot{x}^b}, \tag{5.9}
\end{aligned}$$

[1]Cf. [34], p. 45.

where the expression under the square–root is a polynomial in κ,

$$
\begin{aligned}
g_{ab}\dot{x}^a\dot{x}^b &= g_{tt}\kappa^2 - 2g_{t\varphi}\kappa + g_{\varphi\varphi}, \\
&= \frac{\Delta - a^2\sin^2\vartheta}{\Sigma}\kappa^2 - \frac{2asin^2\vartheta}{\Sigma}\left(r^2 + a^2 - \Delta\right)\kappa \\
&\quad + \frac{\sin^2\vartheta}{\Sigma}\left[\Delta a^2\sin^2\vartheta - \left(r^2 + a^2\right)^2\right].
\end{aligned}
\tag{5.10}
$$

This factor—which will be used later again—depends only on the r– and ϑ–coordinates. The duration should not exceed a reasonable measure compared to the gain in time. In order to optimize this relation, we introduce a quantity "w" providing the ratio at stake:

$$
w \doteq \frac{\Delta t}{\Delta s}.
$$

w is a dimensionless quantity whose absolute value should be large enough to pay out the effort made by the crew. Again, in case the travel leads into the past, w is negative. For our itinerary, we have

$$
w = \frac{\kappa}{\sqrt{g_{ab}\dot{x}^a\dot{x}^b}}
\tag{5.11}
$$

as time gain per travel duration. For frankness sake, we introduce the terminology

$$
F(M, a, Q; r, \vartheta; \kappa) \doteq g_{\mu\nu}\dot{x}^\mu\dot{x}^\nu,
\tag{5.12}
$$

where $\dot{x}^\mu$ is given by the curve (5.4). $F = F(M, a, Q; r, \vartheta; \kappa)$ has the form of a second order polynomial in κ.

A journey like ours will not only take some travelling time, but also cost a considerable amount of energy and this shall be calculated in the next chapter.

5.3   Tidal Forces on the Time Travel

Speaking precisely, what we calculate in this section are not the tidal forces, but rather the relative acceleration per meter between two adjacent geodesics. For this end, we may well profit from work done earlier in this essay. We have seen in section 3.4.2 that the longitudinal relative acceleration per distance is given by

$$
\frac{b_2}{\delta x^2} = -R_{1212},
$$

and the transverse by

$$
\frac{b_3}{\delta x^3} = -R_{1313}.
$$

Using (2.28), we obtain

$$
\begin{aligned}
\frac{b_2}{\delta x^2} &= \frac{1}{\Sigma^3}\left[2Mr\left(r^2 - 3a^2\cos^2\vartheta\right) - Q^2\left(3r^2 - a^2\cos^2\vartheta\right)\right], \\
\frac{b_3}{\delta x^3} &= -\frac{1}{\Sigma^3}\left[Mr\left(r^2 - 3a^2\cos^2\vartheta\right) - Q^2\left(r^2 - a^2\cos^2\vartheta\right)\right].
\end{aligned}
\tag{5.13}
$$

To avoid a catastrophe, tidal forces should not exceed a certain threshold. The relative acceleration per distance should not normally be larger than some 10s^{-2} which corresponds to a stress of about 10^2Nm^{-2}. The tidal forces arising from the strong curvature near the singular ring will thus set limits to our boldness.

5.4 Charge Dependence

We have argued in section 3.5 that the charge of a Kerr–Newman black hole will always remain tiny compared to its angular momentum and to its mass. The argument given there provides good reasons to set $Q = 0$. Furthermore, Δ and $g_{\mu\nu}$ depend only on even powers of Q. Hence, the derivatives of the components of the metric with respect to r and ϑ as well as the inverse metric contain only even powers of Q. As a result, the affine connection and the Riemann curvature tensor are also free of odd powers of Q. Finally, all the quantities $\Delta t, \Delta s, w, b_2/\delta x^2$, and $b_3/\delta x^3$ are only functions of even powers of Q—and of course of the other parameters. We will learn to understand in the following chapter that the acceleration $\wp$ necessary to keep the craft on the trajectory of our time travel depends also only on the square of the charge.

If we construct the derivatives of the above derived entities with respect to Q, we obtain therefore only terms with odd powers of Q. At $Q = 0$ all these derivatives vanish consequently. This means that none of the mentioned quantities largely depends on the charge in the region of $Q = 0$. As the charge will be confined to small sizes relative to the angular momentum and the mass of the singularity, we set

$$Q \;=\; 0$$

for the further analysis. Another choice which dates back to section 3.4.2 regards the mass of the black hole. For the convenience of the travellers, it has proved to be wise to select a galactic nucleus of at least

$$M \;=\; 10^7 M_\odot,$$

as we have already postulated in (3.32). We will keep on calculating within a spacetime where this holds.

5.5 Latitudinal Dependence

It is intuitively clear that the physical quantities introduced in this chapter will strongly be influenced by whether we fly our spirals in the neighbourhood of the equatorial plane or not. The tidal forces are the higher, the closer we get to the singular ring. The duration of one period of the journey depends not only on the ϑ–angle, but also largely on κ. In case κ increases in absolute value, the frontier of the domain where time travel is an option moves towards the equatorial plane. Therefore, timelikeness of the curve has to be carefully watched.

5.5.1   Tidal Accelerations

We investigate the latitudinal behaviour of the relative acceleration of two points of mass at a distance of one meter to each other to start with. According to (5.13), the absolute value of the longitudinal relative acceleration for an uncharged singularity is twice as large as of the transverse one. Regardless of the differing sign, we will confine ourselves to the longitudinal case, assuming that if we are able to control this direction, the other will not cause any trouble.

For a thorough assessment, we will have to develop an idea of an answer to the question: "How strong a relative acceleration could a human resist without being torn asunder?". According to [1], p. 862, a human body will break in case the tension or pressure upon it exceeds 100 atmospheres. Using the same measures as in (3.35), the absolute value of the relative acceleration should not transgress

$$R_{1212}^{\max} \quad \simeq \quad 2.5 \cdot 10^4 \frac{1}{\mathrm{s}^2}. \tag{5.14}$$

Naturally, the tidal forces are not supposed to even come close to this value, because the journey would certainly not be a wholesome one then.

The trajectory parameter κ does certainly not influence the tidal accelerations as the reader can quickly see from (5.13). We shall study their dependence from the rotation of the ring and the distance from it.

For a short analytical account to start with, we calculate the derivative of the longitudinal relative acceleration (5.13) with respect to the angle ϑ,

$$\frac{\partial}{\partial \vartheta}\left(\frac{b_2}{\delta x^2}\right) \quad = \quad -\frac{24Mra^2}{\Sigma^4}\sin\vartheta\cos\vartheta\left(r^2 - a^2\cos^2\vartheta\right), \tag{5.15}$$

which leads us to the three extrema $\vartheta_1 = 0, \vartheta_2 = \pi/2$, and $\vartheta_3 = \arccos|r/a|$. Building the second derivative helps to identify the character of the extremal points:

$$\begin{aligned}
\frac{\partial^2}{\partial\vartheta^2}\left(\frac{b_2}{\delta x^2}\right) \quad = \quad & -\frac{24Mra^2}{\Sigma^5}\Big[\left(r^2 - a^2\cos^2\vartheta\right)\left\{\Sigma\left(\cos^2\vartheta - \sin^2\vartheta\right)\right. \\
& \left. -8a^2\sin^2\vartheta\cos^2\vartheta\right\} + 2\Sigma a^2\sin^2\vartheta\cos^2\vartheta\Big].
\end{aligned}$$

By means of this equation, we easily recognize the principal structure of $\frac{b_2}{\delta x^2}$. Clearly, for different regions of the parameter space, the behaviour of the function in question will be different. We distinguish three parts of the parameter space: (1) $|r| < |a|$, (2) $|r| = |a|$, and (3) $|r| > |a|$. In the first part (1), we find maxima at ϑ_1 and at ϑ_2 because r is always negative in case $Q = 0$, and a minimum at ϑ_3. In case of equality (2), ϑ_3 stops being well defined and we have to be content with two extrema, *viz.* a maximum at ϑ_2 and an inflection point at ϑ_1. This inflection point is at the same time a minimum of the function inside the interval $\vartheta \in [0, \pi/2]$. In the third scenario (3), everything there happens is a minimum at ϑ_1 and a maximum at ϑ_2. As can also be recognized in the subsequent plots for the quantitative analysis, we find a maximum at $\vartheta = \pi/2$ in any case. Let us proceed to some quantitative considerations.

First, then, we have a closer look on the impact of the rotation of the singular ring upon the relative acceleration. Fixing the value of the radial distance r appropriately, we give two plots of the latitudinal dependence for two different angular momenta $\bar{a}$.

<table>
<tr><td>(a) $a = 0.1M$, $|r| > |a|$</td><td>(b) $a = 0.9M$, $|r| < |a|$</td></tr>
</table>
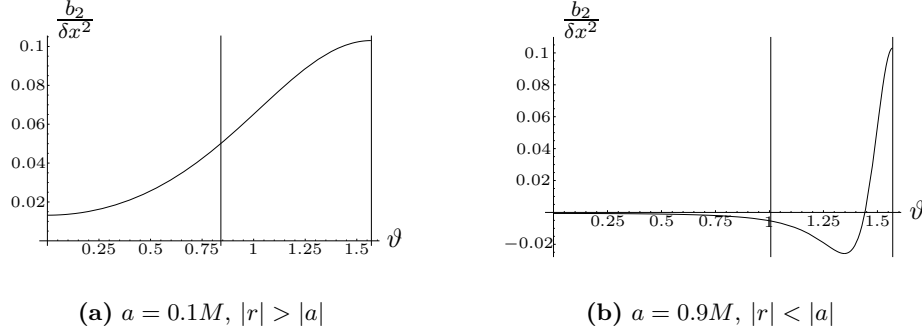
Figure 5.1: Longitudinal relative acceleration in units of s^{-2} as function of angle ϑ for two different $\bar{a}$, where $\vartheta \in [0, \pi/2]$. We have set $M = 10^7 M_\odot$, $Q = 0$ and $r = -0.2M$. The vertical lines indicate the Γ domain. The reader should take into consideration that the border of Γ designates the region where *closed* timelike curves are possible and where $\kappa = 0$ therefore.

Whereas the shape of both Figures 5.1 is quite considerably distinct for different angular momenta, the absolute value of the maximum is not. Clearly, for both $\bar{a}$, the relative acceleration will not even get close to the threshold $R_{1212}^{\max}$ for any ϑ. The same can be said of any other value of the angular momentum within the allowed range.

As we have already stated in section 3.5, the angular momentum of the black hole is expected to be rather large than small. Fixing a at $0.6M$ therefore, we briefly mention the radial dependence of the relative acceleration with two graphical examples. One expects the tidal forces to increase when approaching the singular ring. Indeed, intuition is not misleading in that case, as the plots in Fig. 5.2 indicate.

<table>
<tr><td>(a) $r = -0.05M$, $|r| < |a|$</td><td>(b) $r = -0.6M$, $|r| > |a|$</td></tr>
</table>
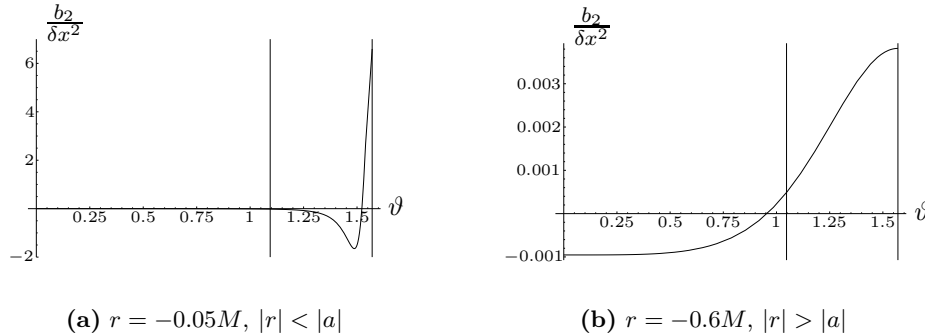
Figure 5.2: Longitudinal relative acceleration in units of s^{-2} as function of angle ϑ for two different radial distances r. We have set $M = 10^7 M_\odot$, $Q = 0$ and $a = 0.6M$. The vertical lines indicate the Γ domain.

Although the tidal accelerations increase near the singularity, even for a small radial distance $r = -0.01M$, the relative acceleration in the equatorial plane is bound by a maximum at about $\frac{b_2}{\delta x^2} = 825\text{s}^{-2}$ for the same values as in Fig. 5.2, which is still small enough. As we shall see later on, it is not advantageous for an efficient time gain to stay too close to the ring. Thus, there are no severe problems emerging from the radial dependence if one stays away from the ring. Summarizing, excluding the immediate neighbourhood of the singularity, all cuts through the parameter space of the latitudinal dependence of the tidal accelerations clearly pose no danger for the bones of the craft's crew.

5.5.2 Duration of Journey

How does the height above the equatorial plane influence the duration of one revolution of the time travel? The duration does not only depend on the parameters ϑ, r, and a—M and Q are still fixed—, but also on κ. The hyperspaces of constant κ of the parameter space are therefore not identical for all values.

Regarding the analytical considerations which are yet to follow in this chapter, we differentiate the function $F = F(M, a, Q; r, \vartheta; \kappa)$ of (5.12) where $Q = 0$, *i.e.*

$$F = \frac{1}{\Sigma}\Big[\left(\Delta - a^2 \sin^2\vartheta\right)\kappa^2 - 4Mra\sin^2\vartheta\kappa$$
$$+ \sin^2\vartheta\left\{\Delta a^2\sin^2\vartheta - \left(r^2 + a^2\right)^2\right\}\Big], \tag{5.16}$$

with respect to ϑ,

$$\frac{\partial F}{\partial \vartheta} = \frac{2\sin\vartheta\cos\vartheta}{\Sigma^2}\Big[-2Mra^2\kappa^2 - 4Mra\kappa\left(r^2 + a^2\right)$$
$$+\Delta a^2\sin^2\vartheta\left(\Sigma + r^2 + a^2\right) - \left(r^2 + a^2\right)^3\Big]. \tag{5.17}$$

Then, the derivative of the duration Δs from (5.9) with respect to ϑ is given by

$$\frac{\partial(\Delta s)}{\partial \vartheta} = \frac{\pi}{\sqrt{F}}\frac{\partial F}{\partial \vartheta}.$$

The extremal points are generally found at $\vartheta_1 = 0$ and $\vartheta_2 = \pi/2$, which is easily acknowledged after reference to (5.17). We spare the somewhat lengthy analysis of these extrema in terms of higher derivatives and confirm that trends from computer analysis show that we find a maximum at ϑ_2 for all but exotic combinations of the parameters. The reader may consult Figures 5.3–5.5 for a pedagogical illustration to this end.

Probing the intersections through the phase space for several values of $\bar{a} \in [0, 1]$, we find that for any given $\bar{r}$ in the allowed range, there appears a domain wherein the curve turns spacelike and should therefore be avoided. This domain usually covers rather the low angular momenta than the high ones. As we presume the rotation to be rather quick, we confine ourselves to the range

(a) $a = 0.5M$ **(b)** $a = 0.9M$
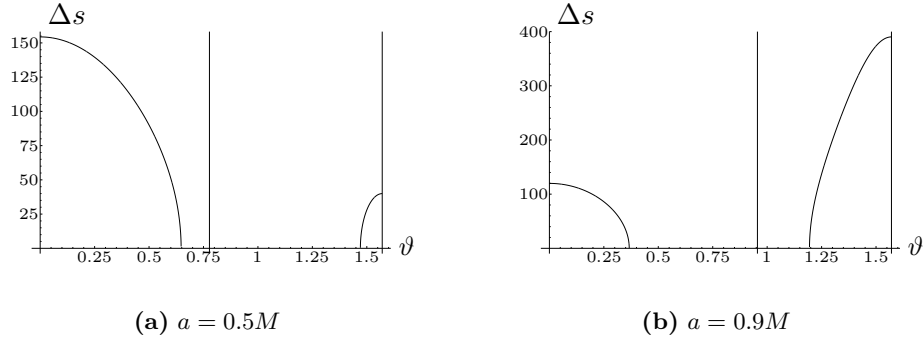
Figure 5.3: Duration Δs in seconds as function of ϑ for two different angular momenta a. Vertical Lines delimit Γ. Parameter fixations: $M = 10^7 M_\odot$, $Q = 0$, $r = -0.3M$, $\kappa = -0.3M$.

above the domain of spacelike curves and give in Fig. 5.3 plots for different angular momenta.

The time necessary to complete a full revolution rises at the same time as the rotation speeds up and the curve moves towards the equatorial plane. On the other hand, the scope of clearance for κ to become more negative—while the curve still stays timelike—grows. Generally speaking, the higher efficiency we obtain in our time travel, the more it costs in terms of temporal expenditure, tidal accelerations, and, as we shall see in the next chapter, energy consumption. We may stress at this point, however, that the closer to the border of the Γ–domain we aim to realize our journey with a fixed κ, the more fuel our engines will burn. As long as we can afford to stay in the centre of Γ without being torn or without turning too old before the returning from the time travel, we should do so in order to save energy.

Turning our attention the voyage's length due to radial variation, we study Fig. 5.4. Again, we see that only a small range of Γ is permitted in case of a very small κ, *viz.* the domain just left of the right vertical line where the graph does not dip into the negative realm.

(a) $r = -0.05M$ **(b)** $r = -0.4M$
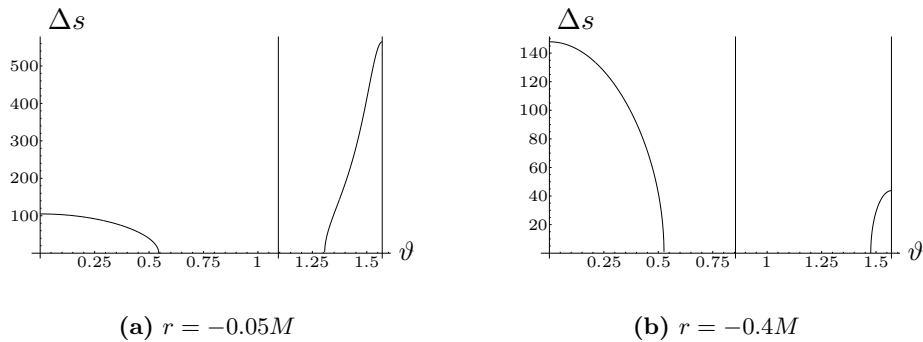
Figure 5.4: Duration Δs in seconds as function of ϑ for two different radial distances r. Vertical Lines delimit Γ. Parameter fixations: $M = 10^7 M_\odot$, $Q = 0$, $a = 0.6M$, $\kappa = -0.3M$.

Since $r = -0.41M$ is situated on the border of Γ for the parameter values used in Fig. 5.4 for calculation, the duration per revolution is smaller for radial coordinate values close to the edge of Γ than for those in its core. However, the potential time gain is, of course, also smaller near the edge and will eventually vanish on the borderline. Evidently, the flying time per period is the longest on the equatorial plane.

The duration is, of course, also a function of the time gain producing variable κ. The investigation of its influence upon the duration per period is due next. Eventually, we read from the plots in Fig. 5.5 that the range for potential causality violations is much broader in the "vertical" direction for smaller absolute values of κ than for curves travelling backwards in time in a more hastily manner. For $\kappa = 0$, we have closed timelike φ–curves orbiting the singular ring. It is therefore clear that in this case, the permitted range of positive flying time extends all over the domain Γ.

(a) $\kappa = 0$ **(b)** $\kappa = -0.45M$
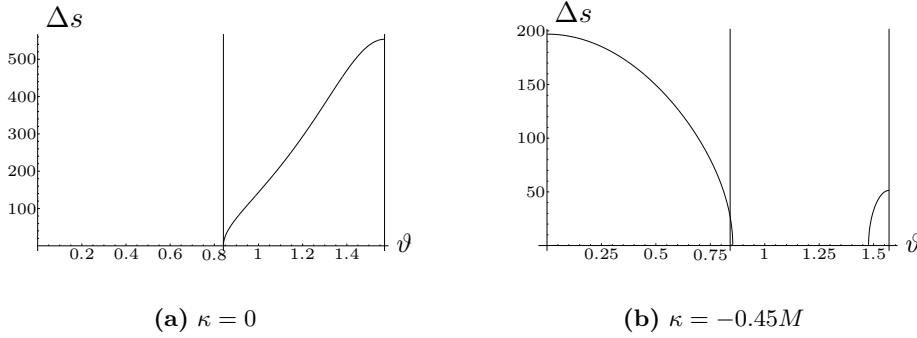
Figure 5.5: Duration Δs in seconds as function of ϑ for two different trajectory parameters κ. Vertical Lines delimit Γ. Parameter fixations: $M = 10^7 M_\odot$, $Q = 0$, $a = 0.6M$, $r = -0.2M$.

Obviously enough, this island we are interested in is peeling off like an onion, layer by layer with an increasingly steep travel into the past. Perhaps surprisingly, for a better κ–value, we get *ceteris paribus* a shorter flying time. For this reason, we shall take the time gain per duration ratio into account.

Finding extrema of $w(\vartheta)$, we differentiate (5.11) with respect to ϑ and find

$$\frac{\partial w}{\partial \vartheta} = -\frac{\kappa}{2\sqrt{F^3}} \frac{\partial F}{\partial \vartheta}$$

From (5.17), we have extrema at $\vartheta_1 = 0$ and $\vartheta_2 = \pi/2$. From the fact that

$$\frac{\partial^2 w}{\partial \vartheta^2} = -\frac{\kappa}{4\sqrt{F^3}} \left[2F \frac{\partial^2 F}{\partial \vartheta^2} - 3 \left(\frac{\partial F}{\partial \vartheta} \right)^2 \right],$$

where the second derivative of F with respect to ϑ is

$$\begin{aligned}
\frac{\partial^2 F}{\partial \vartheta^2} = {} & \frac{1}{\Sigma^3} \left\{ 2\Sigma \left(\cos^2 \vartheta - \sin^2 \vartheta \right) + 8a^2 \sin^2 \vartheta \cos^2 \vartheta \right\} \Big[\Big\{ -2Mra^2\kappa^2 \\
& -4Mra\kappa \left(r^2 + a^2 \right) + \Delta a^2 \sin^2 \vartheta \left(\Sigma + r^2 + a^2 \right) \\
& - \left(r^2 + a^2 \right)^3 \Big\} + 8\Delta\Sigma a^2 \sin^2 \vartheta \cos^2 \vartheta \Big],
\end{aligned} \qquad (5.18)$$

we obtain for the second derivative of w at the extremal point

$$\left.\frac{\partial^2 w}{\partial \vartheta^2}\right|_{\vartheta=\vartheta_2} = -\frac{\kappa}{r^4 \sqrt{F^3}}\Big[2Mra^2\kappa^2 + 4Mra\kappa\left(r^2 + a^2\right)$$
$$+ \left(r^2 + a^2\right)\left\{\left(r^2 + a^2\right)^2 - \Delta a^2\right\} - \Delta r^2 a^2\Big].$$

We see that $w(\vartheta_2)$ is a maximum for small κ. In this case, the terms in the lower line—which are only of first order in κ—contribute more and from (5.6), we make sure that $\partial^2 w(\vartheta)/\partial\vartheta^2 < 0$ for $\vartheta = \pi/2$ and $\kappa < 0$ wherever the curve is timelike.

(a) $\kappa = -0.01M$ (b) $\kappa = -0.45M$
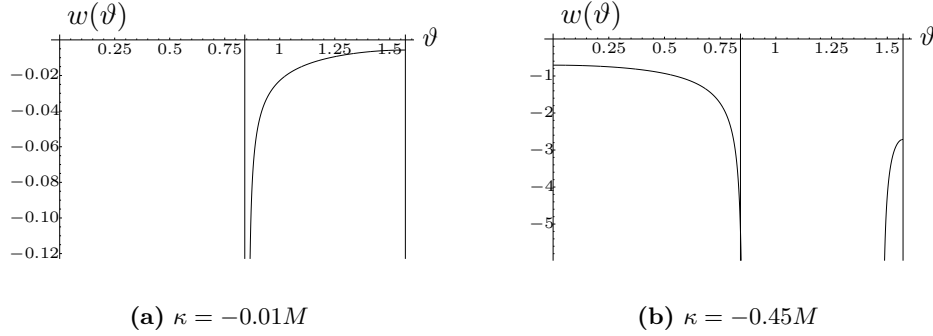
Figure 5.6: Time gain per duration ratio w as function of ϑ for two different trajectory parameters κ. Vertical Lines delimit Γ. Parameter fixations: confer Fig. 5.5.

The rate of time gain per travel duration should be as deep in the negative as possible, because this indicates a quick journey into the past. Examining Fig. 5.6, we find a corroboration that $w(\vartheta)$ has a local maximum in the equatorial plane, which is imaginably improper for our purpose. This maximum does not move outside the plane for varying values of κ. Generally, κ makes a huge difference however. The whole graph of $w(\vartheta)$ inside Γ falls towards much smaller numbers for an increasing κ. Where Δs has its roots, w drops into negative infinity. The only drawback is the astronomical—and eventually diverging—amount of energy necessary to follow these curves, as we will see in the next chapter. We are therefore in urgent need of a compromise.

Summarizing, we may state that for causality violations on curves near singularities of a mass comparable to an average galactic nucleus, tidal forces will not pose a challenge while spiraling into the past—regardless of the angle ϑ. On the other hand, the gain per duration rate is necessarily vital for our journey. We cannot ignore the energy consumption however. As we shall see in the subsequent chapter, the total acceleration—which is vital for the energy consumption—is minimal at the equator for reasonably large distances from the singular ring. Hence, we investigate in the further devolution of this chapter the behaviour of the quantities at stake while confining ourselves to the equatorial plane,

$$\vartheta = \frac{\pi}{2}.$$

The rate w has unfortunately a local maximum in this plane, but if the yield is still high enough to be economically reasonable, we will save large amounts of fuel, which—in turn—enables us to proceed on our journey even further.

5.6 Analysis in the Equatorial Plane

After having chosen a spacetime with a certain fixed M and a vanishing Q and after having restrained ourselves to the equatorial plane, we are left with three varying parameters a, r, and κ for the following analysis. We aim at giving a complete account on the dependence on these parameters of the tidal accelerations, the duration of the journey, and the gain of time to duration ratio.

5.6.1 Tidal Accelerations

Following precisely the argumentation in section 5.5.1, we restrict the considerations on tidal accelerations on the longitudinal direction. The tidal forces are independent of the trajectory parameter κ, and the radial distance r must be between zero and the (negative) minimal value $r_{\max}$ for the uncharged case.[2] The singularity should live up, as always, to the "no–nudity–code" for black holes. Therefore, the angular momentum is restricted to the range $\bar{a} \in [0,1]$.

In the equatorial plane near an uncharged singularity, the longitudinal tidal acceleration originally given in (5.13) simplifies to

$$\frac{b_2}{\delta x^2} \quad = \quad \frac{2M}{r^3}. \tag{5.19}$$

This acceleration is independent of κ and of the angular momentum a. Thus, it is precisely the same as for a Schwarzschild spacetime.[3] However, if we define the radial distance r in terms of the maximal value allowed, the angular momentum exerts an indirect influence on the tidal forces, shown in Fig. 5.8.

The radial dependence of the relative acceleration is determined by

$$\frac{\partial}{\partial r} \left(\frac{b_2}{\delta x^2} \right) \quad = \quad -\frac{6M}{r^4}.$$

As intuitively accessible, the relative accelerations as well as the radial derivative diverge at the singularity. Hence, the gradient increases increasingly the closer we get to $r = 0$.

Although the relative acceleration is independent of the rotation of the black hole, the range for the radial coordinate where time travel may take place is not. Therefore it exerts an indirect influence on the tidal acceleration insofar as it helps to determine this range. In Fig. 5.7, we show the radial dependence of the acceleration and two concrete delimitations for different angular momenta. Clearly, the tidal accelerations grow towards the singular ring for any given rotation. In order to understand the dependence of the range on the rotation

---

[2]Cf. (4.4), where $z = -r$.
[3]According to [1], p. 860.
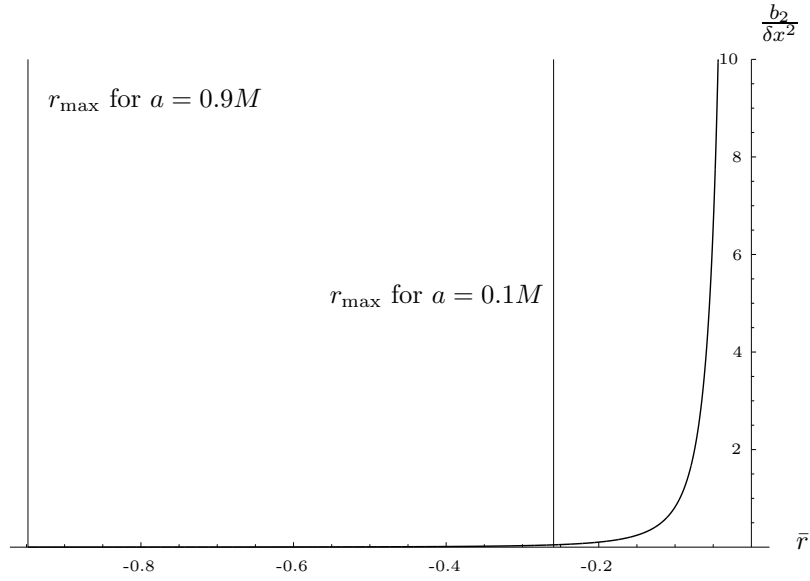
Figure 5.7: Equatorial tidal acceleration in units of s^{-2} as function of radial distance
r for $a = 0.9M$. The respective vertical line and the y–axis delimit Γ for
the different values of a.

of the black hole more accurately, we plot Fig. 5.8, which shows that a higher
angular momenta will widen the range allowed and therefore add comfort on
travel. The dependence on the rotation emerges of the fact that r is defined
in terms of the maximal value $r_{\max}$. But this range is a function of a in turn,
as may be checked in (4.9). For a larger relative distance like $r = 0.9\,r_{\max}$, the
tidal forces are evidently about one thousand times weaker than for a smaller
one such as $r = 0.1\,r_{\max}$.

(a) $r = 0.1r_{\max}$ **(b)** $r = 0.9r_{\max}$
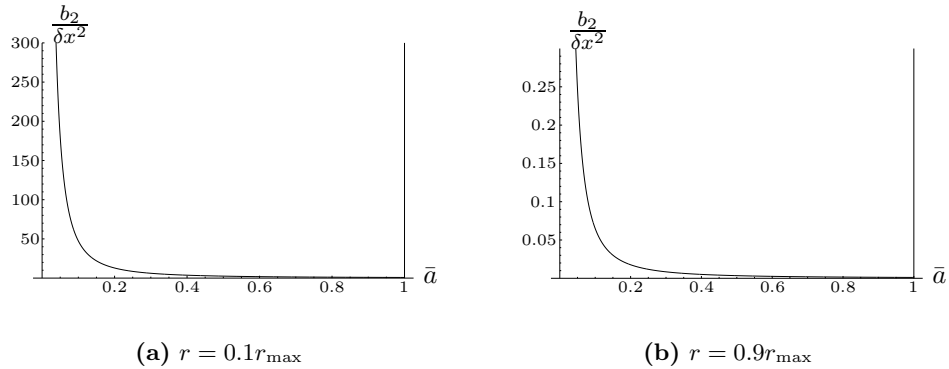
Figure 5.8: Equatorial tidal accelerations in units of s^{-2} as function of angular mo-
mentum $\bar{a}$ for two different relative radial distances. The vertical line and
the y–axis delimit Γ.

We take the issues of these considerations into account when searching for
a black hole with appropriate parameters and a suitable trajectory within Γ.
Regarding the angular momentum, we will not face a problem in reality since

there are good reasons to presume it to be of a considerable size. We have argued for this earlier, *viz.* in section 3.5.

For the trajectory we are heading for, it will prove clever not to fly too close to the singularity. Vicinity to the singular ring is of no necessity to our objective. The optimal radial distance to the ring, where the absolute value of the time gain per flight duration ratio has a maximum, will be away from its immediate contiguity. This maximum, however, will, of course, depend on the rotation of the ring as well as on the trajectory parameter. We leave the tidal accelerations with the knowledge of the desirability of a high angular momentum in order to stretch the range for r, allowing a distance from the ring as large as possible.

5.6.2 Temporal Quantities

First, a word on the time gain in the equatorial plane. The gain is only subject to the trajectory parameter κ. One could therefore—mistakenly—believe that the rest of the parameters is of no relevance to this question. The influence of the angular momentum of the hole as well as of the orbit of the craft is certainly indirect. The rotation and the radial distance determine—apart of course from the mass and the charge of the black hole and from the angle ϑ—the range of permitted κ. We calculate with a "relative" κ, where κ is not fixed but defined in terms of its minimum, *i.e.* of the larger root of $F(M, a, Q; r, \vartheta; \kappa) = g_{\mu\nu}\dot{x}^\mu\dot{x}^\nu$. For the Kerr–Newman metric, we obtain for the roots of (5.12)

$$\kappa_{1/2} \;\; = \;\; \frac{1}{\Delta - a^2\sin^2\vartheta}\left[a\sin^2\vartheta\left(r^2 + a^2 - \Delta\right) \pm \Sigma\sin^2\vartheta\sqrt{\Delta}\right]. \quad (5.20)$$

We christen the larger of the two roots κ_2—the one with the "+"–sign—and set $\kappa = k\kappa_2$, where $k \in [0, 1]$. For different values of the angular momentum $\bar{a}$ and the radial coordinate $\bar{r}$, κ will thus be different in absolute terms. It is evident then, that the time gain strongly depends not only on the trajectory parameter. The time gain Δt from (5.7) and (5.20) in the equatorial plane is differentiated with respect to r,

$$\frac{\partial(\Delta t)}{\partial r} \;\; = \;\; -\frac{2\pi k}{r^2\sqrt{\Delta}(r - 2M)^2}\left[2\Delta\left(Mr^2 + a^2(r - M)\right) + 2\sqrt{\Delta}Mar^2\right.$$
$$\left. -r\left(r^2 + a^2\right)\left(r^2 - 3Mr + 2M^2\right)\right].$$

In this derivative, no general remarks concerning its sign may be made. Computer analysis shows however, that in the region of the parameter space in which our travel will most likely take place, the derivative is negative and has no extremal points. In Fig. 5.9, we provide two concrete examples for Δt as a function of the distance from the ring.

It is clearly visible that the closer to the singularity we choose our trajectory, the quicker we are allowed to travel back in time. By the increasing contiguity to the ring, we achieve an ever larger margin of κ. Another relevant point rises from Fig. 5.9. Having a closer look to the values printed on the Δt–axis, we recognize the difference caused by strongly differing angular momenta. The first term in (5.20) determines the centre of the range of κ where the curve

(a) $a = 0.1M$ (b) $a = 0.9M$
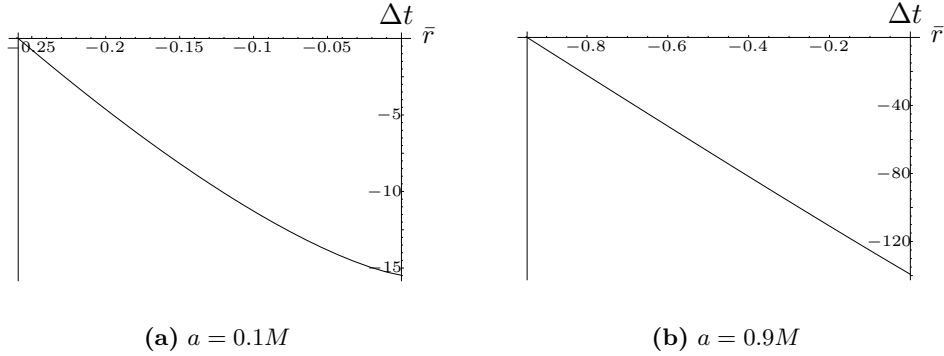
Figure 5.9: Time gain in seconds as function of radial distance $\bar{r}$ for a small and a large angular momentum at $\kappa = 0.5\kappa_2$. Vertical Line at $r = r_{\max}$.

$\dot{x}^\mu$ is spacelike. The translation on the κ–axis towards the values where $\dot{x}^\mu$ is timelike as well as directed to the future comes from the second term in (5.20). This translation indicates the values of κ where our curve becomes lightlike. Obviously, the first term vanishes for a non–rotating black hole. In this case, however, there would be no analytic extension into $r < 0$ and for this reason, no opportunity to travel backwards in time. Therefore, the smaller the angular momentum of the ring is, the smaller is the permitted negative range for κ. This definitely produces another good reason to look for a strongly rotating black hole.

We turn to the analysis of the flight duration in the equatorial plane for a given κ. Introducing, it should be emphasized that the duration is subjected to a change of κ. If we choose the trajectory parameter to be the value of one of the roots (5.20), the duration of a revolution Δs given by (5.9) around the the ring (if "around" is the right preposition...) will tend to vanish. On these grounds, we conclude that we have to try to get a κ as negative as possible, since this will not only bestow a large time gain upon our crew, but also a favourable time of flight. Eventually, the time gain per duration ratio will diverge at $\kappa = \kappa_2$. However, let that ratio pass for the moment and let us come back to the flight duration.

We differentiate the duration Δs with respect to r,

$$\frac{\partial(\Delta s)}{\partial r} \;\; = \;\; \frac{4\pi}{r^2\sqrt{F}}\left[M(\kappa + a)^2 - r^3\right]. \tag{5.21}$$

The sign of the derivative is positive everywhere inside Γ and $\Delta s(r)$ is rising for all parameter values at stake. One can easily recognize that the increment grows towards infinity for $r \longrightarrow 0$. The roots of (5.21) at $r^3 = M(\kappa + a)^2$ lie outside the domain of causality violation.

Fig. 5.10 provides another clear argument not to pass too close to the singularity, for in its vicinity, as we have seen in our previous short analytical account, the duration of one revolution diverges. Since $\Delta s = 2\pi\sqrt{F}$, the reason for this divergence is easily found in the singularity of the metric at $(\bar{r} = 0, \vartheta = \pi/2)$, i.e. in the divergence of g_{tt} and $g_{t\varphi}$, which, in turn, forces F to run into infinity.

(a) $a = 0.1M$ **(b)** $a = 0.9M$
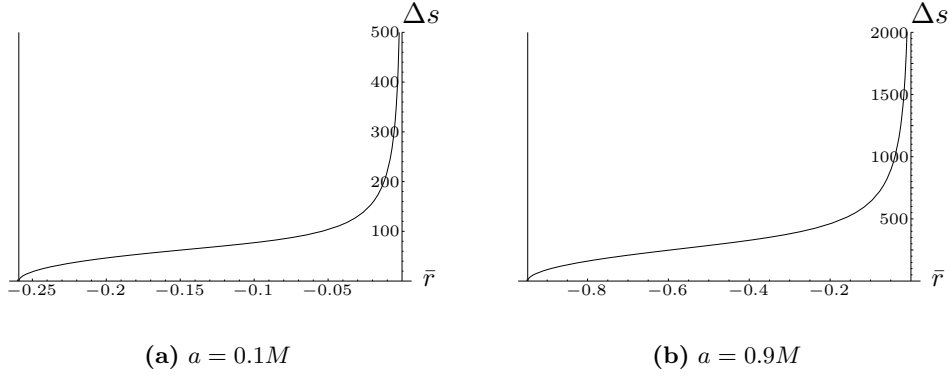
Figure 5.10: Duration in seconds as function of radial distance $\bar{r}$ for a small and a large angular momentum at $\kappa = 0.5\kappa_2$. Vertical Line at $r = r_{\max}$.

The derivative of $\Delta s = \Delta s(a)$ with respect to the angular momentum a is given by

$$\frac{\partial(\Delta s)}{\partial a} \quad = \quad -\frac{2\pi}{r\sqrt{F}}\left[a(r + 2M) + M\kappa\right]. \tag{5.22}$$

The first term in the rectangular bracket is positive, because in Γ we have $|r| < M$ according to (4.6). The second remains negative for all κ enabling time travel. If we manage to prove $|a| > |\kappa| \ \forall \kappa \in [\kappa_2, 0]$, the derivative of the time of flight Δs with respect to the angular momentum a remains positive throughout the domain Γ.

Theorem 2 *Everywhere in the domain Γ, we have $|a| > |\kappa|$, provided that the spiralling curve remains timelike.*

Proof: It is clear that if we show $|a| > |\kappa_2|$, the show is over, since this is the κ with the highest absolute value. The absolute value of any number is defined by $|x| = x \, \mathrm{sgn} x \ \forall x \in \mathbf{R}$. Therefore, we hope to rise a contradiction by assuming $a \, \mathrm{sgn} a < \kappa_2 \, \mathrm{sgn} \kappa_2$, where $\mathrm{sgn} \kappa_2 = -1$ for any travel into the past. Thus,

$$a \, \mathrm{sgn} a \quad < \quad -\frac{1}{r(r - 2M)}\left(2Mra + \left(r^2 + a^2\right)\sqrt{\Delta}\right).$$

Since $r(r - 2M)$ is positive everywhere in the domain, the opponents are both multiplied by this factor without any change regarding which side has a higher absolute value. We obtain

$$ar(r - 2M) \, \mathrm{sgn} a \quad < \quad -2Mra - \left(r^2 + a^2\right)\sqrt{\Delta}.$$

The further argumentation depends on the rotational sense, *i.e.* whether a is a positive or a negative number. In case we have $\mathrm{sgn} a = 1$, we add $2Mra$ on both sides and get

$$a \, r^2 \quad < \quad -\left(r^2 + a^2\right)\sqrt{\Delta}.$$

At this point, it becomes obvious that the left–hand side is greater than the right–hand side throughout Γ and that we have brought about a contradiction to the counter-assumption above. In case $\mathrm{sgn}a = -1$, the same operation yields

$$a\,r^2 + 4Mra \quad < \quad -\left(r^2 + a^2\right)\sqrt{\Delta}.$$

The right–hand side is still negative, whereas the expression on the left is positive due to the negative angular momentum and therefore larger than the one on the right. Again, this contradicts the assumption we made initial to this proof. Hence, we have $|a| > |\kappa_2|$ in both cases and the derivative in (5.22) is positive in Γ. □

Summarizing, apart from the time gain increase due to higher angular momentum, the length of the travel also increases the faster the black hole rotates. Fig. 5.11 shows the dependence of the duration per period Δs on the angular momentum a of the singularity. The plot stays qualitatively the same for all coordinate values r. Thus, we give only one example.
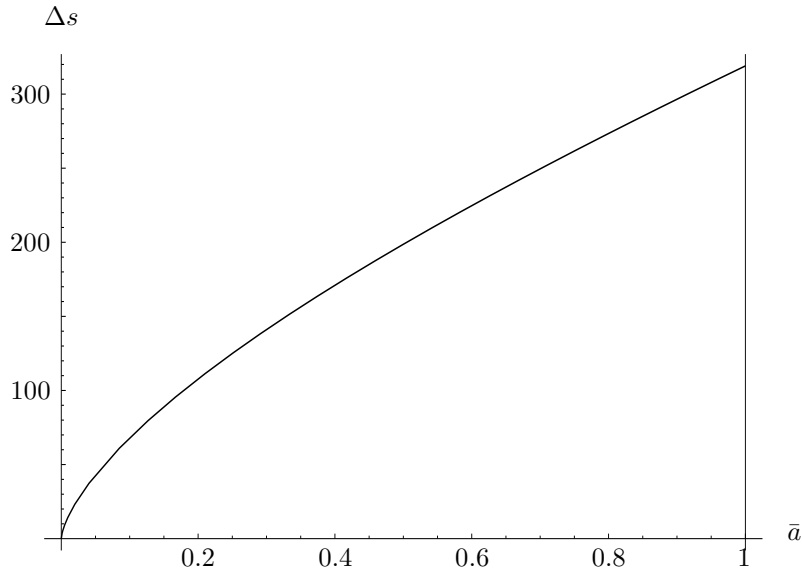

Figure 5.11: Duration Δs in seconds as function of angular momentum $\bar{a}$, which is measured in units of M. Parameter fixes: $\kappa = 0.5\kappa_2$, $r = 0.5r_{\max}$. Angular momenta should not extend beyond the vertical line in order not to violate the cosmic censorship.

The results for the temporal quantities in the equatorial plane are controversial so far. A small distance to the rotating body enables us to travel quickly backwards in time, but obliges us to plan for a longer flight time. Second, a large angular momentum offers the opportunity of a higher time gain for the price of longer flight again. Thus, it is evident to analyze the time gain per duration ratio w in order to settle the dilemma. We investigate the dependence of this ratio on the trajectory parameter κ to start with.

We calculate the derivative of w with respect to κ,

$$\frac{\partial w}{\partial \kappa} \quad = \quad \frac{\kappa(Ma - \kappa(r - 2M)) + rF}{r\sqrt{F^3}}, \qquad (5.23)$$

which has a root at $\kappa = -\frac{r^3 + a^2(r+2M)}{Ma}$. In this case, it depends on the region of parameter space whether the derivative (5.23) is positive or negative and whether the extremal point of $w = w(\kappa)$ lies where our spacecraft moves. The trends in the numerical analysis of this issue tend to favour a positive derivative along the interval $[\kappa_2, 0]$.

(a) $r = 0.1 r_{\max}$ **(b)** $r = 0.9 r_{\max}$
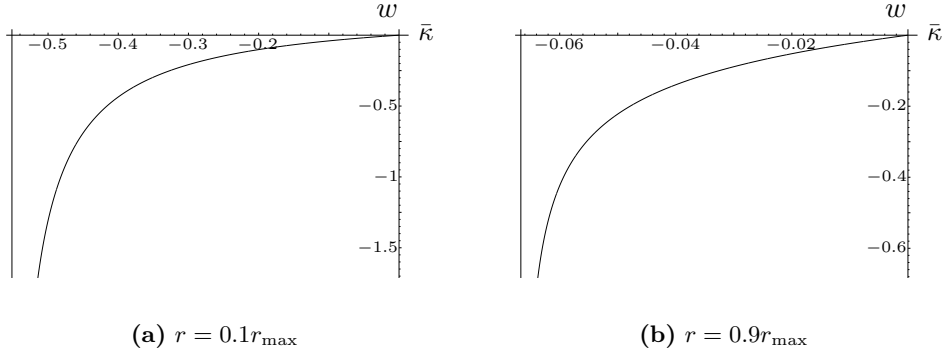
Figure 5.12: Time gain per duration of flight rate for $\bar{a} = 0.6$ as function of trajectory parameter. The vertical lines indicate the zone where the curve is timelike and directed towards the future.

The plots in Fig. 5.12 and Fig. 5.14 presuppose the same angular momentum, as there is no qualitative difference in the plots for several different rotations. The distinction between graphs calculated at different distances turns out to be purely quantitative as well. Regardless of the rotation and the radial coordinate, we recognize that the κ–value for the trajectory which the spacecraft travels along should be the closest possible to the larger root κ_2 of (5.12).

The next step concerns the radial coordinate r, the distance of the trajectory to the singular ring. For the derivative of the gain per duration ratio with respect to the radial distance, we obtain

$$\frac{\partial w}{\partial r} = -\frac{\kappa \left(M(a + \kappa)^2 - r^3 \right)}{r^2 \sqrt{F^3}} \quad (> 0 \ \forall r < 0, \kappa < 0). \qquad (5.24)$$

A maximum is to be found at

$$r = \sqrt[3]{M(a + \kappa)^2},$$

where the second derivative at this root of (5.24) reads $3\kappa/\sqrt{F^2}$. The maximum lies in the positive realm and therefore outside Γ. For pedagogical purposes, the reader may confer Fig. 5.13.

The range of how far the trajectory parameter κ may be chosen on the negative leg naturally depends on in the distance from the singularity that the craft hovers. From a certain distance r on, it is not even possible to find a trajectory of non–spacelike travel into the past anymore. Hence, it does maybe not make sense to insist on defining an "absolute" κ, *i.e.* a κ independent of r as we have done above. We go back to the notion of a "relative" κ, one which is defined in terms of the root κ_2 of (5.20): $\kappa = k\kappa_2$, where $k \in [0, 1]$. We
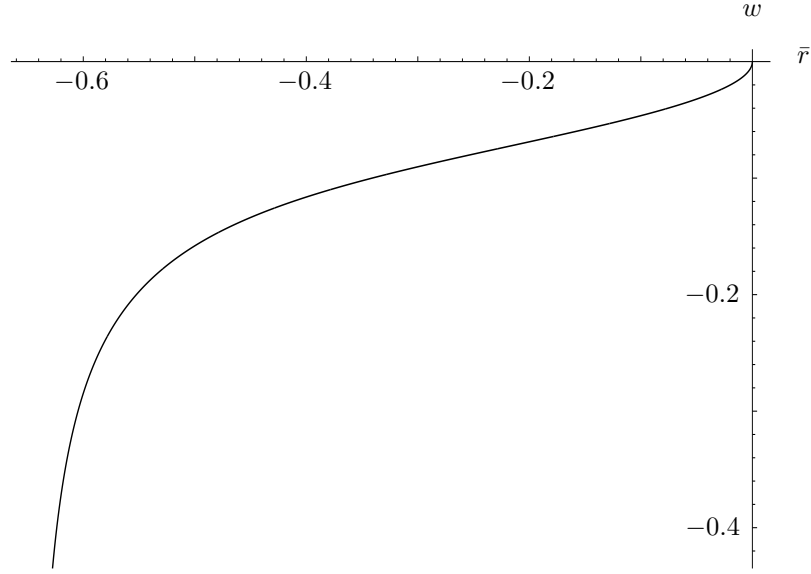
Figure 5.13: The time gain per duration ratio w for fixed $\kappa = -0.1M$ and $\bar{a} = 0.6$. When approaching $r = r_{\max}$ from the right, the ratio diverges because κ is defined in absolute terms.

calculate the derivative the ratio w with respect to r anew, this time with the relative κ,

$$
\begin{aligned}
\left.\frac{\partial w}{\partial r}\right|_{\kappa = k\kappa_2} = \ & \frac{k}{2r^2(r - 2M)^2\sqrt{F^3\Delta}}\Bigg[2F\Big\{ r\left(r^2 + a^2\right)\left(r^2 - 3Mr + 2M^2\right) \\
& -2\sqrt{\Delta}Mar^2 - 2\Delta\left(Mr^2 + a^2r - Ma^2\right)\Big\} \\
& -r\frac{\partial F}{\partial r}\sqrt{\Delta}(r - 2M)\left\{ 2Mar + \left(r^2 + a^2\right)\sqrt{\Delta}\right\}\Bigg],
\end{aligned} \tag{5.25}
$$

where $\partial F/\partial r$ is a fraction of two polynomials in r in both, the numerator and the denominator. The numerator includes up to seven orders of r, which, substituted in the last term of (5.25) would result in a fraction of two polynomials for $\partial w/\partial r$ with something in r^{11} as the highest order of the numerator. It is therefore hopeless to attempt to find the roots of (5.25) analytically. Since the relative κ will vanish at the border of Γ but not in between, where it is negative, we find a minimum at some $r \in [r_{\max}, 0]$. These heuristic considerations are corroborated in the computer analysis of the behaviour of $w = w(r)$. This radial dependence of the time gain per duration ratio is plotted in Fig. 5.14.

As argued beforehand, w has a minimum with respect to the radial coordinate r in the equatorial plane. A detailed computer analysis reveals that the "quicker" the helmsman steers into the past, the closer the minimum migrates towards the singularity. For any given κ and $\bar{a}$, the minimum would provide an ideal orbit. However, the captain of the craft has to take into consideration that the values of the other parameters are more relevant than the finding of the minimum. This is exemplified by the scale of the vertical axes in Fig. 5.14. The absolute value of the minimum in 5.14(a) does not even surpass the three–

(a) $\kappa = 0.1\kappa_2$ **(b)** $\kappa = 0.9\kappa_2$
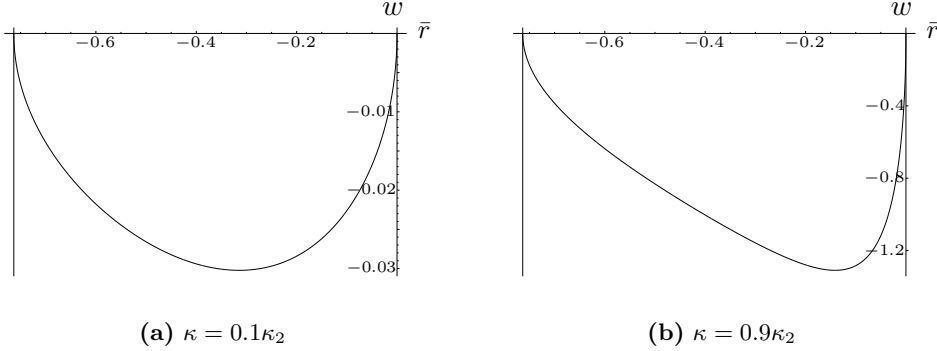
Figure 5.14: Time gain per duration of flight rate for $\bar{a} = 0.6$ as function of radial distance. The vertical lines indicate the zone where the curve is timelike and directed towards the future.

percent–mark of the one in 5.14(b). The principal result which may be read from 5.14 clearly corroborates the intuitive assumption that it is in principle clever to spiral somewhere in the centre of the radial range allowed. If the craft flies only at the edge of the domain, it will hardly be possible to travel back in time. If it gets too close to the singularity, it will eventually crash into an infinite curvature. Regarding the tidal accelerations, the navigator of the craft should choose a curve as far from the singular ring as reasonably possible. Since the tidal forces do not depend upon κ, it may be as high as the energy consumption to be discussed in the next chapter allows. Concluding, Fig. 5.14 gives evidence of the possibility to keep the craft at a larger distance and still have a considerably reasonable time gain per flight duration ratio w.

Let us turn to the last analysis in this chapter. The ratio is not only a function of κ and r, but also of the angular momentum of the black hole. As we have already mentioned above, a strongly rotating singularity allows for quick travel into the past, but only for the price of a longer flight duration. We obtain the derivative

$$\frac{\partial w}{\partial a} \;=\; \frac{\kappa}{r\sqrt{F^2}}\left[a(r+2M)+M\kappa\right], \qquad\qquad (5.26)$$

which is always positive $\forall a \in \Gamma$—$a = 0$ is excluded—, since $|r| < M$ and $|a| > |\kappa|$ for all combinations of parameters allowed. We find an extremal point at $a_{\min} = -M\kappa/(r+2M)$, where

$$\left.\frac{\partial^2 w}{\partial a^2}\right|_{a=a_{\min}} \;=\; \frac{\kappa(r+2M)}{r\sqrt{F^3}} \;>\; 0.$$

The extremal point $a_{\min}$ is a minimum for this reason. At this point, the weakness of the approach with "absolute" parameters may clearly be recognized, for throughout the zone with the permitted combinations of parameters, the derivative of the ratio w is positive, but the minimum for the same function is found at $a_{\min} > 0$. This is interpreted to mean that the angular momentum cannot take values in the range $[0, a_{\min}]$. To be frank however, it makes much

more sense to define the trajectory parameter κ in terms of the other quantities again. We differentiate w with respect to a for $\kappa = k\kappa_2$,

$$\frac{\partial w}{\partial a}\bigg|_{\kappa=k\kappa_2} = \frac{k}{2r(r-2M)\sqrt{F^3\Delta}}\left[2F\left(a\left(r^2+a^2\right)+2\Delta a+2Mr\sqrt{\Delta}\right)\right.$$
$$\left.-\sqrt{\Delta}r(r-2M)\kappa_2\frac{\partial F}{\partial a}\right] \tag{5.27}$$

Closer analytic scrutiny of (5.27) unfortunately turns out to be as hard as it was for (5.25). Therefore, we provide in Fig. 5.15 a plot of the ratio depending on the angular momentum $\bar{a}$, where not only κ, but also r is relativized with respect the angular momentum. We hope to satisfy at least a pedagogical purpose with this plot and its short discussion.

PSfrag replacements
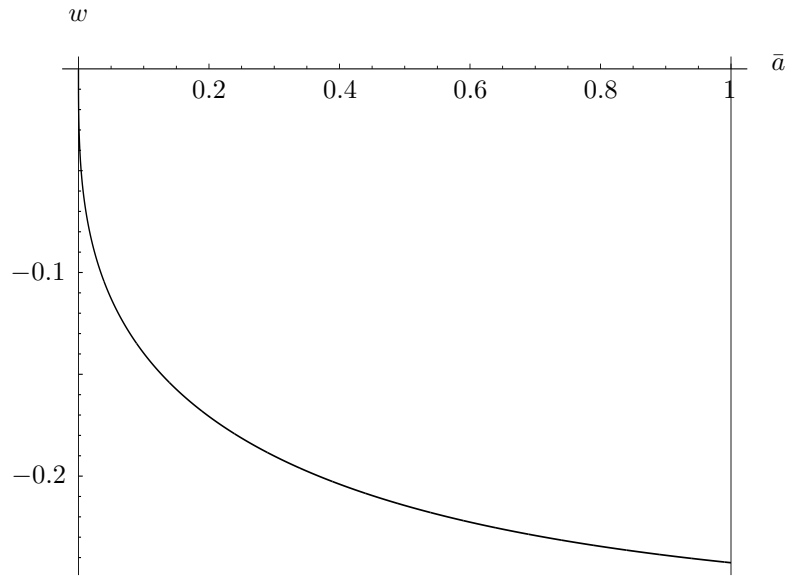
Figure 5.15: Time gain per duration of flight rate for $\kappa = 0.5\kappa_2$ and $r = 0.5r_{\max}$ as a function of the angular momentum $\bar{a}$. Angular momenta should not extend beyond the vertical line in order not to violate the cosmic censorship.

The graph remains qualitatively the same for all combinations of the parameters κ and r. Not surprisingly, the ratio w vanishes if the black hole does not rotate. In this case however, there is no logical possibility to complete a time travel as our crew does. The graph may be separated basically into two legs: a zone where the ratio increases quickly in absolute terms and a second zone where the ratio is not constant, but clearly confined to the region around $w = -0.2$. The absolute value of the ratio grows monotonically over the permitted range of $\bar{a}$. Hence, we will not face problems arising from this issue, for we have assumed in section 3.5 the angular momentum to be high rather than low.

Our next task consists of assessing the energy consumption during the time travel. This question is, of course, vital to the entire enterprise and shall be discussed in the subsequent chapter.

Chapter 6

Energy Consumption during Time Travel

The spacecraft burns energy in order to remain on the trajectory as planned in (5.4). The energy burn is mainly due to the attractive force of the strong curvature inside the domain Γ, which has to be resisted. In principle, we calculate the mass of fuel required to meet a given total acceleration times the duration of the exhaust. This product is what we are interested in.

We execute all subsequent calculations in the proper system of the craft, where its velocity vanishes. Newtonian mechanics is therefore valid for our considerations and no special relativistic formulation will be necessary.

We start with computing the total acceleration on the φ–curve.

6.1 Acceleration on Trajectory

The total acceleration $\wp$ is provided by the subsequent expression,

$$\wp = \sqrt{|g_{\mu\nu}\wp^{\mu}\wp^{\nu}|}. \tag{6.1}$$

In order to compute the *physical* acceleration, the curve has to be reparametrized with the proper time s. Derivatives have to be expressed with respect to the proper time. This is obtained by use of (5.8),

$$\frac{dx^{\mu}}{ds} = \frac{\dot{x}^{\mu}}{\sqrt{g_{ab}\dot{x}^{a}\dot{x}^{b}}},$$

$$\frac{d^{2}x^{\mu}}{ds^{2}} = \frac{\ddot{x}^{\mu}}{|g_{ab}\dot{x}^{a}\dot{x}^{b}|}.$$

The individual components of the physical acceleration are given by

$$\wp^{\mu} = \frac{d^{2}x^{\mu}}{ds^{2}} + \Gamma^{\mu}_{\alpha\beta}\frac{dx^{\alpha}}{ds}\frac{dx^{\beta}}{ds}. \tag{6.2}$$

For the type of curves characterized by (5.4), the second derivatives vanish for all components. Evaluating (6.2) therefore yields

$$\wp^t \;=\; 0,$$

$$\wp^\varphi \;=\; 0,$$

$$\wp^r \;=\; \frac{1}{|g_{ab}\dot{x}^a\dot{x}^b|}\left(\Gamma^r_{tt}\kappa^2 + 2\Gamma^r_{t\varphi}\kappa + \Gamma^r_{\varphi\varphi}\right),$$

$$\wp^\vartheta \;=\; \frac{1}{|g_{ab}\dot{x}^a\dot{x}^b|}\left(\Gamma^\vartheta_{tt}\kappa^2 + 2\Gamma^\vartheta_{t\varphi}\kappa + \Gamma^\vartheta_{\varphi\varphi}\right).$$

The individual components of the affine connection are listed in Appendix C. Concluding, we write down the total acceleration:

$$\wp \;=\; \frac{1}{2|g_{ab}\dot{x}^a\dot{x}^b|}\sqrt{\left|\begin{array}{c}\gamma^{rr}\left(g_{tt,r}\kappa^2 - 2g_{t\varphi,r}\kappa + g_{\varphi\varphi,r}\right)^2 \\ + \;\; \gamma^{\vartheta\vartheta}\left(g_{tt,\vartheta}\kappa^2 - 2g_{t\varphi,\vartheta}\kappa + g_{\varphi\varphi,\vartheta}\right)^2\end{array}\right|}.$$

Using $F(M,a,Q;r,\vartheta;\kappa) = g_{tt}\kappa^2 - 2g_{t\varphi}\kappa + g_{\varphi\varphi}$ from (5.12), renaming yields

$$\wp \;=\; \frac{1}{2|F|}\sqrt{\left|\gamma^{rr}F_{,r}{}^2 + \gamma^{\vartheta\vartheta}F_{,\vartheta}{}^2\right|}, \tag{6.3}$$

the total acceleration which has to be exerted on the craft in order to stay on the curve (5.4).

Although energy saving propulsion devices may be developed in future, minimum total acceleration of our craft is what is needed at the moment. We shall return to this point later in the chapter.

6.2   Tsiolkovsky Equation

In this section, in order to make estimates about the energy consumption, we calculate the mass of fuel burned per flight time by means of the Tsiolkovsky–equation. These considerations assume non–relativistic dynamics, *i.e.* we do our calculations in an inertial frame of the rocket.

The propulsion of the spacecraft is due to the expulsion of gases. Each of these accelerated particles of the exhaust gases takes away its contributions to the total mass and the momentum of the craft. We term the velocity of the craft or the rocket v_R, its mass m_R, its momentum $p_R = m_R v_R$, and the velocity of the exhausted gases relative to the craft v_E, where $v_E < 0$. Every infinitesimal ignition causes an infinitesimal change of the craft's momentum,

$$\frac{dp_R}{dt} \;=\; \frac{dm_R}{dt}\left(v_R + v_E\right), \tag{6.4}$$

where $(v_R + v_E)$ is the absolute velocity of the exhaust fumes—absolute in the sense of relative to the coordinate system in use of course. As long as the velocity of the rocket does not vanish, this formula is only approximately valid,

since we have ignored the second–order–term. In our case, however, we may skip it lightheartedly as a result of the vanishing rocket velocity in the inertial frame we haven chosen.

Generally, there will be external forces acting on the craft in addition. Naturally, these forces also exist in our case, where the gravitational pull tends to attract the craft towards the singularity. It is important to note at this point that we work within the framework of General Relativity, though we calculate non–relativistically with respect to Special Relativity. The core of GR, however, is the idea that gravitational forces are inertial in the sense of the underlying equivalence principle. Therefore, the metric describes the geometry of the spacetime which, in turn, shapes the inertial forces. Gravitation has thus already been included in the acceleration in (6.3) and does therefore not contribute to the external forces referred to.

The idea now is that many infinitesimal ignitions do change the craft's properties macroscopically, thus we have $m_R = m_R(t)$ and $v_R = v_R(t)$. Subtracting the term with the rocket velocity on both sides of (6.4) then yields

$$m_R \frac{dv_R}{dt} \quad = \quad v_E \frac{dm_R}{dt}. \tag{6.5}$$

Thus, the acceleration of the craft and the rate at which its mass decreases may be brought into connection to each other. The Tsiolkovsky equation (or rocket equation as it is sometimes referred to) is obtained by integration of (6.5),

$$\Delta v_R \quad = \quad -v_E \ln \frac{m_0}{m_1}, \tag{6.6}$$

where the Δv_R is the velocity increment during the whole period of the burn, m_0 the total mass of the craft before and m_1 after the burn. Of course, we always have $m_1 < m_0$.

Adopted to our situation with the temporarily constant acceleration $\wp$ from (6.3), we may easily compute the fuel exhaust in kilograms per travel time in seconds necessary to obtain the desired acceleration. To this end, we use (6.5) and get the following differential equation:

$$\frac{\wp}{v_E} \quad = \quad \frac{1}{m_R} \frac{dm_R}{dt}.$$

The function

$$m_R(t) \quad = \quad m_0 \exp\left(\frac{\wp}{v_E} t\right) \tag{6.7}$$

solves the differential equation, provided that the "decay rate" $\wp/v_E$ remains constant over time. The exhaust velocity is subject to the propulsion system and given once the spacecraft is constructed. The geometry is invariant under rotations around the axis of symmetry and the curvature is thus identical for all values of the φ–coordinate. As we travel along φ–curves, it makes therefore sense to assume a time–independent decay rate. The total mass of the craft will not increase from burning fuel. For this reason, the decay rate should be

negative—for otherwise we would not term it thus—which is secured by $v_E < 0$ as already stated above and $\wp > 0$ from (6.1).

Defining $m_F \doteq m_0 - m_R$ as the fuel burnt after the time t of spiralling in the domain Γ and introducing

$$\mu(\wp, t) \quad = \quad \frac{m_F(\wp, t)}{m_0},$$

where $\mu(\wp) \in [0, 1]$, we have constructed a quantity well suited for analysis. Holding $\wp$ constant, we may try to generate an idea of the time dependence of $\mu(t)$. From its first and second derivative with respect to t, we learn that the function is monotonically increasing and that its rate of growth diminishes. In Fig. 6.1, we give an instructive plot of $\mu(t)$.

PSfrag replacements
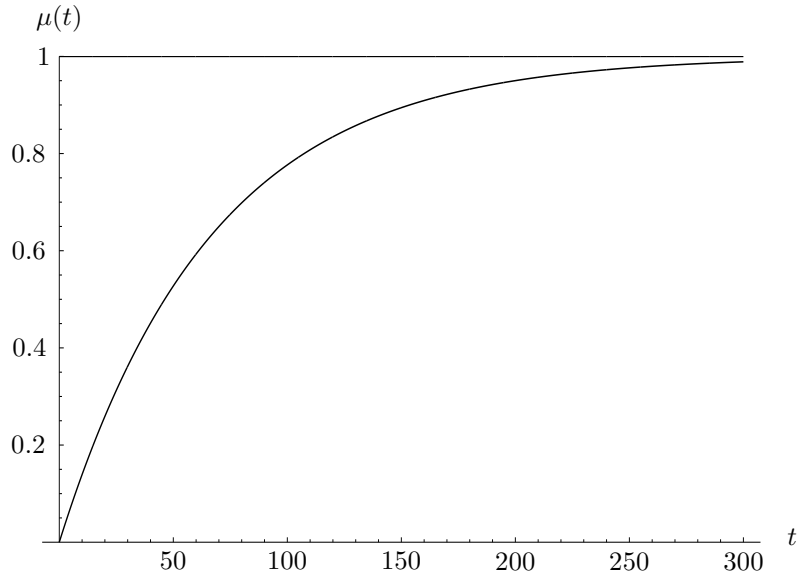
Figure 6.1: The relative mass exhaust μ as function of the time. The relative mass exhaust is unitless, since it indicates the share of the fuel in the total mass of the spacecraft burned within a certain period of travelling time. We have set $\wp = 0.005\mathrm{ms}^{-2}$ and $v_E = -10^8\mathrm{ms}^{-1}$.

We quickly see from (6.7) that the relative mass of fuel per time necessary for the completion of one revolution ($t = \Delta s$) exhausted in order to produce a certain demanded and therefore given acceleration is

$$\mu(\wp \cdot \Delta s) \quad = \quad 1 - \exp\left(\frac{\wp \cdot \Delta s}{v_E}\right). \tag{6.8}$$

$\mu(\wp \cdot \Delta s) = 0$ means the solution to all our problems, since in this case, no fuel is needed at all, whereas $\mu(\wp \cdot \Delta s) = 1$ signifies that practically the entire mass of the craft will be exhausted within the first revolution (or even earlier) in order to keep on track.

6.3 Analysis of Relative Mass Exhaust

6.3.1 Propulsion Systems

Rockets and spacecrafts may have different propulsion systems. It is relevant for us to give an overall impression of the state of the art in order to have reliable assumptions concerning the exhaust velocity v_E and thus to assess the possibility of time travel.

The classification of propulsion systems distinguishes among thermal, electric, and nuclear drives. The thermal systems are subdivided into chemical (solid and liquid), solar or laser drives. The electric systems contain electrothermal (resistojet, arcjet), electromagnetic (plasma), and electrostatic powerings. The latter works with electrical power which provides an accelerating potential. The particles accelerated are either ions or colloids, *i.e.* aerosol particles.[1]

Development of propulsion systems has focused mainly on thermal and electric rockets. Different systems do have different applications according to their respective performance on various important parameters, such as thrust acceleration, exhaust velocity, and specific power, *i.e.* kinetic power $P = \frac{1}{2}\frac{dm}{dt}v_E^2$ per vehicle mass m, where $\frac{dm}{dt}$ is the exhaust mass flow rate. The thrust acceleration is given by the vehicle acceleration (or vehicle thrust–to–weight ratio) divided by the surface acceleration of the concerned celestial body due to gravity.

Unfortunately, all existing propulsion systems are either *power* or *energy limited*. Nuclear or chemical rockets offer poor propellant utilization through limited exhaust velocity while having high specific power and thrust acceleration —they are energy limited. Operations from planetary surfaces like launching vehicles into orbit (where high power is needed) are thus restricted to this category. Electrically powered systems on the other hand are power limited. They are characterized by high exhaust velocities, but also by unacceptably large engine weigh of the apparatus necessary for the electrical conversion in high–power applications. These systems are confined to operations of very small accelerations like orbit raising manoeuvres, interplanetary missions, and spacecraft attitude and orbit control.

According to J. Barrie Moss in [37], p. 109, electrically powered propulsion systems like ion accelerators reach exhaust velocities up to $10^2\mathrm{ms}^{-1}$, whereas drives on a nuclear or chemical basis remain at least one order below that velocity. On the other side of the coin, we find the fact that electric systems are only able to produce thrust accelerations of maximal 10^{-3} times Earth's surface acceleration g. Nuclear and chemical systems on the other hand may sustain or produce accelerations up to $10g$.

Our craft has to be equipped with a drive capable of speeding the exhaust gases to a velocity as high as technically possible as well as having a large thrust acceleration at its disposal. Clearly, the higher v_E is in (6.8), the smaller gets $\mu(\wp)$, the relative mass of fuel per second necessary to produce a given acceleration $\wp$. This connection is also intuitively accessible, for under *ceteris paribus* conditions, the faster the gases are ejected, the more the craft will gain

---

[1]For a more detailed account, cf. Moss, J. B. 'Propulsion Systems', in [37], pp. 107–143.

in velocity. A problem of quite another scope is the acceleration we need to produce in order to stay on the planned trajectory.

6.3.2   Analysis of Total Acceleration

The less the total acceleration measures, the less energy we burn on our journey. In this subsection, we focus our investigation on the acceleration $\wp$ therefore. For the whole section, we assume the black hole to be uncharged, $Q = 0$.

Latitudinal Dependence

Let us analyse $\wp$ as a function of ϑ. Our hope is to find a minimum within the range $[\vartheta_{\min}, \pi/2]$, where it would be favourable to time travel. To this end, we differentiate $\wp$ with respect to ϑ,

$$
\begin{aligned}
\frac{\partial \wp}{\partial \vartheta} &= \frac{1}{2M} \frac{1}{F^2 \sqrt{\left| \gamma^{rr} F_{,r}{}^2 + \gamma^{\vartheta\vartheta} F_{,\vartheta}{}^2 \right|}} \Big[2F \left(\gamma^{rr} F_{,r} F_{,r,\vartheta} + \gamma^{\vartheta\vartheta} F_{,\vartheta} F_{,\vartheta,\vartheta} \right) \\
&\quad + F_{,r}{}^2 \left(\gamma^{rr}{}_{,\vartheta} F - \gamma^{rr} F_{,\vartheta} \right) + F_{,\vartheta}{}^2 \left(\gamma^{\vartheta\vartheta}{}_{,\vartheta} F - \gamma^{\vartheta\vartheta} F_{,\vartheta} \right) \Big],
\end{aligned} \tag{6.9}
$$

where

$$
\begin{aligned}
\frac{\partial F}{\partial r} &= \frac{2}{\Sigma^2} \Big[M \left(r^2 - a^2 \cos^2 \vartheta \right) \left(\kappa^2 + 2a\kappa \sin^2 \vartheta \right) \\
&\quad \sin^2 \vartheta \left\{ Ma^2 \sin^2 \vartheta \left(r^2 - \cos^2 \vartheta \right) - r\Sigma^2 \right\} \Big],
\end{aligned}
$$

and therefore

$$
\begin{aligned}
\frac{\partial^2 F}{\partial \vartheta \partial r} &= \frac{4 \sin \vartheta \cos \vartheta}{\Sigma^2} \Big[Ma^2 \kappa^2 - 2Ma\kappa \left(r^2 + a^2 \left(\sin^2 \vartheta - \cos^2 \vartheta \right) \right) \\
&\quad + Ma^2 \sin^2 \vartheta \left(2r^2 - a^2 \sin^2 \vartheta \right) - r\Sigma \left(r^2 - a^2 \sin^2 \vartheta \right) + \frac{a^2}{\Sigma} \frac{\partial F}{\partial r} \Big].
\end{aligned}
$$

The search for roots of equation (6.9) is somehow hopeless, since the numerator is a polynomial of trigonometric functions of ϑ of order twelve. Far from recognizing obvious simplifications or helpful substitutions, we choose a slightly different approach: we argue that in the equatorial plane, due to the the $\vartheta \to \pi - \vartheta$ symmetry of the Kerr–Newman spacetime, the first derivative of any quantity with respect to ϑ vanishes in the equatorial plane and that for this reason, $\vartheta = \pi/2$ is at least one solution of $\partial \wp / \partial \vartheta = 0$.

The function $\wp(\vartheta)$ has therefore an extremal point at $\vartheta = \pi/2$. Differentiating (6.9) one more time with regard to ϑ yields for $\vartheta = \pi/2$

$$
\left. \frac{\partial^2 \wp}{\partial \vartheta^2} \right|_{\vartheta = \frac{\pi}{2}} = \frac{1}{2M} \frac{1}{F^2 \sqrt{\left| \gamma^{rr} F_{,r}{}^2 \right|}} \Big[F_{,r}{}^2 \left(\gamma^{rr}{}_{,\vartheta,\vartheta} F - \gamma^{rr} F_{,\vartheta,\vartheta} \right) + 2F \gamma^{rr} F_{,r} F_{,r,\vartheta,\vartheta} \Big],
$$

where

$$\gamma^{rr}_{,\vartheta,\vartheta}\Big|_{\vartheta=\frac{\pi}{2}} = -\frac{2\Delta a^2}{r^4} < 0,$$

$$F_{,\vartheta,\vartheta}\Big|_{\vartheta=\frac{\pi}{2}} = \frac{4M}{r^3}\left(a\kappa + r^2 + a^2\right)^2 + 2\Delta,$$

$$F_{,r,\vartheta,\vartheta}\Big|_{\vartheta=\frac{\pi}{2}} = -\frac{4}{r^3}\left[3Ma^2(a+\kappa)^2 + 2Mar^2(a+\kappa) - r^5\right] > 0.$$

Since there seems to be no direct proof as to whether the second derivative is positive or negative at $\vartheta = \pi/2$—due to the fact that $F_{,\vartheta,\vartheta}$ changes sign for different zones in parameter space—we try to find answers numerically. Computer analysis reveals that close to the singularity at small values of r, we find a local maximum at $\vartheta = \pi/2$. In this case, the total acceleration in the equatorial plane is only slightly above the two minima nearby at $\vartheta_1 < \pi/2$ and $\vartheta_2 > \pi/2$. With increasing r, this elevation in the equatorial plane will eventually vanish and becomes a valley for large enough radial distances. Unfortunately, it is not clear how to find the dividing ridge in the parameter space analytically. The reader may consult Fig. 6.2 in order to obtain an idea of the behaviour of the total acceleration as a function of ϑ. The mass M of the singular ring is assumed to be fixed at $M = 10^7 M_\odot$ as in (3.32) unless stated differently.


(a) $r = 0.1r_{\max}$

(b) $r = 0.6r_{\max}$
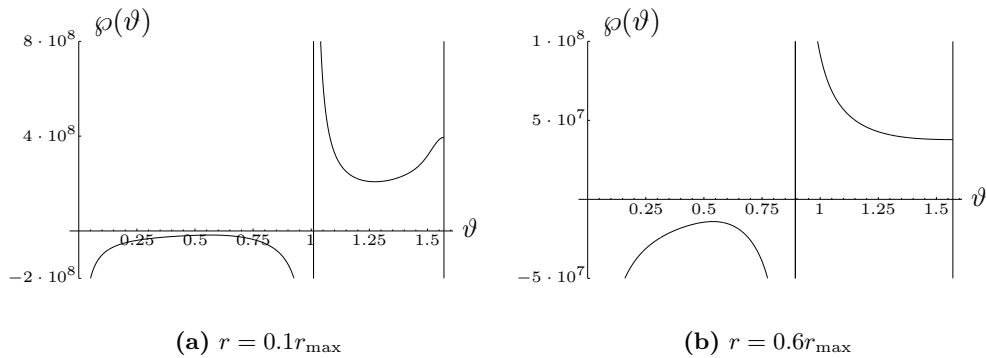
Figure 6.2: Total acceleration $\wp$ as function of ϑ in ms^{-2}. Two typical examples are chosen which are supposed to show the subsiding of the maximum in the equatorial plane for growing r. The angular momentum is fixed at $\bar{a} = 0.6$, the trajectory parameter at $\kappa = 0.1\kappa_2$.

If we consider the factor $\wp \cdot \Delta s$ in the exponent of (6.8), what has been said in the analytical argument regarding the acceleration remains valid, due to the fact that

$$\wp \cdot \Delta s = \frac{\pi}{\sqrt{F}}\sqrt{\left|\gamma^{rr}F_{,r}{}^2 + \gamma^{\vartheta\vartheta}F_{,\vartheta}{}^2\right|} \tag{6.10}$$

has a very similar structure to $\wp$. In Fig. 6.3, we give plots of this factor with exactly the same parameters as in Fig. 6.2. The minima rise relative to their neighbourhood for increasing distances.

(a) $r = 0.1r_{\max}$ **(b)** $r = 0.6r_{\max}$
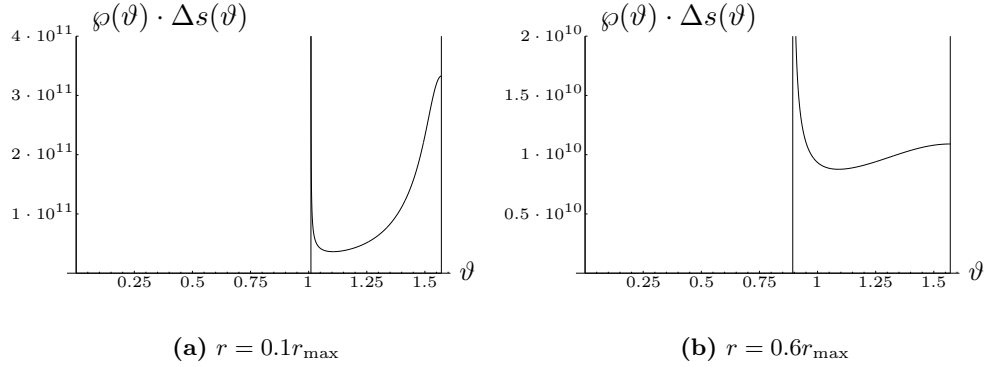
Figure 6.3: Total acceleration $\wp$ times duration of one revolution Δs as function of ϑ in ms^{-1}. The angular momentum is fixed at $\bar{a} = 0.6$, the trajectory parameter at $\kappa = 0.1\kappa_2$.

The amount of energy which may be saved by strictly looking for the minimum of $\wp(\vartheta)$—or rather of $\wp(\vartheta) \cdot \Delta s(\vartheta)$—does not justify the calculatory complications it would take to include the latitudinal dependence in our further analysis. What promises to be of much higher relevance is the distance r from the singular ring. To this end, compare the scales of Fig. 6.3(a) and Fig. 6.3(b). From here onwards, we will therefore certainly get on all right if we confine our investigation to the equatorial plane. For larger distances r, the total accelerations drops, as we will soon learn. Therefore, we will argue to keep a certain distance from the ring anyway. As we already did in the preceding chapter, we set again

$$\vartheta = \frac{\pi}{2}.$$

In the equatorial case, we find for the total acceleration $\wp$

$$\wp^\star = \frac{1}{2F^\star}\sqrt{\left|(\gamma^{rr})^\star \left(F_{,r}^\star\right)^2\right|},$$

where quantities with stars indicate their respective value in the equatorial plane. Thus, we have

$$F^\star = \frac{r - 2M}{r}\kappa^2 - \frac{4Ma}{r}\kappa - \frac{1}{r}\left(r^3 + a^2 r + 2Ma^2\right) > 0,$$

$$(\gamma^{rr})^\star = -\frac{\Delta}{r^2} < 0,$$

$$\left(\frac{\partial F}{\partial r}\right)^\star = \frac{2}{r^2}\left[M(a + \kappa)^2 - r^3\right] > 0.$$

Finally, rearranging yields

$$(\wp \cdot \Delta s)^\star = -\frac{2\pi}{r^3}\sqrt{\frac{\Delta}{F^\star}}\left[M(a + \kappa)^2 - r^3\right] > 0. \qquad (6.11)$$

Our subsequent analysis is based on this quantity.

Mass Dependence

Scaling the angular momentum a and the coordinate r to units of M has the obvious consequence that both become proportional to M. The shortcuts Δ and Σ are then proportional to M^2 and g_{tt} to 1, $g_{t\varphi}$ to M, and $g_{\varphi\varphi}$ to M^2. From considerations regarding units follows the proportionality of the trajectory parameter κ to M. From all this, we conclude that $F \propto M^2$ and finally $\wp \propto M^{-1}$. On the other hand, Δs is also proportional to M. As μ is only a function of the product of $\wp$ and Δs, the energy required to complete a full revolution on the curve (5.4) is independent of the mass of the black hole.

Since the time gain Δt goes proportionally with M as well, the energy consumption per time gain remains proportional to M^{-1} however. The larger the mass of the black hole is, the less energy a given time gain will therefore cost. The argument here is independent of ϑ.

κ–Dependence

If we differentiate the function F with respect to κ, we obtain at $\vartheta = \pi/2$

$$\left(\frac{\partial F}{\partial \kappa}\right)^{\star} = -\frac{2}{r}\left[(2M - r)\kappa + 2Ma\right]. \tag{6.12}$$

This equation shows that for the most likely parameter combinations, $(\partial F/\partial \kappa)^{\star}$ is positive. It will definitely be positive for all r in Γ if $2a > 3|\kappa|$. For the derivation of the derivative in (6.12), we implicitly assumed $\text{sgn}\,a = 1$, therefore we omitted the dashes indicating the absolute value. According to theorem 2 in chapter 5, we argue analogously and come across

$$\frac{2}{3}ar\left(r + M\right) < -\left(r^2 + a^2\right)\sqrt{\Delta},$$

where the left–hand side is unfortunately also negative because of (4.6). The counterassumption can therefore not be strictly ruled out as it was in the proof of theorem 2. This means that no conclusive statement regarding the comparison of $2a$ with $3|\kappa|$ may be made. Generally however, the derivative in (6.12) will be positive.

The derivative of the total acceleration $\wp^{\star}$ times the duration per revolution $(\Delta s)^{\star}$ with respect to κ is given by

$$\frac{\partial(\wp \cdot \Delta s)}{\partial \kappa}\Big|_{\vartheta = \frac{\pi}{2}} = \frac{\pi}{r^3}\sqrt{\frac{\Delta}{(F^{\star})^3}}\Big[-4M(a + \kappa)F^{\star}$$
$$+ \left\{M(a + \kappa)^2 - r^3\right\}\left(\frac{\partial F}{\partial \kappa}\right)^{\star}\Big]. \tag{6.13}$$

The first term in the square bracket remains negative in Γ and the second has the sign of the derivative in (6.12) and will most likely be positive therefore. No unambiguous evidence concerning the overall sign of $\partial(\wp \cdot \Delta s)^{\star}/\partial\kappa$ may thus be given. Clearly though, there must be at least three extremal points at the roots of the square bracket which is a cubic expression in κ. In order to avoid

a costly and lengthy analysis of uncertain success however, we jump from this point to the discussion of the computational investigations into $(\wp \cdot \Delta s)^\star(\kappa)$.

Broad numerical study reveals that the derivative of $\wp \cdot \Delta s$ with respect to κ is negative within Γ, for all parameter combinations checked. Obviously, in these cases, the second term of the square bracket in (6.13) dictates the sign—with a positive derivative $(\partial F/\partial \kappa)^\star$. The output graphs appear nearly identical for most combinations. What is varying is the range of κ, since κ is not allowed to fall below κ_2, which, in turn, depends upon M, a and r. The scale on the y–axis also changes for different combinations of assumed values. As a general rule, the swifter the singularity rotates and the further from it we stay, the lower is the total acceleration required.

PSfrag replacements
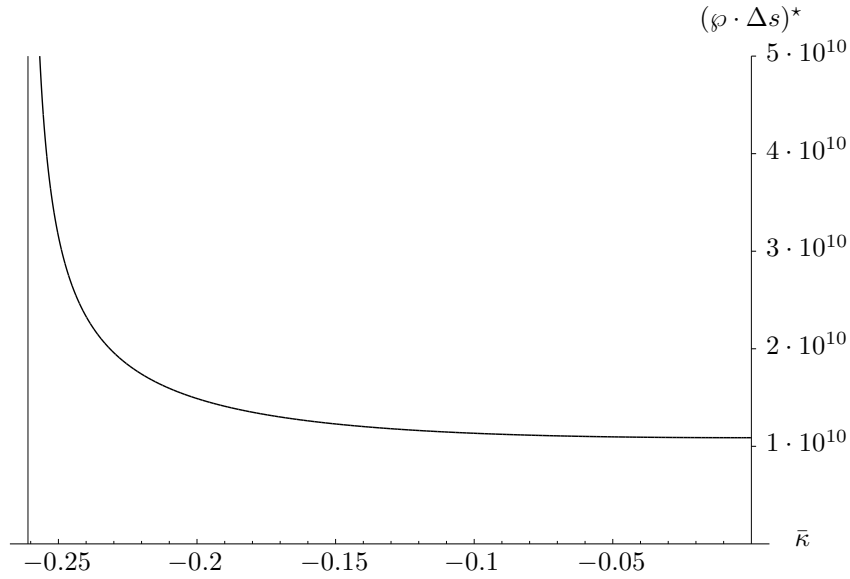
Figure 6.4: A typical graph for $(\wp \cdot \Delta s)^\star$ as function of $\bar{\kappa}$ in ms^{-1}. We stay in the equatorial plane and fix the values for $\bar{a}$ at 0.6 and of r at $0.6 r_{\max}$. The vertical line indicates κ_2, where the φ–curves turn out to be lightlike and even spacelike beyond that limit.

In Fig. 6.4, we provide an example which may give an illustration of the κ–dependence of the acceleration necessary to travel backwards in time times the duration of one full revolution. The divergence of $\wp \cdot \Delta s$ at $\kappa = \kappa_2$ is due to the impossibility to achieve a lightlike trajectory for our massive spacecraft. This means that we have $\mu(\wp \cdot \Delta s) = 1$ in the limit $\kappa \to \kappa_2$. Of course, the least energy consuming way to travel would be to do it without moving back in time and to set $\kappa = 0$. The factor $(\wp \cdot \Delta s)^\star$ from (6.11) would, in this case, reduce to

$$(\wp \cdot \Delta s)^\star \Big|_{\kappa=0} \;=\; -\frac{2\pi}{r^3} \sqrt{\frac{-\Delta r}{r^3 + a^2 r + 2Ma^2}} \left(Ma^2 - r^3\right) \;>\; 0,$$

where $g^\star_{\varphi\varphi} = -\frac{1}{r}\left(r^3 + a^2 r + 2Ma^2\right) > 0$ inside Γ, as we argued in chapter 4.

Since we would indeed be delighted to complete our time travel as planned, setting $\kappa = 0$ does not offer an option. It is important to note, however, that

for the sake of the energy consumption of the spacecraft, κ is to be kept as low as possible.

Radial Dependence

If we differentiate $(\wp \cdot \Delta s)^\star$ with respect to the radial distance r, we obtain

$$\frac{\partial(\wp \cdot \Delta s)^\star}{\partial r} \quad = \quad \frac{\pi}{r^4 \sqrt{F^\star \Delta}} \left[6\Delta M(a + \kappa)^2 - 2r(r - M) \left\{ M(a + \kappa)^2 - r^3 \right\} \right].$$

Here again, it depends on the region of the parameter space whether the derivative is positive or negative. As the analytical search for extremal points turns out to be annoyingly complicated—we have to find roots of a polynomial of eighth order—, we compute the total acceleration to be mastered when approaching the singular ring. Naturally, intuition is not led astray and the limit of (6.11) towards the singularity diverges,

$$\lim_{r \to 0}(\wp \cdot \Delta s)^\star \quad = \quad -2\pi M(a + \kappa)^2 \lim_{r \to 0} \frac{1}{r^3} \sqrt{\frac{\Delta}{F^\star}}$$
$$-\pi \sqrt{2M} a(a + \kappa) \lim_{r \to 0} \frac{1}{\sqrt{-r^5}}.$$

As we shall learn from the numerical analysis, $(\wp \cdot \Delta s)^\star$ diverges also at $r \to r_{\max}$. Since $(\wp \cdot \Delta s)^\star$ is positive for all r, $(\wp \cdot \Delta s)^\star$ has to be minimal for some $r \in [r_{\max}, 0]$. Therefore, we infer from the numerical analysis that at an intermediate radial distance—its exact location depending on the values of M, a and κ—, the product of the total acceleration and the duration becomes minimal and thus the most favourable. In Fig. 6.5, we give an illustrative graph for the radial dependence of $(\wp \cdot \Delta s)^\star$.

Rotational Dependence

We differentiate (6.11) with respect to the angular momentum a,

$$\frac{\partial(\wp \cdot \Delta s)^\star}{\partial a} \quad = \quad -\frac{2\pi}{r^3 \sqrt{(F^\star)^3 \Delta}} \left[\left(M(a + \kappa)^2 - r^3 \right) \frac{3\Delta}{2} \frac{\partial F^\star}{\partial a} \right.$$
$$\left. + F^\star \left\{ 2\Delta M(a + \kappa) + a \left(M(a + \kappa)^2 - r^3 \right) \right\} \right].$$

The maximum range in the radial direction depends through (4.4) on the angular momentum a, as does the relative trajectory parameter $\kappa = k\kappa_2$ through (5.20). In order to avoid the exploding effort necessary for further calculations, we switch to a quantitative analysis of $\wp(a) \cdot \Delta s(a)$.

The computer analysis reveals unambiguously that the derivative of $\wp^\star$ with respect to a has a minimum for all combinations of M, r and κ within the domain Γ, provided that r and κ are defined relatively to the angular momentum. If we define the relevant parameters in absolute terms, we would always encounter some pathological region where the acceleration would diverge—in Fig. 6.6 as well as in Fig. 6.4 and Fig. 6.5. Remarkably, we spot a rather wide
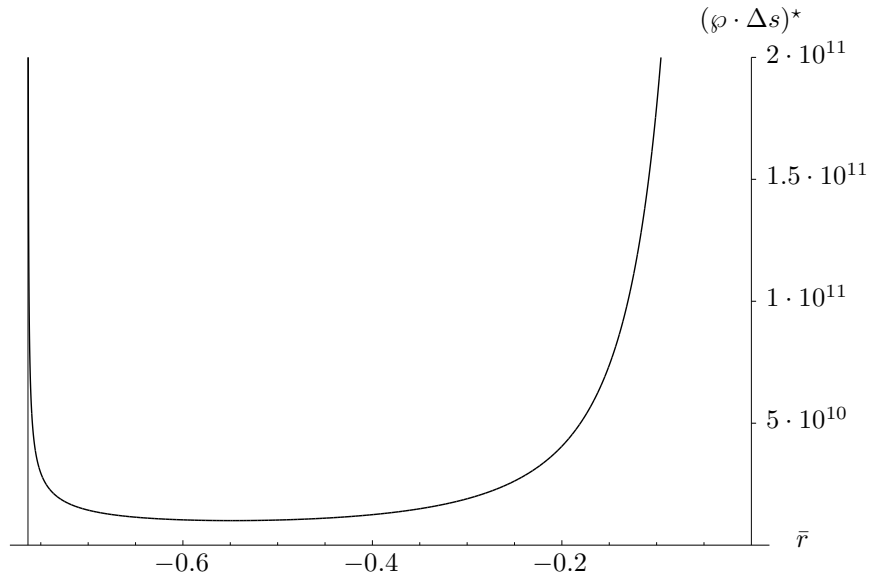
Figure 6.5: A typical graph for $(\wp \cdot \Delta s)^\star$ as function of $\bar{r}$ in ms^{-1}. We stay in the equatorial plane and fix the values for $\bar{a}$ at 0.6 and of κ at $0.1\kappa_2$. The vertical line indicates $r = r_{\max}$ and hence the limit of the domain Γ.

region where $(\wp \cdot \Delta s)^\star$ remains nearly constant with respect to a. The plot in Fig. 6.6 provides another case where the crew of the spacecraft should avoid a singularity with low angular momentum.

Having completed the considerations on the total accelerations encountered on the equatorial plane, we pass to the final section on energy consumption in terms of the relative mass of fuel per time, $\mu(\wp \cdot \Delta s)$.
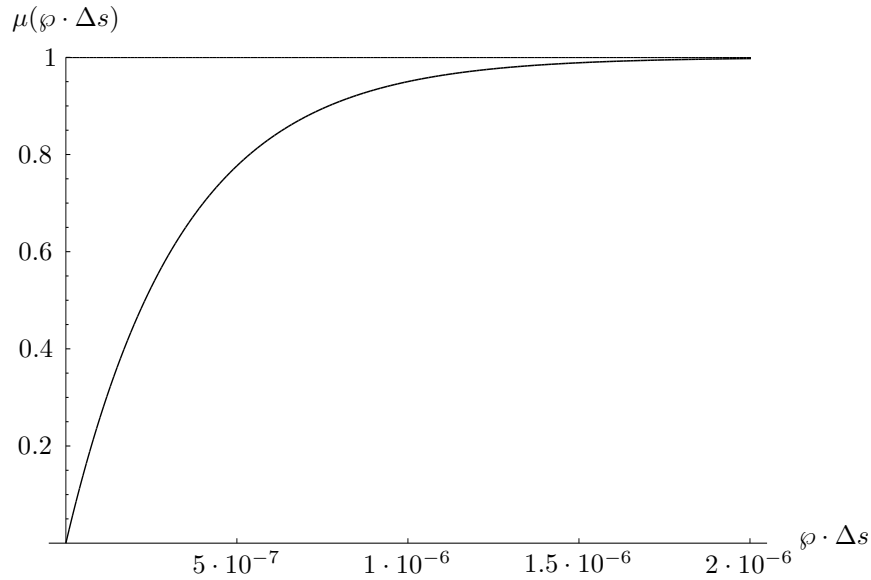
6.4   Relative Mass Exhaust

In this section, we hope to settle the tiresome energy issue. The relative mass exhaust per revolution is a function of the total acceleration $\wp$, the duration of one period Δs, and of the exhaust velocity v_E. In section 6.3.1, we have argued that the velocity at which the gases are exhausted basically depends on the propulsion system and may therefore only hypothetically be varied. We will assume $v_E = -10^2$ms^{-1} to start with, according to [37], p. 109.

Starting from (6.8), we point out that—fixing the exhaust velocity at a constant level—the first derivative of $\mu(\wp \cdot \Delta s)$ with respect to $\wp \cdot \Delta s$ is positive for all values of $\wp \cdot \Delta s$ since the exhaust velocity v_E is taken to be negative. On the other hand, the second derivative is negative everywhere. Thus, $\mu(\wp \cdot \Delta s)$ is a monotonically increasing function over the whole range of $\wp \cdot \Delta s$, but its rate of increase decreases the more we move towards higher $\wp \cdot \Delta s$. Corroboration of the physical intuition predicting a similar behaviour may be found in Fig. 6.7. It illustrates the necessity of low total accelerations, since for an acceleration of only $2 \cdot 10^{-6}$ms^{-2}, our spacecraft's fuel evaporates within a second of travelling time.
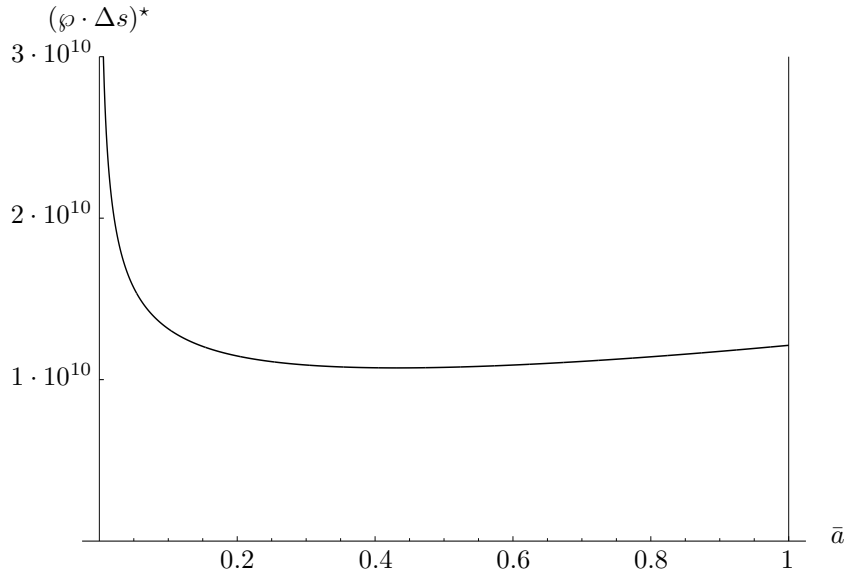
Figure 6.6: A typical graph for $(\wp \cdot \Delta s)^\star$ as function of $\bar{a}$ in ms^{-1}. We stay in the equatorial plane and fix the values for r at $0.6r_{\max}$ and of κ at $0.1\kappa_2$. The vertical line indicates $\bar{a} = 1$, where the singularity turns out to be naked with respect to observers in EKN+ beyond that limit.

Figure 6.7: The relative mass exhaust μ as function of the total acceleration $\wp$ times the duration per revolution Δs. The relative mass exhaust is unitless, since it indicates the share of the fuel in the total mass of the spacecraft burned per revolution. We have set $v_E = -10^2$ms^{-1}.

We are hence in urgent need of strategies of how to save energy. An obvious first hope would be the development of propulsion systems with much higher exhaust velocities than those available today. What is important is the ratio of total acceleration $\wp$ divided by the exhaust velocity v_E. A 10^6 times higher exhaust velocity (a third of the light speed) would naturally allow for 10^6 times higher accelerations. However, even such an improvement would not suffice. The accelerations encountered during the trip are of order $10^8 \mathrm{ms}^{-2}$, as we have seen in section 6.3.2, taking the durations discussed in section 5.6.2 into account. Even if the spacecraft consists of 99% of fuel, the tank would be empty within a split second.

We should therefore try to find an alternative solution to the problem. Even if we minimize $\wp(r, a, \kappa)$, we will never be able to reduce the total acceleration below, say, $10^7 \mathrm{ms}^{-2}$ for a fixed mass of $M = 10^7 M_\odot$. There is one last way out of the difficulty though. In section 6.3.2, we concluded that the total acceleration $\wp$ is proportional to $1/M$ and the duration Δs to M. If we do not have the ambition to complete entire revolutions and thus restrict the time spent spiralling inside Γ below the one necessary for one period. The larger the mass of the black hole grows, the smaller becomes the φ–angle covered during the duration of our stay inside Γ as well as the time gain remain unchanged. By virtue of this fact, we may cut the order of $\wp$ as much as we like. The only restriction to be observed is nature, *i.e.* the mass boundary for a black hole.

Imagine a black hole of the mass of the entire known universe in the visible range. Such an unphysical object would possess a total mass of approximately $10^{22} M_\odot$, assuming the existence of 10^{11} visible galaxies in the known domain with an average total mass of $10^{11} M_\odot$ each.[2] With contemporary rocket technology ($v_E = -10^2 \mathrm{ms}^{-1}$), even when orbiting such a super–supermassive object, the spacecraft would have exhausted half of its mass as propulsion gases within less than five seconds of travelling time! In case of an uncharged, strongly rotating object ($a = 0.9M$), a decent distance from the singular ring ($r = 0.6r_{\max}, \vartheta = \pi/2$), and an intermediate trajectory parameter ($\kappa = 0.5\kappa_2$), the time gain to duration of flight ratio is $w = -0.219$, *i.e.* for every second of time gain on orbit in Γ, we have to return to base camp to have our tanks refilled.

Perhaps the most massive galactic black hole known to man is the nucleus of the galaxy NGC 4486 (M87), 50 million light years away from earth. It has an estimated mass $M_{\mathrm{M87}} = 3 \cdot 10^9 M_\odot$.[3] As we have learnt, even this huge mass is far from being sufficient to confine the energy consumption to a reasonable level. And this is where our project fails. If the crew of the craft has mastered all odds, they still face a challenge only to be matched in science fiction stories but not in physical reality. As theoretical an enterprise our journey was launched, as impracticable it thus comes to an end.

---

[2]According to Ruedi von Steiger (International Space Science Institute, Berne), private communication.

[3]Cf. Press Release No.: STScI–PR97–01 of the Space Telescope Science Institute at http://oposite.stsci.edu/pubinfo/pr/1997/01/PR.html.

Chapter 7

Conclusion

In chapter 2 we introduced some of the basic structures of the Kerr–Newman electrovacuum solution of the Einstein equations. Maybe the most startling feature was the fact that an observer in negative infinity of the external Kerr–Newman spacetime would detect a singular ring of a negative mass at $r = 0$. We have found that it is impossible to eliminate this problem by applying the transformation $r \mapsto -r$, since the horizons would only flip to the other side of the singularity and the observer in the former *positive* infinity would now see a naked singularity with mass $-M$. The spacetime is symmetrical with respect to sign–changing transformations such as above.

When starting off from the well–known Newman–Penrose formalism, we chose two null vectors to be in the two principal null directions of the Kerr–Newman spacetime and constructed a tetrad in advanced Eddington–Finkelstein type of coordinates. By means of the Weyl tensor and the Weyl scalars, we then calculated the components of the Riemann curvature tensor of the Kerr–Newman solution. The approach followed had the remarkable advantage that the invariance of the Riemann tensor under boosts in the plane of the principal null directions and rotations around the axis of symmetry was clearly manifest. Apart from the study of the structure of Kerr–Newman spacetime, our preliminary remarks in chapter 2 involved the preparation for the calculation of the tidal forces.

The calculations performed in the preliminary considerations were purely analytical in character. However, the methods applied in the following chapters changed. Our investigation often started out from broad numerical analysis carried out with the aid of computer algebraic programmes. After having fed the machine with data, we tried to read prevailing trends from the output. Thereafter, our ambition was to corroborate these trends with analytical calculations or proofs. In some instances, our efforts were successful, while in others we had to surrender to high–order polynomials or other obstacles to our analytical approach. In the latter cases, we supported our conclusions with numerical data.

In chapter 3, we split the travel to EKN− into two legs, which were called the tangential and the radial journey respectively: we first travel from anywhere in the asymptotic region to the axis of symmetry, whence we then continue

our journey along the axis. However, the latter is by far more interesting. Although the spacecraft travels along a geodesic (the axis of symmetry), a minimal energy is necessary in order to surmount the maximum of the effective potential, which, unfortunately, is higher than its—the potential's—value in positive infinity. Equation (3.19) shows the minimal kinetic energy necessary to follow the entire axis of symmetry for an uncharged black hole. The minimal kinetic energy is $e_{\mathrm{kinmin}} = m(\sqrt{2} - 1)$ even for an extreme black hole of an angular momentum per unit mass of $a = M$, which was found at the end of section 3.3.1 to be the most promising.

We estimated the elapsed proper time for both legs of the trip in (3.6) and (3.22) and obtained numerical results in Fig. 3.9. Remarkably, the time elapsed for the tangential part increased for lower angular momenta of the black hole, while the one for the radial part decreased. However, for the mass M of a galactic nucleus and an initial distance of one hundred times the distance of the horizon at $r = r_+$ from the singularity, the radial leg should be covered within a few hours only.

The longitudinal and transverse stresses encountered on the radial part of the astronaut's journey were obtained in equation (3.31), where rescaling to units of the mass M has been performed precedingly. This rescaling allowed us to recognize the simple $1/M^2$ dependence of the stress. If we chose a galactic nucleus of at least $M = 10^7 M_\odot$ and an angular momentum not smaller than, say, $a = 0.2M$, the tidal stresses did not exceed some $20\mathrm{Nm}^{-2}$. Closing section 3.4, we discussed the results obtained and concluded that the tidal forces are endurable for both crew and craft.

Chapter 4 on the extension of the realm of causality violation was split into two sections, the first dealing with Kerr spacetime and the second with Kerr–Newman spacetime. The domain of closed timelike φ–curves was termed Γ. In the uncharged case, we calculated the range of Γ in the radial direction in (4.4) and in the latitudinal direction in (4.8). On page 47, we proved that for any value of $a \in [0, M]$, Γ is restricted radially to $r \in [0, -M]$, i.e. our calculations yield for the maximal radial extension towards negative infinity $|r_{\mathrm{max}}| < M$, which is of the order of the horizon radii $r_\pm$—consult equation (2.8). For low angular momenta, the latitudinal range may even reach the vicinity of the axis. We give concrete graphs for several values of the angular momentum in Fig. 4.1 and 4.2. In the second section, we were occupied with the extension of Γ for charged black holes. This part was not only mathematically more complicated, but also physically less interesting, since the influence of the charge upon the domain is only relevant for large Q. However, it might be interesting to take note of the penetration of Γ into positive values of r in case of $Q \neq 0$.

A further project in this context would be the investigation whether we could still access the domain of causality violation in case the singularity were filled with matter, in analogy to what may be done in the Schwarzschild case. The energy–momentum tensor $T^{\mu\nu}$ of this matter should, of course, satisfy the usual conditions such as the positive definiteness of energy density, and having a vanishing divergence, $\nabla_\mu T^{\mu\nu} = 0$. If the matter would form a complete disk, journeys into the domain Γ would no longer be possible.

In chapter 5 we introduced several quantities in order to assess timelike

curves with $t = -\kappa\varphi$, spiralling within Γ and pointing towards the future. We showed that these spirals, satisfying properties (5.1) to (5.3), are found in the same domain Γ as the closed φ–curves. We started with the introduction of the gain of time per revolution $\Delta t = 2\pi\kappa$. The absolute value of the parameter κ, as was proved in theorem 2, is to remain smaller than the absolute value of the angular momentum a in case that the spirals have properties (5.1) to (5.2).

However, Δt alone did not tell us much about the quality of the trajectory for time travelling purposes. Hence, we related Δt to the duration per revolution in Γ, $\Delta s = 2\pi\sqrt{g_{ab}\dot{x}^a\dot{x}^b}$. For reasons elaborated in chapter 3, we set $Q = 0$ subsequently. The duration per revolution as well as the time gain per duration ratio w were proven to be most unfavourable in the equatorial plane, consult Fig. 5.3 to 5.6 to this end. The total acceleration $\wp$ necessary to remain on the intended trajectory turned out to be the most restricting quantity in chapter 6 and as we recognized there, spiralling in the equatorial plane offers a good way to keep it low. Therefore, we still decided to devote the further analysis of chapter 5 to the equatorial plane.

The results of the analysis in the equatorial plane show in Fig. 5.9 that Δt increases with decreasing r, whereas Fig. 5.10 gives testimony of the growth of Δs towards the singular ring. To settle these "contradicting" arguments, we investigated the radial dependence of the time gain per duration ratio w. Fig. 5.12 revealed that it has a minimum for an $r \in [r_{\max}, 0]$, provided that the fixed parameters are defined in terms of their respective maximal values. It vanishes at the edge of the allowed radial range. Of course, the more steeply we travel back in time—i.e. the larger κ gets—, the better the ratio becomes.

The longitudinal relative accelerations—or the tidal accelerations as we were inclined to term them—are independent of κ as can be seen from (5.13). We argued with the aid of (5.14) and Fig. 5.1 and 5.2 that not even the maximal tidal accelerations met at $\vartheta = \pi/2$ pose a dangerous travelling hazard. In the equatorial plane of an uncharged black hole, the tidal accelerations are given by the same simple expression in (5.19) as we have calculated for the Schwarzschild solution in section 3.4.2. Thus, it is independent of the angular momentum a.

In chapter 6 we calculated the mass of the gases exhausted in order to hold course. This was completed by means of the Tsiolkovsky–equation (6.6), which lead to the formula (6.8) indicating the relative mass exhaust μ necessary per revolution to produce the needed acceleration $\wp$. This acceleration was calculated aforehand in section 6.1, where (6.3) resulted.

Preceding to the closer analysis of the relative mass exhaust μ, we gave a short account of propulsion systems. We investigated the latitudinal dependence of the total acceleration $\wp$ as well as of the factor of the acceleration $\wp$ times the duration per revolution Δs, since that is where the action is in (6.8). We found out that especially for distances larger than, say, $0.2r_{\max}$ from the singularity, the calculatory effort of trying to minimize the exponential of (6.8) is not justified by the modest profit of a factor two at the utmost which may be drawn from that. For this reason, we focussed our considerations on the equatorial plane.

Subsequent to the latitudinal dependence, we studied the influence of the mass M of the black hole upon the energy consumption on the time travel.

The total energy used to perform a complete revolution is, rather surprisingly, independent of the mass. However, the energy loss per time gain goes with $1/M$ and may thus be improved by a higher mass. The trajectory parameter κ should remain rather small in order to save the craft's fuel, since the acceleration $\wp$ times the duration per revolution Δs decreases monotonically in the interval $[\kappa_2, 0]$, where κ_2 denotes the minimal value allowed for κ if the spirals have to satisfy the properties (5.1) to (5.3). Unfortunately though, we have not been able to prove this in a strict way. The factor $\wp \cdot \Delta s$ was found to diverge for $\kappa \to \kappa_2$, meaning that an infinite amount of fuel would have to be burnt in case our ambition were to follow a trajectory with $\kappa = \kappa_2$.

Studying the radial dependence of $\wp \cdot \Delta s$, we recognized its divergence for $r \to r_{\max}$ as well as for $r \to 0$. The consequence of such a behaviour on parts of the factor near the limits of Γ was its minimum for any intermediate value $r \in [r_{max}, 0]$, varying for different sets of parameters. Regarding the variation of $\wp \cdot \Delta s$ resulting from the angular momentum, we argued that over large parts of the permitted range of a, the factor remains well–behaved and nearly constant. However, it diverges for $a \to 0$, which would shatter our prospect for finding a passage into EKN− anyway, as the singularity would then no longer form a Kerr *ring* singularity, but a Schwarzschild *point* singularity. In this case, no analytical extension into negative values of r may be pasted to the "Schwarzschild–patch" and no domains of causality violation emerge.

In the last section of chapter 6, we had to admit that the time travel eventually is rendered impossible due to an extremely high energy consumption. Given an exhaust velocity common to contemporary state–of–the–art propulsion systems, the tank of the spacecraft would be empty within a time of the order $\sim 10^{-15}$s. There has been no way of solving this energy problem when insisting on completing one full revolution in Γ. If we content ourselves with spiralling on the curve for less than one revolution, we may concentrate on achieving a certain time gain and then quit for the purpose of refuelling. The energy consumption per time gain ratio is proportional to $1/M$ and may thus be tuned by choosing a black hole with a mass as large as possible. However, any known—or even conceivable—black hole will not even approach what is required in terms of masses if time travel were to be realistic. The mass required should lie above $10^{22} M_\odot$. Therefore, the time travel envisioned remains nothing but an intellectual game. □

Acknowledgments

First of all, I would like to express my gratitude towards Prof. Petr Hájíček. I am much indebted to his expert comments and his competent advice.

My colleagues at the Institute for Theoretical Physics in Berne have provided a relaxed working atmosphere. Jan Kazil discussed many conceptual questions with me and Markus Leibundgut and Thomas Jörg helped me out with stubborn problems regarding information technology. Alan Held and John T. Whelan copyread earlier drafts of this essay.

Special thanks go to my parents—Margreth and Fritz Wüthrich—who have encouraged me to keep going and who have provided financial support throughout my studies. Last but not least, I would like to thank Evelyne Schlup from the bottom of my heart.

Appendix A

Units

We would like to add a few remarks concerning the units used in this essay. On the one hand, we calculate in natural units where $c = G = \mu_0 = 1$. This shortens many expressions considerably. As a consequence, we express every quantity in units of meters m^z where $z \in \mathbf{Z}$. On the other hand, for any numerical calculations, the SI–system is applied. It has the undoubted advantage of being a more comprehensible approach to numerical quantities. Its fundamental units are meters m, seconds s, kilograms kg, and Ampères A. The fundamental constants of nature have the following numerical values in the SI–system:[1]

$$
\begin{aligned}
c &= 299 \ 792 \ 458 \mathrm{ms}^{-1}, \\
G &= 6.672 \ 59(85) \times 10^{-11} \mathrm{m}^3 \mathrm{kg}^{-1} \mathrm{s}^{-2}, \\
\mu_0 &= 4\pi \times 10^{-7} \mathrm{NA}^{-2}.
\end{aligned}
$$

A combination of these factors will convert expressions from one system to the other. This conversion can thus be formalized,

$$
\mathrm{m}^a \left[c^x G^y \mu_0^z \right] = \mathrm{m}^b \mathrm{s}^c \mathrm{kg}^d \mathrm{A}^e,
$$

where $a, b, c, d, e, x, y, z \in \mathbf{Q}$. The square brackets symbolize the units of the quantities embraced and no numerical values whatsoever. The exponentials x, y, z are uniquely given by a, b, c, d, e. These considerations lead us to Figure A.

Since the metric ds^2 is a sort of "quadratic distance" and the coordinates t and r are measured in m according to Figure A, the units of the metrical tensor (in Boyer–Lindquist coordinates) are given by

$$
\begin{aligned}
[g_{tt}] = [g_{tr}] = [g_{rr}] &= 1, \\
[g_{t\varphi}] = [g_{t\vartheta}] = [g_{r\varphi}] = [g_{r\vartheta}] &= \mathrm{m}, \\
[g_{\varphi\varphi}] = [g_{\varphi\vartheta}] = [g_{\vartheta\vartheta}] &= \mathrm{m}^2.
\end{aligned}
$$

---

[1]All numerical data from [38]

Quantity	Acronym	Natural Units	Conversion Factor	SI Units
Distance	r	m	1	m
Time	t	m	c^{-1}	s
Mass	M	m	$G^{-1}c^2$	kg
Angular Momentum	a	m	c	m^2s^{-1}
	J	m^2	$G^{-1}c^3$	$\text{kgm}^2\text{s}^{-1}$
Charge	Q	m	$(G\mu_0)^{-1/2}c$	C = A s
Force	F	1	$G^{-1}c^4$	$\text{N} = \text{kgms}^{-2}$
Energy	E	m	$G^{-1}c^4$	$\text{J} = \text{kgm}^2\text{s}^{-2}$
Power	P	1	$G^{-1}c^5$	$\text{W} = \text{kgm}^2\text{s}^{-3}$

Figure A.1: Conversion of physical quantities between natural and SI-units.

Appendix B

Advanced and Retarded Coordinates

Sometimes it will prove useful to carry out the calculations in an Eddington–Finkelstein type of coordinates. Therefore, we introduce the advanced (AKN) and retarded Kerr–Newman (RKN) coordinates through the following transformations:

$$t = u + X(r), \quad \varphi = \xi + Y(r) \tag{B.1}$$

for the retarded and

$$t = v - X(r), \quad \varphi = \eta - Y(r) \tag{B.2}$$

for the advanced coordinates, where

$$X'(r) = \frac{r^2 + a^2}{\Delta},$$
$$Y'(r) = \frac{a}{\Delta}.$$

A simple integration yields:

$$X(r) = r - A \log|r - r_-| + B \log|r - r_+|, \tag{B.3}$$

where

$$A = \frac{2m^2 - Q^2}{r_+ - r_-} - m > 0,$$
$$B = \frac{2m^2 - Q^2}{r_+ - r_-} + m > 0,$$

and

$$Y(r) = \frac{a}{r_+ - r_-} \log\left|\frac{r - r_+}{r - r_-}\right|. \tag{B.4}$$

To complete the transformation of the metric (2.4) from the Boyer–Lindquist to the retarded and advanced Kerr–Newman coordinates, we compute the corresponding differentials:

$$
\begin{aligned}
dt - a\sin^2\vartheta\,d\varphi &= du - a\sin^2\vartheta\,d\xi + \frac{\Sigma}{\Delta}dr, \\
adt - (r^2 + a^2)d\varphi &= adu - (r^2 + a^2)d\xi, \\
dt - a\sin^2\vartheta\,d\varphi &= dv - a\sin^2\vartheta\,d\eta - \frac{\Sigma}{\Delta}dr, \\
adt - (r^2 + a^2)d\varphi &= adv - (r^2 + a^2)d\eta.
\end{aligned}
$$

Finally, we obtain for the transformed line element

$$
\begin{aligned}
ds^2 &= \frac{\Delta}{\Sigma}(du - a\sin^2\vartheta\,d\xi)^2 + 2(du - a\sin^2\vartheta\,d\xi)dr \\
&\quad - \frac{\sin^2\vartheta}{\Sigma}[adu - (r^2 + a^2)d\xi]^2 - \Sigma d\vartheta^2, \qquad\qquad \text{(B.5)} \\
ds^2 &= \frac{\Delta}{\Sigma}(dv - a\sin^2\vartheta\,d\eta)^2 - 2(dv - a\sin^2\vartheta\,d\eta)dr \\
&\quad - \frac{\sin^2\vartheta}{\Sigma}[adv - (r^2 + a^2)d\eta]^2 - \Sigma d\vartheta^2, \qquad\qquad \text{(B.6)}
\end{aligned}
$$

and for its potential

$$
\begin{aligned}
A_\mu dx^\mu &= \frac{Qr}{\Sigma}(du - a\sin^2\vartheta\,d\xi) + \frac{Qr}{\Delta}dr, \\
A_\mu dx^\mu &= \frac{Qr}{\Sigma}(dv - a\sin^2\vartheta\,d\eta) + \frac{Qr}{\Delta}dr.
\end{aligned}
\qquad\qquad \text{(B.7)}
$$

As can easily be derived, we have

$$
\det g_{\mu\nu} = -\Sigma^2 \sin^2\vartheta. \qquad\qquad \text{(B.8)}
$$

This metric is regular everywhere except for $\Sigma = 0$ or $\vartheta = 0, \pi$. The latter is the ever arising coordinate singularity, whereas the former is the real McCoy.

Appendix C

Affine Connection of Kerr–Newman Spacetime

Leaving the familiar field of linear theories and the trusted global inertial systems of the Newtonian physics, we are in urgent need of providing a formal construction which enables the astrophysicist to compare physical quantities in distant places. Such a means is put at disposal by the components of the affine connection which establishes a connection between adjoining points of the respective spacetime. Parallel (*not equal!*) vectors are unambiguously propagated from one point to its neighbour by means of the affine connection. For this reason, it is vital to know the components of the affinity for the concerned spacetime. As it is a general procedure in physics to postulate a *metric* affine connection—where the components are equal to the Christoffel symbols of the geodesic equation—, we may compute these components in the following manner:

$$\Gamma^{\rho}_{\mu\nu} \;=\; \frac{1}{2}g^{\rho\kappa}\left(g_{\kappa\nu,\mu} + g_{\kappa\mu,\nu} - g_{\mu\nu,\kappa}\right) \tag{C.1}$$

Generally, however, this tedious calculation may be considerably shortened. If we fall back to the variational principle using the action

$$\mathcal{S} \;=\; \frac{1}{2}\int d\lambda\, g_{\mu\nu}\dot{x}^{\mu}\dot{x}^{\nu}$$

with the Lagrangian

$$\mathcal{L} \;=\; \frac{1}{2}g_{\mu\nu}\dot{x}^{\mu}\dot{x}^{\nu}, \tag{C.2}$$

the computational effort decreases significantly. Subsequently, we decompose the Kerr–Newman metric in (C.2) for a more convenient use,

$$\mathcal{L} \;=\; \frac{1}{2}g_{ab}\dot{x}^{a}\dot{x}^{b} + \frac{1}{2}\gamma_{\alpha\beta}\dot{x}^{\alpha}\dot{x}^{\beta}, \tag{C.3}$$

where Latin letters indicate sums over t and φ whereas α and β run over the other two coordinates r and ϑ and $\gamma_{\alpha\beta}$ designates the induced metric in this

two–dimensional subspace. This economic splitting is possible since there are no mixed terms between the two groups of Boyer–Lindquist coordinates. Now, (C.3) is inserted in the Euler-Lagrange equations

$$\frac{\partial \mathcal{L}}{\partial x^\mu} - \frac{d}{d\lambda}\frac{\partial \mathcal{L}}{\partial \dot{x}^\mu} = 0. \tag{C.4}$$

Bearing in mind that the tensor product of a symmetrical tensor with an antisymmetrical one always vanishes, and that therefore in some terms of (C.4) only the symmetrical parts matter, an easy calculation yields

$$\ddot{x}^a + \tfrac{1}{2}g^{ab}(g_{bc,\alpha} + g_{b\alpha,c})\dot{x}^c\dot{x}^\alpha = 0,$$
$$\ddot{x}^\alpha - \tfrac{1}{2}\gamma^{\alpha\beta}g_{ab,\beta}\dot{x}^a\dot{x}^b + \tfrac{1}{2}\gamma^{\alpha\beta}(\gamma_{\beta\rho,\sigma} + \gamma_{\beta\sigma,\rho} - \gamma_{\rho\sigma,\beta})\dot{x}^\rho\dot{x}^\sigma = 0,$$

where ρ and σ also run over the r and ϑ coordinates of the Boyer–Lindquist metric. Some of the derivatives of the metric vanish, and the components of the affine connection can easily be read out of these four equations:

$$\Gamma^a_{c\alpha} = \frac{1}{2}g^{ab}g_{bc,\alpha},$$
$$\Gamma^\alpha_{ab} = -\frac{1}{2}\gamma^{\alpha\beta}g_{ab,\beta}, \tag{C.5}$$
$$\Gamma^\alpha_{\rho\sigma} = \gamma^{\alpha\beta}(\gamma_{\beta\rho,\sigma} + \gamma_{\beta\sigma,\rho} - \gamma_{\rho\sigma,\beta}).$$

If written out explicitly, we obtain the list of all non–vanishing components,

$$\Gamma^t_{tr} = \frac{r^2 + a^2}{\Delta\Sigma^2}\left[M\left(r^2 - a^2\cos^2\vartheta\right) - rQ^2\right],$$

$$\Gamma^t_{t\vartheta} = -\frac{a^2\sin\vartheta\cos\vartheta}{\Sigma^2}\left(r^2 + a^2 - \Delta\right),$$

$$\Gamma^t_{\varphi r} = -\frac{a\sin^2\vartheta}{\Delta\Sigma^2}\left[\left(M\left(r^2 - a^2\cos^2\vartheta\right) - rQ^2\right)\left(r^2 + a^2\right) + r\Sigma\left(r^2 + a^2 - \Delta\right)\right],$$

$$\Gamma^t_{\varphi\vartheta} = \frac{a^3\sin^3\vartheta\cos\vartheta}{\Sigma^2}\left(r^2 + a^2 - \Delta\right),$$

$$\Gamma^\varphi_{tr} = \frac{a}{\Delta\Sigma^2}\left[M\left(r^2 - a^2\cos^2\vartheta\right) - rQ^2\right],$$

$$\Gamma^\varphi_{t\vartheta} = -\frac{a\cot\vartheta}{\Sigma^2}\left(r^2 + a^2 - \Delta\right),$$

$$\Gamma^\varphi_{\varphi r} = -\frac{1}{\Delta\Sigma^2}\left[\left(M\left(r^2 - a^2\cos^2\vartheta\right) - rQ^2\right)a^2\sin^2\vartheta - r\Sigma\left(\Delta - a^2\sin^2\vartheta\right)\right],$$

$$\Gamma^\varphi_{\varphi\vartheta} = \frac{\cot\vartheta}{\Sigma^2}\left[\Sigma\left(\Delta - a^2\sin^2\vartheta\right) + \left(r^2 + a^2\right)\left(r^2 + a^2 - \Delta\right)\right],$$

$$\Gamma^r_{tt} = \frac{\Delta}{\Sigma^3}\left[M\left(r^2 - a^2\cos^2\vartheta\right) - rQ^2\right],$$

$$\Gamma^r_{t\varphi} = -\frac{\Delta a\sin^2\vartheta}{\Sigma^3}\left[M\left(r^2 - a^2\cos^2\vartheta\right) - rQ^2\right],$$

$$\Gamma^r_{\varphi\varphi} = -\frac{\Delta\sin^2\vartheta}{\Sigma^3}\left[r\Sigma^2 - a^2\sin^2\vartheta\left(M\left(r^2 - a^2\cos^2\vartheta\right) - rQ^2\right)\right],$$

$$\Gamma^r_{rr} = -\frac{1}{\Delta\Sigma}\left[r(\Delta-\Sigma)+M\Sigma\right],$$

$$\Gamma^r_{r\vartheta} = -\frac{a^2\sin\vartheta\cos\vartheta}{\Sigma},$$

$$\Gamma^r_{\vartheta\vartheta} = -\frac{\Delta r}{\Sigma},$$

$$\Gamma^\vartheta_{tt} = -\frac{a^2\sin\vartheta\cos\vartheta}{\Sigma^3}\left(r^2+a^2-\Delta\right),$$

$$\Gamma^\vartheta_{t\varphi} = \frac{a\sin\vartheta\cos\vartheta}{\Sigma^3}\left(r^2+a^2\right)\left(r^2+a^2-\Delta\right),$$

$$\Gamma^\vartheta_{\varphi\varphi} = -\frac{\sin\vartheta\cos\vartheta}{\Sigma^3}\left[\Delta\Sigma^2+\left(r^2+a^2\right)^2\left(r^2+a^2-\Delta\right)\right],$$

$$\Gamma^\vartheta_{rr} = \frac{a^2\sin\vartheta\cos\vartheta}{\Delta\Sigma},$$

$$\Gamma^\vartheta_{r\vartheta} = \frac{r}{\Sigma},$$

$$\Gamma^\vartheta_{\vartheta\vartheta} = -\frac{a^2\sin\vartheta\cos\vartheta}{\Sigma}. \tag{C.6}$$

With the label (C.6), we imply the entire list.

Bibliography

[1] Misner, C. W., Thorne, K. S., and Wheeler, J. A., *Gravitation*, Freeman, 1973.

[2] Schwarzschild, K., Sitzber. Deut. Akad. Wiss. Berlin, Kl. Math.–Phys. Tech. (1916) 189.

[3] Kruskal, M. D., Phys. Rev. **119** (1960) 1743.

[4] Kerr, R. P., Phys. Rev. Lett. **11** (1963) 237.

[5] Newman, E. T. et al., J. Math. Phys. **6** (1965) 918.

[6] Lifshitz, E. M. and Khalatnikov, I. M., Soviet Physics JETP **12** (1961) 108.

[7] Lifshitz, E. M. and Khalatnikov, I. M., Adv. Phys. **12** (1963) 205.

[8] Penrose, R., Phys. Rev. Lett. **14** (1965) 58.

[9] Hawking, S. W., Proc. Roy. Soc. Lond. **A 294** (1966) 511.

[10] Israel, W., Phys. Rev. **164** (1967) 1776.

[11] Israel, W., Commun. Math. Phys. **8** (1968) 245.

[12] Robinson, D. C., Phys. Rev. Lett. **34** (1975) 905.

[13] Penrose, R., Riv. del Nuovo Cimento **1** (1969) 252 (Numero Speciale).

[14] Mazur, P. O., J. Phys. **A15** (1982) 3173.

[15] de Felice, F., Nature **273** (1978) 429.

[16] Hawking, S. W., The event horizon, in *Black Holes*, edited by DeWitt, C. and DeWitt, B. S., pages 5–55, Gordon and Breach, 1973.

[17] Hájíček, P., Phys. Rev. D **7** (1973) 2311.

[18] Carter, B., Black hole equilibrium states, in *Black Holes*, edited by DeWitt, C. and DeWitt, B. S., pages 57–214, Gordon and Breach, 1973.

[19] Mazur, P. O., Black hole uniqueness theorems, in *General Relativity and Gravitation*, edited by MacCallum, M. A. H., Proceedings of GR11, Cambridge UP, 1987.

[20] de Felice, F., Nuovo Cim. **B57** (1968) 351.

[21] Stewart, J. and Walker, M., Black holes: The outside story, in *Springer tracts in Modern Physics*, volume 69, pages 69–115, Springer, 1973.

[22] Bičák, J. and Stuchlík, Z., Bull. Astr. Inst. Czech. **27** (1976) 129.

[23] Boyer, R. H. and Lindquist, R. W., J. Math. Phys. **8** (1967) 265.

[24] Carter, B., Phys. Rev. **141** (1966) 1242.

[25] Carter, B., Phys. Rev. **174** (1968) 1559.

[26] Hawking, S. W. and Penrose, R., Proc. Roy. Soc. Lond. **A314** (1970) 529.

[27] Tipler, F. J., Phys. Rev. Lett. **37** (1976) 879.

[28] Calvani, M. and de Felice, F., Gen. Rel. Grav. **9** (1978) 155.

[29] Calvani, M. and de Felice, F., Gen. Rel. Grav. **9** (1978) 889.

[30] de Felice, F. and Calvani, M., Gen. Rel. Grav. **10** (1979) 335.

[31] Newman, E. and Penrose, R., J. Math. Phys. **3** (1962) 566.

[32] Novikov, I. D. and Frolov, V. P., *Physics of Black Holes*, Kluwer Academic Publishers, 1989.

[33] Chandrasekhar, S., *The Mathematical Theory of Black Holes*, Oxford U. P. , 1983.

[34] Hájíček, P., *Allgemeine Relativitätstheorie*, Vorlesungsskript, 1998.

[35] Estabrook, F. B. and Wahlquist, H. D., J. Math. Phys. **5** (1964) 1629.

[36] Goenner, H., *Einführung in die spezielle und allgemeine Relativitätstheorie*, Spektrum, 1996.

[37] Fortescue, P. and Stark, J., *Spacecraft Systems Engineering*, John Wiley and Sons, 1991.

[38] Particle physics booklet, July 1998.